Design Optimization Procedure for Monocoque Composite Cylinder Structures Using Response Surface Techniques

by

Jonathan E. Rich

Thesis submitted to the faculty of the
Virginia Polytechnic Institute and State University
in partial fulfillment of the requirements for the degree of

Master of Science
in
Engineering Mechanics

APPROVED
Zafer Gürdal, Chairman
Michael W. Hyer
Romesh C. Batra

September 12, 1997
Blacksburg, VA

Design Optimization Procedure for Monocoque Composite Cylinder Structures Using Response Surface Techniques

by

Jonathan E. Rich

Zafer Gürdal, Chairman

Engineering Science and Mechanics

(ABSTRACT)

An optimization strategy for the design of composite shells is investigated. This study differs from previous work in that an advanced analysis package is utilized to provide buckling information on potential designs. The Structural Analysis of General Shells (STAGS) finite element code is used to provide linear buckling calculations for a minimum buckling load constraint. A response surface, spanning the design space, is generated from a set of design points and corresponding buckling load data. This response surface is incorporated into a genetic algorithm for optimization of composite cylinders. Laminate designs are limited to those that are balanced and symmetric. Three load cases and four different variable formulations are examined. In the first approach, designs are limited to those whose normalized in-plane and out-of-plane stiffness parameters would be feasible with laminates consisting of two independent fiber orientation angles. The second approach increases the design space to include those that are bordered by those in the first approach. The third and fourth approaches utilize stacking sequence designs for optimization, with continuous and discrete fiber orientation angle variation, respectively. For each load case and different variable formulation, additional runs are made to account for inaccuracies inherent in the response surface model. This study concluded that this strategy was effective at reducing the computational cost of optimizing the composite cylinders.

Table of Contents

List of Figures

List of Tables

Chapter 1—Introduction and Literature Review

1.1—Introduction

Cylindrical shells are structures which find uses in a large number of applications. In the aerospace field, they are used extensively as rocket bodies and aircraft fuselage. As designers look for methods of further reducing the weight of such shell structures, fiber reinforced composite materials are finding wider usage. However, the process of designing with composites is much more difficult than traditional design methods. Composites introduce a number of design variables which affect both the strength and stiffness of the structure. The capability to optimize these structures will allow designers to produce minimum weight designs which satisfy determined design requirements.

This project began as an effort to develop a global-local optimization strategy for the overall design of composite cylindrical shells. The global optimization portion would optimize the structural design with respect to global design variables and global constraints. Features such as numbers of stiffeners and shell wall thickness might be possible design variables, while buckling load and allowable deflections would be potential global constraints. Local optimization would focus on local design variables and design constraints. Design features around cutouts and stress constraints would be included at the local level. Stacking sequence optimization could potentially be applied at either level.

Work in this study focuses on the global optimization. Structures were optimized with respect to global shell variables and a minimum buckling load was implemented as a design constraint. As with virtually any optimization problem, computational efficiency presented the

primary challenge. The number of times the design constraints and objective function must be evaluated and the speed with which they can be evaluated must be held to a minimum for an optimization strategy to be an effective tool. While this study focuses on buckling load as the primary analytical constraint, the optimization strategy should still apply to other constraints.

For this study, a finite element analysis package was used for the buckling load calculations. For simple shell structures, an exact analytical solution for buckling load can be found. However, more complex shell structures, such as those incorporating stiffening structures and cutouts, require numerically intensive approximate methods. The finite element method is one such approximate method.

Structural Analysis of General Shells (STAGS) is a finite element code designed specifically to handle the requirements of analyzing a shell structure. Lockheed's Research and Development Division has developed the code with sponsorship from U.S. government agencies and Lockheed's Independent Research program [1,2]. It is currently regarded as one of the best codes for analyzing shell structures, completing the structural analysis in a minimum of processor time. STAGS is capable of performing linear, as well as nonlinear, analyses of various structures.

Initially, work proceeded using STAGS directly, utilizing a gradient based optimization algorithm. A number of routines were constructed which allowed the automated construction and analysis of STAGS models, as well as retrieval of analysis results. Optimization runs for ring and stringer stiffened aluminum cylinders were completed. While this method was found to be capable of converging to a minimum, it presented a number of potential problems, primarily computational efficiency.

Upon discovery of this problem, an alternate optimization strategy which utilizes response surface techniques was investigated. In this strategy, the evaluation of the buckling load constraint in the optimization algorithm was accomplished using a response surface, rather than using STAGS analyses directly. Since evaluation of the response surface was significantly faster than a corresponding STAGS analysis, the computational cost of optimization was significantly reduced. This reduction in cost would benefit the use of a gradient based optimization algorithm, but also makes the use of a genetic algorithm (GA) feasible.

Genetic algorithms are ideally suited to optimization problems which involve discrete design variables, like composite material stacking sequence design. For this reason, a genetic algorithm optimization code was determined to be the most suitable, and was utilized to examine composite cylinder designs.

1.2—Literature Review

A number of studies have examined optimization of composite cylinders. The earliest work focused on laminates which consisted of single fiber orientation angles and utilized equation-based analysis techniques. Later efforts increased the complexity of the problems, including discrete fiber orientation angles and number of layers in the laminate as design variables. Each of these studies uses some sort of closed form expression to evaluate a buckling load constraint, as opposed to a more complex analysis. In this respect, these studies differ from the work presented in this thesis in that the optimization technique used here includes the STAGS finite element analysis, and a method for possibly incorporating other analysis techniques.

Chao, Sun and Koh [3] utilized shell theory equations and golden section search techniques to maximize the strength of a cylinder subjected to various loadings. The cylinder was made up of balanced symmetric laminates composed of a single fiber orientation angle. The fiber orientation angle which maximized the strength of the cylinder, according to the theory of maximum work, was then found.

A similar study was performed by Prucz, Sivan, and Upadhyay [4]. Composite ducts were optimized for weight minimization. Various normalized geometric and material parameters were considered in the study. The Tsai-Wu Quadratic failure criterion and a buckling failure criterion are used as constraints, and a single fiber orientation angle is varied, with minimum thickness being determined from resulting plots.

Further work was done by ZitzEvancih [5]. The analytical tool chosen for his optimization research were NASA buckling equations for orthotropic cylinders. Using this criteria, the buckling capability to weight ratio of the cylinders was maximized, with the cylinders being subjected to axial, pressure and bending loads. Balanced symmetric laminates, consisting of 0^o, $\pm 45^o$, and 90^o fiber orientations, were used to construct the laminates. The relative volume

ratio of the laminates to each other and the stacking sequence were used as design variables for the study.

Zimmerman [6] presented a study which examined the mass minimization of axially compressed composite cylinders. Shallow shell theory was utilized to calculate the classical buckling load of the cylinders being examined. Zimmerman did not limit the design of the laminates to be symmetric. Fiber failure and matrix cracking constraints were also included. Fiber orientation angles were utilized as design variables and comparisons were made between continuous variation and discrete variation of the design variables. Continuous optimization was facilitated by the use of the CADOP optimization package, while an exhaustive lattice search was used to search for the optimum discrete combination. Zimmerman also concluded from the study that the optimal fiber orientations for a cylinder are independent of the length, radius and wall thickness of the cylinder.

Chattopadhyay and Ferreira [7] performed a study to investigate the maximum buckling load of a cylinder, subject to ply stress constraints, using material and geometric design variables. A closed form shell equation was utilized for the buckling load calculation. Laminates were constrained to be symmetric, and the number of laminates was included in the design variables. Fiber orientation angles were permitted to vary continuously. The computer code CONMIN was employed as the optimizer. Results were found for graphite-epoxy, glass-epoxy, and Kevlar-epoxy models, with 2 to 10 plies.

Response surface models have been utilized throughout scientific research to fit expressions to experimental data. However, they have also found use in optimization work to approximate more complex systems, for which the governing equation is unknown or too expensive to solve many times. Response surfaces can also be used in instances when the analysis suffers from numerical noise and, as a result, contains numerous local minima. A few recent studies have examined the use of response surfaces in optimization work.

Narducci *et al.* [8] utilized a response surface model to approximate a non-smooth objective function. The study tackles a fluid design optimization problem which involves a non-smooth objective function. The response surface is used to approximate the objective function

across the entire design space with a smooth least-squares fit polynomial. Optimization was then performed to find the minimum of the response surface. The minimum of the response surface was taken to be close to the minimum of the objective function and final minimization was performed. Comparisons were made between using a gradient based optimization strategy, starting at the response surface minimum, and using a second response surface model, constructed in the vicinity of the response surface minimum.

Ragon *et al.* [9] incorporated a response surface model into a global-local optimization strategy. A response surface was used to model the weights of optimized composite panels, subject to a series of load and stiffness requirements, over a range of local design variables. This response surface was then referenced by a global optimization algorithm, instead of directly referencing the local optimization code. The use of the response surface allowed coupling between the global and local design process, without requiring modifications to either the global or local codes.

The concepts of cylinder optimization and the response surface techniques investigated in these studies gives a basis for this work. Optimization of composite cylinders has been performed using small numbers of design variables and simplified analysis techniques in the interests of computational efficiency. Work with response surface models has been done in order to replace a computationally expensive process with an inexpensive process. This work attempts to combine the optimization of composite cylinders with the response surface techniques to improve the computational cost of optimization and make use of currently available analysis technologies.

1.3—Scope of the present work

In this work, a procedure has been investigated for finding the minimum mass design of a monocoque composite cylinder. The problem used to test the procedure was that of an axially loaded cylinder. A linear buckling analysis contained within a finite element analysis package (STAGS) is used to calculate the buckling loads of the model. Response surfaces were used to model the minimum buckling load in terms of the design variables of the problem, reducing the computational cost of the optimization procedure. To further simplify the problem, only balanced symmetric laminate constructions were permitted. Design variables were used to represent the in-

plane and bending stiffness characteristics of the composite laminates. Results are presented for three minimum buckling load targets.

Chapter 2—Analysis

This chapter includes a discussion on classical laminate theory and a brief overview of the STAGS analysis. A major focus of the design study presented in this thesis is the use of normalized laminate stiffness parameters, which simplify the description of a laminate to four parameters, regardless of stacking sequence. Derivation of the laminate stiffness parameters is included in the Classical Laminate Theory section. Use of these parameters as design variables allows complex stacking sequence optimization, while maintaining the low number of design variables necessary for optimization.

2.1—Classical Laminate Theory

Consider the following expression of the generalized Hooke's law in matrix form [10]:

$$\begin{bmatrix} \sigma_1 \\ \sigma_2 \\ \sigma_3 \\ \tau_{23} \\ \tau_{31} \\ \tau_{12} \end{bmatrix} = \begin{bmatrix} c_{11} & c_{12} & c_{13} & c_{14} & c_{15} & c_{16} \\ c_{12} & c_{22} & c_{23} & c_{24} & c_{25} & c_{26} \\ c_{13} & c_{23} & c_{33} & c_{34} & c_{35} & c_{36} \\ c_{14} & c_{24} & c_{34} & c_{44} & c_{45} & c_{46} \\ c_{15} & c_{25} & c_{35} & c_{45} & c_{55} & c_{56} \\ c_{16} & c_{26} & c_{36} & c_{46} & c_{56} & c_{66} \end{bmatrix} \begin{bmatrix} \varepsilon_1 \\ \varepsilon_2 \\ \varepsilon_3 \\ \gamma_{23} \\ \gamma_{31} \\ \gamma_{12} \end{bmatrix} \quad \{1\}$$

For orthotropic materials, the number of independent elastic constants reduces from 21 to 9.

$$\begin{bmatrix} \sigma_1 \\ \sigma_2 \\ \sigma_3 \\ \tau_{23} \\ \tau_{31} \\ \tau_{12} \end{bmatrix} = \begin{bmatrix} c_{11} & c_{12} & c_{13} & 0 & 0 & 0 \\ c_{12} & c_{22} & c_{23} & 0 & 0 & 0 \\ c_{13} & c_{23} & c_{33} & 0 & 0 & 0 \\ 0 & 0 & 0 & c_{44} & 0 & 0 \\ 0 & 0 & 0 & 0 & c_{55} & 0 \\ 0 & 0 & 0 & 0 & 0 & c_{66} \end{bmatrix} \begin{bmatrix} \varepsilon_1 \\ \varepsilon_2 \\ \varepsilon_3 \\ \gamma_{23} \\ \gamma_{31_5} \\ \gamma_{12} \end{bmatrix} \quad \{2\}$$

Assuming a state of plane stress in the 1-2 material plane gives:

$$\sigma_3 = 0 \quad \{3\}$$
$$\tau_{23} = 0$$
$$\tau_{31} = 0$$

which reduces Hooke's law to:

$$\begin{bmatrix} \sigma_1 \\ \sigma_2 \\ \tau_{12} \end{bmatrix} = \begin{bmatrix} Q_{11} & Q_{12} & 0 \\ Q_{12} & Q_{22} & 0 \\ 0 & 0 & Q_{66} \end{bmatrix} \begin{bmatrix} \varepsilon_1 \\ \varepsilon_2 \\ \gamma_{12} \end{bmatrix} \quad \{4\}$$

The Q_{ij}'s are referred to as reduced stiffness, and are defined in terms of material properties:

$$Q_{11} = \frac{E_1}{1-\nu_{12}\nu_{21}} \quad \{5\}$$
$$Q_{22} = \frac{E_2}{1-\nu_{12}\nu_{21}}$$
$$Q_{12} = \frac{\nu_{12}E_2}{1-\nu_{12}\nu_{21}} = \frac{\nu_{21}E_1}{1-\nu_{12}\nu_{21}}$$
$$Q_{66} = G_{12}$$

Generally, Equation 4 must be transformed to reflect rotated fiber orientation angles. The following relationship reflects this transformation [11]:

$$\begin{bmatrix} \sigma_{x1} \\ \sigma_y \\ \tau_{xy} \end{bmatrix} = \begin{bmatrix} \overline{Q}_{11} & \overline{Q}_{12} & \overline{Q}_{16} \\ \overline{Q}_{12} & \overline{Q}_{22} & \overline{Q}_{16} \\ \overline{Q}_{16} & \overline{Q}_{16} & \overline{Q}_{66} \end{bmatrix} \begin{bmatrix} \varepsilon_x \\ \varepsilon_y \\ \gamma_{xy} \end{bmatrix} \quad \{6\}$$

where:

$$\overline{Q}_{11} = Q_{11}\cos^4\theta + 2\left(Q_{12} + 2Q_{66}\right)\sin^2\theta\cos^2\theta + Q_{22}\sin^4\theta \quad \{7\}$$
$$\overline{Q}_{12} = \left(Q_{11} + Q_{22} - 4Q_{66}\right)\sin^2\theta\cos^2\theta + Q_{12}\left(\sin^4\theta + \cos^4\theta\right)$$
$$\overline{Q}_{22} = Q_{11}\sin^4\theta + 2\left(Q_{12} + 2Q_{66}\right)\sin^2\theta\cos^2\theta + Q_{22}\cos^4\theta$$
$$\overline{Q}_{16} = \left(Q_{11} - Q_{22} - 2Q_{66}\right)\sin\theta\cos^3\theta + \left(Q_{12} - Q_{22} + 2Q_{66}\right)\sin^3\theta\cos\theta$$
$$\overline{Q}_{26} = \left(Q_{11} - Q_{22} - 2Q_{66}\right)\sin^3\theta\cos\theta + \left(Q_{12} - Q_{22} + 2Q_{66}\right)\sin\theta\cos^3\theta$$
$$\overline{Q}_{66} = \left(Q_{11} + Q_{22} - 2Q_{12} - 2Q_{66}\right)\sin^2\theta\cos^2\theta + Q_{66}\left(\sin^4\theta + \cos^4\theta\right)$$

Often, it is useful to express these relationships independent of the fiber orientation angle. The following invariant U terms are solely a function of material properties.

$$U_1 = \frac{1}{8}\left(3Q_{11} + 3Q_{22} + 2Q_{12} + 4Q_{66}\right) \quad \{8\}$$

$$U_2 = \frac{1}{2}\left(Q_{11} - Q_{22}\right)$$

$$U_3 = \frac{1}{8}\left(Q_{11} + Q_{22} - 2Q_{12} - 4Q_{66}\right)$$

$$U_4 = \frac{1}{8}\left(Q_{11} + Q_{22} + 6Q_{12} - 4Q_{66}\right)$$

$$U_5 = \frac{1}{8}\left(Q_{11} + Q_{22} - 2Q_{12} + 4Q_{66}\right)$$

Thus, the transformed reduced stiffnesses are given by:

$$\overline{Q}_{11} = U_1 + U_2\cos 2\theta + U_3\cos 4\theta \quad \{9\}$$

$$\overline{Q}_{12} = U_4 - U_3\cos 4\theta$$

$$\overline{Q}_{22} = U_1 - U_2\cos 2\theta + U_3\cos 4\theta$$

$$\overline{Q}_{16} = -\frac{1}{2}U_2\sin 2\theta - U_3\sin 4\theta$$

$$\overline{Q}_{26} = -\frac{1}{2}U_2\sin 2\theta + U_3\sin 4\theta$$

$$\overline{Q}_{66} = U_5 - U_3\cos 4\theta$$

For classical laminate theory (CLT), it is assumed that N layers of material are perfectly bonded together, with infinitely thin, non-shear-deformable boundaries. Using Kirchoff plate theory, which assumes in-plane displacements vary linearly through-thickness and zero through-thickness strains, displacement relationships are defined by the following equations. Midplane displacements are denoted by the 0 subscript.

$$u = u_0 - z\frac{\partial w_0}{\partial x} \quad \{10\}$$

$$v = v_0 - z\frac{\partial w_0}{\partial y}$$

$$w = w_0$$

$$\varepsilon_z = \gamma_{xz} = \gamma_{yz} = 0$$

Combining these relationships with equation 6 gives the following expression for the k[th] layer:

$$\begin{Bmatrix}\sigma_x\\ \sigma_y\\ \tau_{xy}\end{Bmatrix}_k = \begin{bmatrix}\overline{Q}_{11} & \overline{Q}_{12} & \overline{Q}_{16}\\ \overline{Q}_{12} & \overline{Q}_{22} & \overline{Q}_{16}\\ \overline{Q}_{16} & \overline{Q}_{16} & \overline{Q}_{66}\end{bmatrix}_k \left(\begin{Bmatrix}\varepsilon^0{}_x\\ \varepsilon^0{}_y\\ \gamma^0{}_{xy}\end{Bmatrix} + z\begin{Bmatrix}\kappa_x\\ \kappa_y\\ \kappa_{xy}\end{Bmatrix} \right) \quad \textbf{\{11\}}$$

By integrating through the thickness of the laminate, the net stress resultants and moment resultants can be calculated.

$$\begin{Bmatrix}N_x\\ N_y\\ N_{xy}\end{Bmatrix} = \int_{-\frac{h}{2}}^{\frac{h}{2}} \begin{Bmatrix}\sigma_x\\ \sigma_y\\ \tau_{xy}\end{Bmatrix}_k dz \quad \textbf{\{12\}}$$

$$\begin{Bmatrix}M_x\\ M_y\\ M_{xy}\end{Bmatrix} = \int_{-\frac{h}{2}}^{\frac{h}{2}} \begin{Bmatrix}\sigma_x\\ \sigma_y\\ \tau_{xy}\end{Bmatrix}_k z dz$$

Following the laminate stacking convention shown in Figure 1, the above integrals can be expresses as summations:

Figure 1 Laminate stacking convention [12]

$$\begin{Bmatrix} N_x \\ N_y \\ N_{xy} \end{Bmatrix} = \sum_{k=1}^{N} \int_{z_{k-1}}^{z_k} \begin{Bmatrix} \sigma_x \\ \sigma_y \\ \tau_{xy} \end{Bmatrix}_k dz \qquad \{13\}$$

$$\begin{Bmatrix} M_x \\ M_y \\ M_{xy} \end{Bmatrix} = \sum_{k=1}^{N} \int_{z_{k-1}}^{z_k} \begin{Bmatrix} \sigma_x \\ \sigma_y \\ \tau_{xy} \end{Bmatrix}_k z dz$$

Combining these relationships with equation 11 gives:

$$\begin{Bmatrix} N_x \\ N_y \\ N_{xy} \end{Bmatrix} = \begin{bmatrix} A_{11} & A_{12} & A_{16} \\ A_{12} & A_{22} & A_{16} \\ A_{16} & A_{16} & A_{66} \end{bmatrix} \begin{Bmatrix} \varepsilon^0{}_x \\ \varepsilon^0{}_y \\ \gamma^0{}_{xy} \end{Bmatrix} + \begin{bmatrix} B_{11} & B_{12} & B_{16} \\ B_{12} & B_{22} & B_{16} \\ B_{16} & B_{16} & B_{66} \end{bmatrix} \begin{Bmatrix} \kappa_x \\ \kappa_y \\ \kappa_{xy} \end{Bmatrix} \qquad \{14\}$$

$$\begin{Bmatrix} M_x \\ M_y \\ M_{xy} \end{Bmatrix} = \begin{bmatrix} B_{11} & B_{12} & B_{16} \\ B_{12} & B_{22} & B_{16} \\ B_{16} & B_{16} & B_{66} \end{bmatrix} \begin{Bmatrix} \varepsilon^0{}_x \\ \varepsilon^0{}_y \\ \gamma^0{}_{xy} \end{Bmatrix} + \begin{bmatrix} D_{11} & D_{12} & D_{16} \\ D_{12} & D_{22} & D_{16} \\ D_{16} & D_{16} & D_{66} \end{bmatrix} \begin{Bmatrix} \kappa_x \\ \kappa_y \\ \kappa_{xy} \end{Bmatrix}$$

where:

$$A_{ij} = \sum_{k=1}^{N} \left(\overline{Q}_{ij}\right)\left(z_k - z_{k-1}\right) \qquad \{15\}$$

$$B_{ij} = \frac{1}{2} \sum_{k=1}^{N} \left(\overline{Q}_{ij}\right)\left(z_{k-1}^2 - z_k^2\right)$$

$$D_{ij} = \frac{1}{3} \sum_{k=1}^{N} \left(\overline{Q}_{ij}\right)\left(z_{k-1}^3 - z_k^3\right)$$

The integral form of these three equations can be written as:

$$\left\{A_{ij} \quad B_{ij} \quad D_{ij}\right\} = \int_{-\frac{h}{2}}^{\frac{h}{2}} \overline{Q}_{ij} \left\{1 \quad z \quad z^2\right\} dz \qquad \{16\}$$

Using this form of the expressions, the invariant relationships expressed earlier can be incorporated into the matrix expressions. Assuming that each layer of the laminate uses the same material, the first term of each matrix is given by:

$$\left\{A_{11} \quad B_{11} \quad D_{11}\right\} = U_1 \left\{h \quad 0 \quad \frac{h^3}{12}\right\} + U_2 \int_{-\frac{h}{2}}^{\frac{h}{2}} \cos 2\theta \left\{1 \quad z \quad z^2\right\} dz + U_3 \int_{-\frac{h}{2}}^{\frac{h}{2}} \cos 4\theta \left\{1 \quad z \quad z^2\right\} dz \qquad \{17\}$$

The remaining elements in the matrices can also be found via a similar expression. Table 1 shows summarizes these expressions.

Table 1 A, B, D Matrices in terms of lamina invariants [12]

	$V_{0\{A,B,D\}}$	$V_{1\{A,B,D\}}$	$V_{2\{A,B,D\}}$	$V_{3\{A,B,D\}}$	$V_{4\{A,B,D\}}$
$\{A_{11}, B_{11}, D_{11}\}$	U_1	U_2	0	U_3	0
$\{A_{22}, B_{22}, D_{22}\}$	U_1	$-U_2$	0	U_3	0
$\{A_{12}, B_{12}, D_{12}\}$	U_4	0	0	$-U_3$	0
$\{A_{66}, B_{66}, D_{66}\}$	U_5	0	0	$-U_3$	0
$2\{A_{16}, B_{16}, D_{16}\}$	0	0	$-U_2$	0	$-2U_3$
$2\{A_{26}, B_{26}, D_{26}\}$	0	0	$-U_2$	0	$2U_3$

where:

$$V_{0\{A,B,D\}} = \left\{h, 0, \frac{h^3}{12}\right\} \quad \{18\}$$

$$V_{1\{A,B,D\}} = \int_{-\frac{h}{2}}^{\frac{h}{2}} \cos 2\theta \left\{1, z, z^2\right\} dz$$

$$V_{2\{A,B,D\}} = \int_{-\frac{h}{2}}^{\frac{h}{2}} \sin 2\theta \left\{1, z, z^2\right\} dz$$

$$V_{3\{A,B,D\}} = \int_{-\frac{h}{2}}^{\frac{h}{2}} \cos 4\theta \left\{1, z, z^2\right\} dz$$

$$V_{4\{A,B,D\}} = \int_{-\frac{h}{2}}^{\frac{h}{2}} \sin 4\theta \left\{1, z, z^2\right\} dz$$

For balanced, symmetric laminates, normalized V_1 and V_3 parameters can be used to describe an entire laminate. By normalizing these parameters with respect to the overall thickness of the laminate, h, the in-plane stiffness characteristics of the laminate are defined. A similar, but

somewhat more complex normalization is performed for the bending stiffness parameters, W_1^* and W_3^*. These parameters were introduced by Miki as a part of a graphical design technique [12].

$$V_1^* = \frac{V_{1A}}{h} = \sum_{k=1}^{I} v_k Cos(2\theta_k) \quad \{19\}$$

$$V_3^* = \frac{V_{3A}}{h} = \sum_{k=1}^{I} v_k Cos(4\theta_k) \quad \{20\}$$

$$W_1^* = \frac{12V_{1D}}{h^3} = \sum_{k=1}^{I} s_k Cos(2\theta_k) \quad \{21\}$$

$$W_3^* = \frac{12V_{3D}}{h^3} = \sum_{k=1}^{I} s_k Cos(4\theta_k) \quad \{22\}$$

where:

$$v_i = \frac{2(z_i - z_{i-1})}{h} \text{ , } i = 1, \text{k} \quad \{23\}$$

$$s_i = \left(\frac{2z_i}{h}\right)^3 - \left(\frac{2z_{i-1}}{h}\right)^3 \text{ , } i = 1, \text{k} \quad \{24\}$$

The (V_1^*, V_3^*) parameters determine the in-plane stiffness characteristics for the laminate being analyzed, while the (W_1^*, W_3^*) parameters determine the bending stiffness characteristics. From these four parameters, the A and D wall stiffness matrices can be calculated. These four parameters now fully describe the cylinder wall stiffness properties.

$$\begin{Bmatrix} A_{11} \\ A_{22} \\ A_{12} \\ A_{66} \end{Bmatrix} = \begin{bmatrix} U_1 & V_{1A} & V_{3A} \\ U_1 & -V_{1A} & V_{3A} \\ U_4 & 0 & -V_{3A} \\ U_5 & 0 & -V_{3A} \end{bmatrix} \begin{Bmatrix} h \\ U_2 \\ U_3 \end{Bmatrix} \quad \{25\}$$

$$\begin{Bmatrix} D_{11} \\ D_{22} \\ D_{12} \\ D_{66} \end{Bmatrix} = \frac{h^3}{12} \begin{bmatrix} U_1 & W_1^* & W_3^* \\ U_1 & -W_1^* & W_3^* \\ U_4 & 0 & -W_3^* \\ U_5 & 0 & -W_3^* \end{bmatrix} \begin{Bmatrix} 1 \\ U_2 \\ U_3 \end{Bmatrix} \quad \{26\}$$

Bending-stretching coupling is eliminated from these designs by the symmetric lay-up of the laminated design ($B_{ij} = 0$) and the balanced requirement produces orthotropic laminate designs ($A_{16} = A_{26} = D_{16} = D_{26} = 0$), further simplifying the relationships.

For this study, the four parameters described above are used as design variables in the optimization of composite cylinders. The advantage of using the parameters is that they can be used to represent the in-plane and bending stiffness properties of any balanced, symmetric laminate, regardless of its thickness or number of fiber orientation angles. For optimization, this is an important reduction in the complexity of the problem. Consider a balanced symmetric laminate with 10 fiber orientations. Use of the parameters reduces the problem from a ten design variable problem to a four design variable problem.

Each of the four parameters is bounded by $-1 \le V_1^*, V_3^*, W_1^*, W_3^* \le 1$, and the two pairs of parameters are bounded by a parabola [12], given by Equations 27 and 28. The shaded region of Figure 2 shows the feasible region for the parameters.

$$V_3^* \ge 2V_3^{*2} - 1 \quad \textbf{\{27\}}$$

$$W_3^* \ge 2W_3^{*2} - 1 \quad \textbf{\{28\}}$$

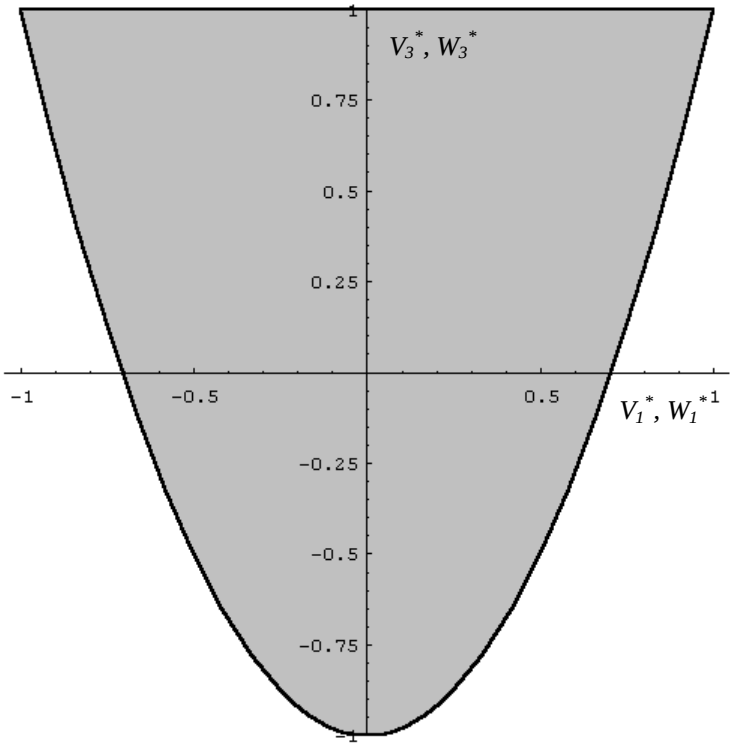

Figure 2 V_1^***-**V_3^***,** W_1^***-**W_3^* **Limiting Parabola**

For a laminate comprised of only two fiber orientation angles, it is possible for find closed form expressions for those angles in terms of V_1^*, V_3^*, and the relative percentages of each fiber orientation angle in the laminate. These expressions are given by Equations 29 and 30. The fiber orientation angles are assumed to be continuous variables.

$$\theta_1 = \frac{1}{2} Cos^{-1}\left(T_1\right) \quad \{29\}$$

$$\theta_2 = \frac{1}{2} Cos^{-1}\left(T_2\right) \quad \{30\}$$

where:

$$T_1 = \frac{2v_1 V_1^* \pm \sqrt{2v_1 v_2\left(1 + V_3^* - 2\left(V_1^*\right)^2\right)}}{2v_1} \quad \{31\}$$

$$T_2 = \frac{V_1^* - v_1 T_1}{v_2} \quad \{32\}$$

By assuming a stacking sequence of $[\pm\theta_1, \pm\theta_2]_s$ and a laminate thickness of h = 1, a relationship between the four parameters can be determined. For this laminate,

$$z = \{1, 1-t, 0\} \quad \{33\}$$

which gives:

$$v = \{t, 1-t\} \quad \{34\}$$

$$s = \left\{1-(1-t)^3, (1-t)^3\right\} \quad \{35\}$$

By manipulating these expressions, the following expressions for W_1^* and W_3^* were determined.

$$W_1^* = V_1^* \pm 2C \quad tC \quad \{36\}$$

$$W_3^* = (1-t)^3\left(2\left(\frac{V_1^* - tV_1^* \quad C}{1-t}\right)^2 - 1\right) + t\left(3 - 3t + t^2\right)\left(2\left(V_1^* \pm \frac{C}{t}\right)^2 - 1\right) \quad \{37\}$$

where:

$$C = \frac{1}{\sqrt{2}}\sqrt{(1-t)(t)(1 - 2V_1^{*2} + V_3^*)} \quad \{38\}$$

The curves defined by Equations 36 and 37 bound a region of feasible $\left(W_1^*, W_3^*\right)$ for a given $\left(V_1^*, V_3^*\right)$ point. Figures 3 and 4 show examples of this feasible region. The $\left(V_1^*, V_3^*\right)$ is plotted as a black point, while the $\left(W_1^*, W_3^*\right)$ curves are plotted in red and green parametrically as t varies. The interior region is feasible if *s* is allowed to vary independently of *v*.

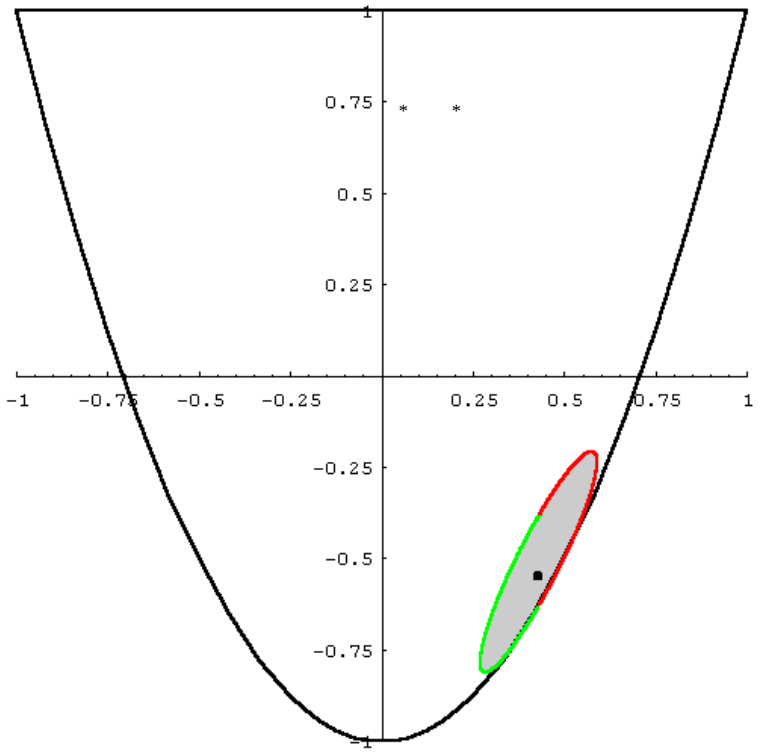

Figure 3 Feasible region for $\left(W_1^*, W_3^*\right)$ for $\left(V_1^*, V_3^*\right) = (0.430, -0.548)$

This relationship between $\left(V_1^*, V_3^*\right)$ and $\left(W_1^*, W_3^*\right)$ is important. Constraining an optimization problem with this relationship ensures that a realistic laminate design can be determined which matches the design variable values. Without such a relationship, the optimizer is likely to select parameter pairings which cannot be produced with true laminates. The drawback is that the relationship limits the design to two independent fiber orientation angles.

Laminates with more than two fiber orientations can have $\left(W_1^*, W_3^*\right)$ values which are outside the bounded region.

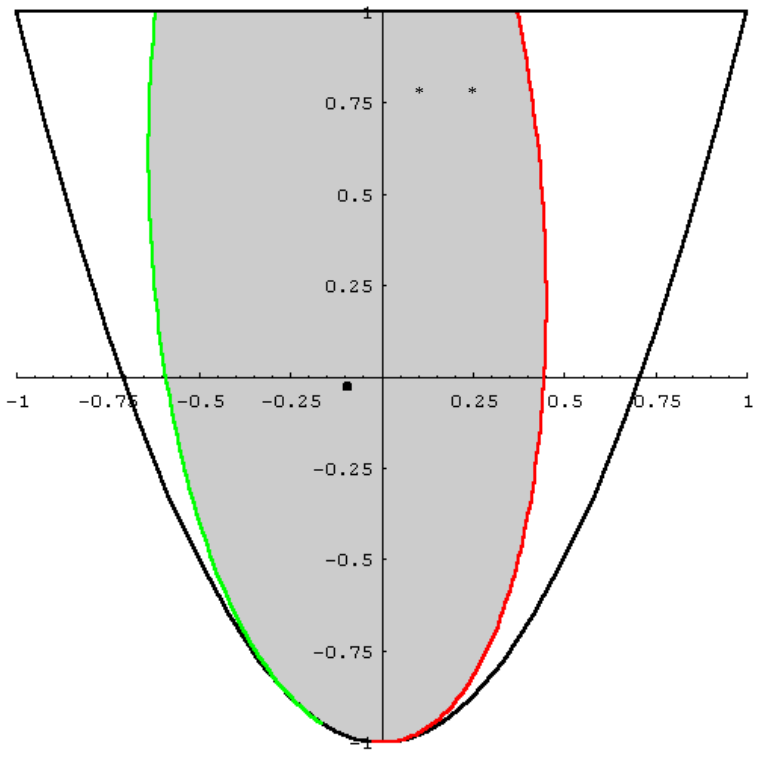

Figure 4 Feasible region for $\left(W_1^*, W_3^*\right)$ for $\left(V_1^*, V_3^*\right) = \left(-0.0931, -0.0284\right)$

2.2—STAGS Shell Analysis

Shells, while seemingly simple, react to the loads they are subjected to in their environment in a complex manner. However, while their reactions are complex, they are still governed by the same physical laws which govern all structures.

By simultaneously satisfying the structure's constitutive equations, kinematic requirements, and differential equations of motion, the structure's behavior can be determined. Combining the constitutive and kinematic relationships, which express stresses as functions of strains and strains as functions of displacements, respectively, into the equations of motion results

in equations in only the displacements. It can then be shown that the solution to this resulting governing equation is equivalent to a minimum potential energy state of the structure. This is given by [13]:

$$\delta(U+W)=0 \quad \textbf{\{39\}}$$

where U is the strain energy of the structure and W is the potential of the force system that created those strains. For linear elastic analysis of a continuum, this is expressed as:

$$\delta\Pi_T(u)=0 \quad \textbf{\{40\}}$$

where the total potential energy is given by [14]:

$$\Pi_T(u)=\frac{1}{2}\int_V \varepsilon(u)^T C\varepsilon(u)dV-(\int_V u^T f^b dV+\int_S u^T f^s dS) \quad \textbf{\{41\}}$$

Displacements, u, are represented in vector form as functions of position vector, x. Body and surface forces are symbolized as f^b and f^s. Incorporating the Kirchoff-Love hypothesis, transverse shear strains and shell normal stress are assumed to be zero. This gives a displacement field that is defined by:

$$u(x,y,z)=\bar{u}(x,y)-z\bar{w}_{,x}(x,y) \quad \textbf{\{42\}}$$
$$v(x,y,z)=\bar{v}(x,y)-z\bar{w}_{,y}(x,y)$$
$$w(x,y,z)=\bar{w}(x,y)$$

Subsequently, strains can be defined as:

$$\varepsilon(u)=\frac{1}{2}(\nabla u+(\nabla u)^T) \quad \textbf{\{43\}}$$

$$\varepsilon=\{\varepsilon_{11}\quad \varepsilon_{22}\quad 2\varepsilon_{12}\quad 2\varepsilon_{31}\quad 2\varepsilon_{32}\quad \varepsilon_{33}\} \quad \textbf{\{44\}}$$

In-plane local coordinates are given by (x,y) on the reference surface of the shell. The reference surface is defined by z=0. The reference surface displacements are given by $\{\bar{u},\bar{v},\bar{w}\}$ and displacements of all other points are given by $\{u,v,w\}$.

This displacement field relationship can be rewritten as the following for convenience:

$$u(x,y,z)=\bar{u}(x,y)+zu'(x,y) \quad \textbf{\{45\}}$$

where:

$$u = \{u \quad v \quad w\}^T \qquad \{46\}$$

$$\bar{u} = \{\bar{u} \quad \bar{v} \quad \bar{w}\}^T$$

$$u' = \{-\bar{w}_{,x} \quad -\bar{w}_{,y} \quad 0\}^T$$

Combining these displacement definitions with the total potential energy functional gives the "shell" total potential energy functional.

$$\tilde{\Pi}_T(\bar{u}) = \frac{1}{2}\int_S \tilde{\varepsilon}(\bar{u})^T \tilde{C}\tilde{\varepsilon}(\bar{u})dS - (\int_S \tilde{u}^T(\tilde{f}^b + \tilde{f}^s)dS + \int_L \tilde{u}^T \tilde{f}^l dL) \qquad \{47\}$$

where the following definitions are used:

$$\tilde{u} = \{\bar{u} \quad u'\}^T \qquad \text{shell displacement vector} \qquad \{48\}$$

$$\varepsilon = Z\tilde{\varepsilon} \qquad \text{reduced strain vector} \qquad \{49\}$$

$$\tilde{C} = \int_z Z^T C Z dz \qquad \text{resultant constitutive matrix} \qquad \{50\}$$

$$\tilde{\sigma} = \int_z Z^T \sigma dz \qquad \text{stress resultant vector} \qquad \{51\}$$

$$\tilde{f}^{b,s,l} = \{\int_z f^{b,s,l} dz \quad \int_z f^{b,s,l} z dz\}^T \qquad \text{shell body, surface, line forces} \qquad \{52\}$$

$$Z(z) = [I_3 \quad zI_3] \qquad \{53\}$$

Enforcing the zero shear strain and zero normal stress assumptions,

$$\varepsilon_{zx} = \varepsilon_{zy} = \sigma_{zz} = 0 \qquad \{54\}$$

reduces the σ, ε, and C arrays from 6 dimensions to 3 dimensions.

$$\sigma = \{\sigma_{xx} \quad \sigma_{yy} \quad \sigma_{xy}\}^T \qquad \{55\}$$

$$\varepsilon = \{\varepsilon_{xx} \quad \varepsilon_{yy} \quad 2\varepsilon_{xy}\}^T \qquad \{56\}$$

$$C_{ij} = C_{ij} - \frac{C_{i6}C_{6j}}{C_{66}^L} \qquad \{57\}$$

The kinematic relationships for a continuum in three dimensions are:

$$\varepsilon_{ij} = \frac{\partial u_i}{\partial x_j} \qquad \{58\}$$

Applying the above relationship to a general shell represented by a reference surface gives strain relationships in terms of in-plane membrane strains and out-of-plane bending strains, or changes in curvature.

$$\tilde{\varepsilon} = \begin{Bmatrix} \bar{\varepsilon} \\ \kappa \end{Bmatrix} \quad \{59\}$$

where:

$$\bar{\varepsilon} = \begin{Bmatrix} \bar{\varepsilon}_x \\ \bar{\varepsilon}_y \\ \bar{\varepsilon}_{xy} \end{Bmatrix} = \begin{Bmatrix} \dfrac{\partial \bar{u}}{\partial \bar{x}} \\ \dfrac{\partial \bar{v}}{\partial \bar{y}} \\ \dfrac{\partial \bar{u}}{\partial \bar{y}} + \dfrac{\partial \bar{v}}{\partial \bar{x}} \end{Bmatrix} \quad \text{membrane strains} \quad \{60\}$$

$$\kappa = \begin{Bmatrix} \kappa_x \\ \kappa_y \\ \kappa_{xy} \end{Bmatrix} = \begin{Bmatrix} -\dfrac{\partial^2 \bar{w}}{\partial \bar{x} \partial \bar{x}} \\ -\dfrac{\partial^2 \bar{w}}{\partial \bar{y} \bar{y}} \\ -2\dfrac{\partial^2 \bar{w}}{\partial \bar{x} \partial \bar{y}} \end{Bmatrix} \quad \text{bending strains} \quad \{61\}$$

The membrane and bending strains are then combined to give the required strain expression:

$$\varepsilon = \bar{\varepsilon} + z\kappa \quad \{62\}$$

A similar relationship exists for the stress resultants, $\tilde{\sigma}$. The stress resultants include stresses due to in-plane membrane forces and out-of-plane bending forces. For shells with anisotropic wall compositions, there are also coupling terms in which in-plane stress resultants and out-of-plane strains and out-of-plane stress resultants and in-plane strains are coupled. The stress resultants are given by:

$$\tilde{\sigma} = \begin{Bmatrix} N \\ M \end{Bmatrix} = K\tilde{\varepsilon} \quad \{63\}$$

where

$$K = \begin{bmatrix} \int C dz & \int C z dz \\ \int C z dz & \int C z^2 dz \end{bmatrix} = \begin{bmatrix} A & B \\ B & D \end{bmatrix} \quad \{64\}$$

2.2.1—STAGS Finite Element Formulation and Analysis

To solve Equation 40, a finite element approach is used. The structure is broken down into a finite number of elements, and their individual potential energies are summed to give the potential energy of the structure as a whole. Thus, Equation 41 becomes:

$$\Pi_T = \sum_{e=1}^{N_{el}} \Pi_T^e \qquad \{65\}$$

where the total number of elements is given by N_{el}.

For an individual element, an element stiffness matrix, K_e^{matl}, and element external force vector, f_e^{ext}, are defined. Thus, the element potential energy is given by:

$$\Pi_T^e = \frac{1}{2} d_e^T K_e^{matl} d_e - d_e^T f_e^{ext} \qquad \{66\}$$

For a linear static analysis of a structure, the following system of linear equations must be solved:

$$K^{matl} d = f^{ext} \qquad \{67\}$$

where K^{matl} and f^{ext} are the global stiffness matrix and global external force vector, assembled from the element stiffness matrix and element external force vector. The system displacement vector is the combination of all element displacement vectors.

The portion of STAGS used extensively in this design study is the linear bifurcation buckling analysis. The for this analysis, Equation 67 is modified to:

$$\left(K^{matl} + \lambda K^{geom} \sigma_o\right) d_\lambda = 0 \qquad \{68\}$$

The structure is subjected to a pre-stress field, σ_o. Solving the eigenvalue problem gives the shape of the deformed structure in the eigenvector, d_λ, and the eigenvalue, λ, gives the value of the pre-stress load multiplier. K^{geom} is the geometric stiffness matrix [14].

A subroutine in the STAGS code, zbuck.f, was modified to allow the easy retrieval of the buckling load from the analysis. This modified subroutine is shown in Appendix A.

2.2.2—STAGS 410 element

The element used in the finite element model for this study is the STAGS 410 element. Figure 5 shows the topology of this element.

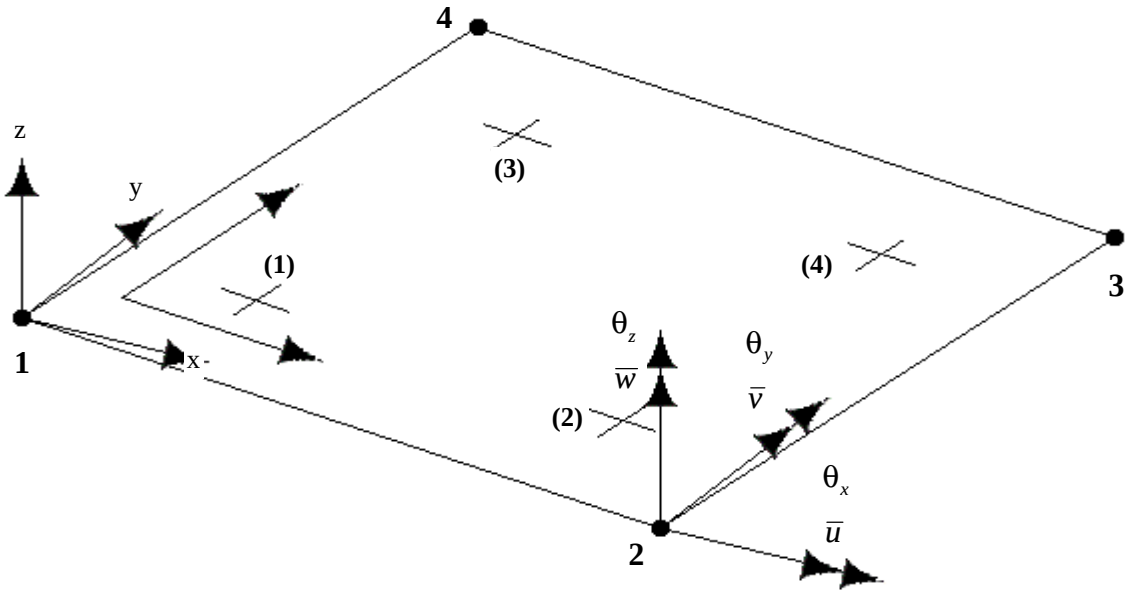

Figure 5 STAGS 410 element topology [11]

Each node of the element has six degrees of freedom, describing translations in the x, y, and z directions and rotations about the x, y, and z axes. Large rotational deformations (>10^o) are permitted by the large rotation algorithm present in STAGS [15].

$$d_a = \begin{Bmatrix} \bar{u}_a \\ \theta_a \end{Bmatrix} = \begin{Bmatrix} \bar{u}_a & \bar{v}_a & \bar{w}_a & \theta_{xa} & \theta_{ya} & \theta z_a \end{Bmatrix} \quad \{69\}$$

At the four Gauss integration points ((1), (2), (3), and (4)) for each element, also shown in Figure 4, the stress and strain resultants are calculated.

The 410 element is a flat, slope-continuous element. The geometry used to define the finite element mesh is a projection of the actual geometry on to a best fit plane for each element. This can potentially make the element sensitive to warping deformations. The displacement shape

functions used for the element are linear-cubic for in-plane deformations and cubic for bending deformations [14].

Chapter 3—Optimization Strategy

The definition of an optimum design is, taken from Haftka and Gurdal [12], *"the best feasible design according to a preselected quantitative measure of effectiveness."* Thus, an optimum design is one which has the proper combination of characteristics (design variables) to give the best value of a performance measure (objective function) and satisfies all of the given requirements (constraints). For structural optimization, it is often desirable to minimize the weight of a structure, yet have it be able to withstand a given load. For a ring and stringer stiffened aircraft fuselage, design variables might be skin thickness and ring and stringer dimensions. Shrinking the values of these design variables would obviously reduce the weight of the structure. However, a likewise reduction in the structure's resistance to loads would also result. Optimization is concerned with finding this balance.

An optimum design can be defined mathematically. For a given objective function, an unconstrained optimum can be found by setting the first order derivatives equal to zero and solving for the values of the design variables. In practical optimization, this approach has two major flaws. The first is that most practical optimization problems are subject to constraints. The unconstrained optimum of an objective function is likely far from the constrained optimum. Second, many times closed form expressions for an objective function (or constraints) are not known. Thus, mathematical manipulation of symbolic expressions is not possible. To get around this problem, various optimization strategies have been developed [16].

Primarily, two optimization strategies were investigated in this study. Sequential linear programming (SLP) is a gradient based search algorithm which iteratively searches a design space from an initial design until it cannot improve upon it. SLP algorithms excel at handling

constrained optimization problems, but at high computational expense. Genetic algorithms (GAs) perform a global search of a design space, successively producing generations of designs which converge towards an optimal design based on the theory of evolution. GAs are well suited to highly non-linear problems and problems with discrete design variables. Included in the discussion on SLP is a brief discussion on an initial design study using ring and stringer stiffened aluminum cylinders. This study indicated reasons for pursuing an alternate strategy.

In this chapter is also a discussion on response surfaces and description of the process utilized to develop the response surface model used in this study. While not directly an optimization technique, response surfaces are often used to model systems in which a governing relationship remains unknown. In this study, response surfaces are used to replace the comparatively computationally expensive STAGS analysis with an inexpensive approximating polynomial.

3.1—Sequential Linear Programming

The optimization strategy initially investigated for use in this project is sequential linear programming (SLP). Given an optimization problem (design variables, objective function, constraints), the algorithm searches the design space for the optimum design by performing mini-optimizations on linear approximations to the problem. Consider the following problem formulation.

Minimize $\quad f(\tilde{x}),\ \tilde{x} = \{x_i\},\ i = 1, \quad , n$

subject to $\quad g_j(\tilde{x}) \geq 0,\ j = 1, \quad , n_g$

At an initial design point, $\tilde{x}_0$, Taylor series expansions are calculated, and the following linear optimization problem is formed.

Minimize $\quad f(\tilde{x}_0) + \sum_{i=1}^{n} (x_i - x_{0i}) \left(\frac{\partial f}{\partial x_i} \right)_{x_0}$

subject to

$$g_j\left(\tilde{x}_0\right) + \sum_{i=1}^{n}\left(x_i - x_{0i}\right)\left(\frac{\partial g_j}{\partial x_i}\right)_{x_0} \geq 0,$$

$$j = 1, \quad , n_g$$

Upon solving this linearized optimization problem, a new design point is found. Using this new point as $\tilde{x}_0$, the process of linearization and optimization is repeated until no further improvement in the objective function is made. A further description of the SLP algorithm is found in Haftka and Gurdal [12].

The SLP optimization strategy offers some significant benefits. Of primary benefit is the algorithm's ability to handle constrained optimization problems. This allows it to be applied directly to practical optimization problems, without the use of a penalty function for infeasible designs [12]. In addition, the optimization process of solving the linear programming problem is comparatively simple. In fact, a number of software packages already exist for solving such a linear problem. The package used in the investigated formulation is the ConstrainedMin function contained in Mathematica® [17].

On the other hand, there are some drawbacks to the SLP algorithm which require attention on the part of the user to ensure success in the solution of the optimization problem. Since SLP is a gradient based search algorithm, it is best suited to problems involving continuous design variables. Problems with discrete design variables are not well suited to SLP. The discrete design variables in composite laminate design optimization pose such difficulties.

The use of an initial design point in the SLP strategy adds additional difficulty for the user. Since the algorithm begins from an initial point, it proceeds to search the design space from this point. Selection of the initial point to close to a local minimum in the design space can cause the algorithm to get caught in that local minimum. To avoid this, it is often necessary to make a number of optimization runs from different initial points to ensure that a global minimum has been found.

In addition, the design point is required to be feasible (satisfy all constraints), or nearly feasible. If the initial design is not in the feasible range of the design space, the resulting linear

programming problem will likely have no solution, and the algorithm will crash. Subsequent designs must also remain within the feasible range for the same reason. Often, the solution of the linear programming problem will move the design point outside of the feasible range. For this reason, additional constraints called move limits are implemented. These move limits constrain how far the solution to the linear programming problem can move from the initial design point, usually keeping the design point within the feasible range. However, the use of move limits also tends to increase the number of iterations required to converge to the optimum. This increases the computational cost of the optimization process.

The major hindrance to the use of the SLP strategy is the high degree of calculation required for its use. Each linearization and linear programming cycle requires evaluation of the objective function at the initial point, calculation of the gradient of the objective function at the initial point, evaluation of each constraint at the initial point and calculation of the gradient of each constraint at the initial point. While this is an extremely simple calculation to make if closed form, symbolic expressions are known for the objective function and constraints, the situation becomes rapidly more complex for other problems.

A series of optimization runs were made using SLP. An initial design was determined and then subsequent alternatives were designed. Each design was optimized using the optimization tool to determine the minimum weight structure. The initial cylinder design was based on a stiffened aluminum shell used in experiments by Davis and Carder at the NASA Langley Research Center to determine the buckling loads of an aluminum shell with cutouts [18]. Subsequent designs, which varied the number of stiffeners (both rings and stringers) were then optimized in a similar process. In this manner, a relationship between the number of stiffeners and the minimum weight structure could be determined.

The initial design, shown in Figures 6 and 7, is a simplified version of the cylinder tested in Davis and Carder. The Davis and Carder geometry is an aluminum stiffened cylinder with 126 stringers and 22 rings. The models in this study use the same length, radius, and skin thickness of the Davis and Carder cylinder (94.125 in., 60.33 in., and 0.10 in., respectively), but has a much more simplified stiffener structure, with only 4 rings and 20 stringers.

A STAGS model of the initial cylinder design was created to determine the buckling load of the shell under an axial compression load. A linear bifurcation analysis was performed, calculating the first four buckling modes.

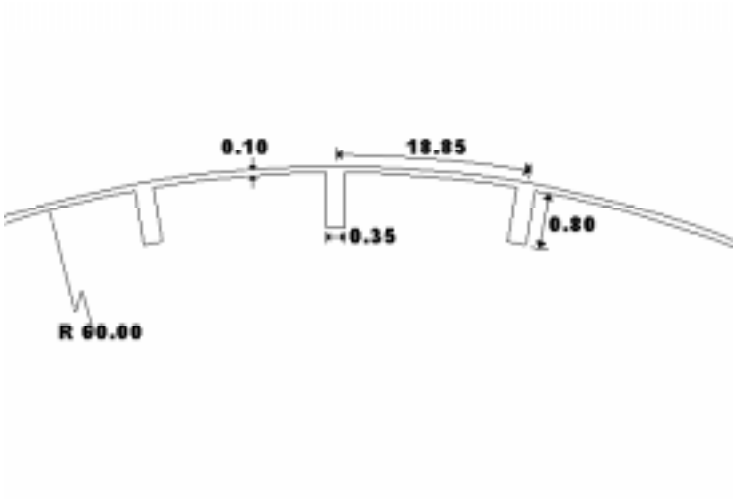

Figure 6 Initial model stringer details

The information learned from the initial model analysis was then incorporated in to the optimization process for nine subsequent cylinder designs. Using the buckling load determined by the initial analysis, a constraint was placed on each of the new designs.

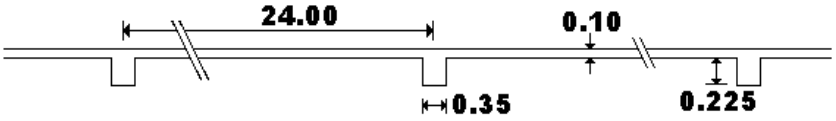

Figure 7 Initial model ring details

The scope of this design study was limited to five design variables. The five design variables used for this study were the skin thickness of the cylinder and the dimensions of the blade stiffeners (ring height and width and stringer height and width). Constraints were placed on

the range of feasible values for each of these design variables, in order to produce realistic designs, and the buckling load of the cylinder.

Together with objective function, the linear constraints on the design variable values and the non-linear constraint placed on the buckling load, the optimization problem can be formulated. This formulation is shown in Table 2.

Table 2 SLP problem formulation

Minimize:	The weight of the stiffened cylinder.
Subject to:	Buckling load 1500 pounds
	0.10 in Ring height 5.0 in
	0.10 in Ring width 5.0 in
	0.10 in Stringer height 5.0 in
	0.10 in Stringer width 5.0 in
	0.10 in Skin thickness 5.0 in

New designs were derived from the initial design of the stiffened cylinder. These designs differ from both the initial design analyzed and the design of the Davis/Carder cylinder in the number of stiffeners used. Figure 8 shows the various stiffener geometries of the new models.

The optimization tool utilized for the optimization runs is a combination of the STAGS finite element analysis package and an optimization algorithm programmed in Mathematica®. The Mathematica® algorithm is the dominant process, performing the optimization iterations and generating new designs as required by the optimization. A slightly modified version of STAGS is called by Mathematica® for the required analysis steps.

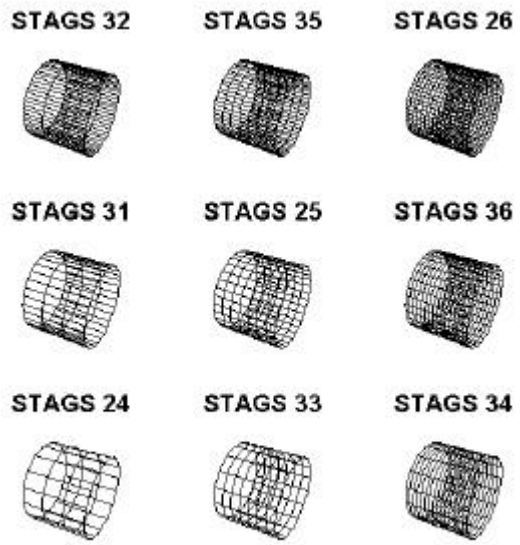

Figure 8 Frame Geometries

The majority of the formulation for the problem is programmed in Mathematica®. A symbolic expression can be derived for the weight of the cylinder, given the fixed values of length, outer radius, number of rings, and number of stringers, and the values of the design variables. Symbolic expressions are also constructed for each of the constraints on the range of values for the skin thickness and stiffener dimensions. The use of symbolic expressions allows efficient gradient calculation within Mathematica®.

The remaining constraint, on the buckling load of the cylinder, is not only programmed in Mathematica®, but also requires the use of the STAGS analysis package. A number of Mathematica® routines were programmed in a Mathematica® package called MathSTAGS. These routines are responsible, given the values of the design variables, for constructing the STAGS input files (casename.inp and casename.bin), moving the files to the computer STAGS is being executed on (if necessary), executing the modified STAGS analysis, and reading the results back into Mathematica® for use by the optimization routine.

The modifications made to STAGS are minimal. A single subroutine, zbuck.f, was modified to export the bifurcation buckling eigenvalues to an external file, buckling.DAT. The

modified subroutine is in Appendix A. The buckling.DAT file is then read by a MathSTAGS routine to import the data into the Mathematica® optimization package.

For the optimization strategy used in this design study, a flexible linearization program was required. Non-linear expressions coded in Mathematica® and those that were not coded in Mathematica® required a linear approximation. A linear approximation was not required for the linear constraints, but was for the objective function and the non-linear STAGS constraint. A Mathematica® program, Linearize, was developed to accomplish this task. Linearize takes as arguments the symbolic expressions for the constraint or objective function and the value of the design point about which the approximation is being made. For the calculation of the first order Taylor series approximation, a gradient calculation is required. An option is included in the Linearize program which instructs Mathematica® to either calculate a symbolic gradient of the expression or use a gradient calculation supplied to it as an argument. The gradient supplied is function which takes the given design point and calculates the numeric gradient vector. This gradient function can either be a symbolic function programmed in Mathematica® or a combination of Mathematica® functions and external applications.

The ability of the linearization module to accept external gradient calculations is necessary for the use of the optimization algorithm with STAGS. Since STAGS is a finite element code, it is impossible to form a symbolic expression for its gradient. To calculate the gradient of the buckling load of the structures being analyzed, it is necessary to perform finite difference derivative calculations. An initial STAGS run is performed, with all design variables set to the values of the design point. Subsequent STAGS runs are then performed, with each design variable perturbed by a small amount. For n design variables, this gradient calculation requires n + 1 STAGS runs.

Each of the SLP runs was allowed to progress for 100 cycles. After evaluation of the data, it was found that most of the runs had converged to an optimum after approximately 40 cycles. For forty cycles, approximately 280 STAGS analyses were required. For some of the more complex models, more than three minutes of computer processor was required to evaluate a

single model. Therefore, at a minimum, over 800 minutes of processor time was required to complete a single SLP run.

At the conclusion of the design study in aluminum cylinders, the problems with implementing SLP were apparent. Utilizing a gradient based optimization algorithm and direct STAGS analysis would be prohibitively expensive. The extremely high computational cost of a single optimization run was too high to make a useful design tool. The multiple optimization runs from independent initial design points would require excessive computer time. In addition, the automated execution of the STAGS program did not allow the user to examine the results of the STAGS analysis before the algorithm could continue. Occasional failures of the STAGS analysis were observed, likely due to busy computer systems; this represents a significant problem. Alternate strategies for reducing the computational cost of the optimization and for allowing the user access to the analysis data were subsequently investigated.

3.2—Response Surface Models

The use of response surface models offered solutions to the challenges made apparent by the implementation of SLP. Historically, response surface models have been used by scientists to fit mathematical models to experimental data when the actual mathematical relationship was unknown. In the field of optimization, the use of response surface models has been expanded. Response surfaces can be used to replace complex function analyses with simple, less expensive mathematical relationships. In terms of this study, a response surface model polynomial is used in place of a computationally costly finite element analysis.

The response surface is created by fitting a polynomial to a set of data. Data from a number of different designs throughout the design space are calculated. From this data, using a least squares fit, constants for a polynomial of a given degree are then calculated. This polynomial now represents a local approximation to the actual system being modeled. Since the data is generated before an optimization run, the user has an opportunity to review it. It would be possible at this stage for the user to find and eliminate problems that occurred during the execution of STAGS.

The area of the design space the response surface represents accurately depends on the selection of the data used to generate the polynomial. For small regions of a design space, a low order response surface can be used. To model a larger region of the design space, a higher order model may be required.

The amount of data required to generate the polynomial depends on the number of design variables and the order of the model to be generated. Equation 70 gives the formula for the number of terms in the response surface model.

$$N_{term} = \left(\frac{n_{vars} + n_{order}}{n_{order}} \right) \left(\frac{n_{vars} + \left(n_{order} - 1 \right)}{\left(n_{order} - 1 \right)} \right) \left(\frac{n_{vars} + \left(n_{order} - 2 \right)}{\left(n_{order} - 2 \right)} \right) \quad \left(\frac{n_{vars} + 1}{1} \right) \qquad \{70\}$$

Given exactly N_{term} data points would give a response surface model which fits the supplied data exactly (N_{term} equations and N_{term} unknowns). Such a model would be adequate if it was known that the polynomial being fitted to the data would represent the system exactly. Since this is highly unlikely, it is desirable to over specify the system of equations, and perform a least squares fit to the data.

The response surface approach offers some distinct advantages over the direct optimization approach. First comes in terms of the computational cost of optimization. Consider the previously discussed cylinder optimization problem. For the five design variable problem, upwards of 240 finite element runs may be required for a single optimization problem run. If a response surface was used to model the buckling load of the cylinder, as opposed to direct use of the finite element code, no finite element analyses would be required during the optimization process itself. Function evaluations and gradient calculations could all be made using the polynomial expression, reducing computational cost. While a large number of finite element analyses may be required to generate the response surface data initially, the polynomial can be used for multiple optimization runs without great computational expense.

On the other hand, there are some drawbacks to using response surface models. Response surfaces are approximate methods. Unless the physical system being modeled is governed by a polynomial expression, the response surface will contain inherent errors. Response surfaces are used to fit a simple function (i.e., a polynomial) to a more complex function (in this case, a finite

element analysis). Therefore, a response surface model will never give the exact same result as the actual system. In addition, the response surface model will only be valid over a limited range of data. Consider the following system, governed by Equation 71 and plotted in Figure 9.

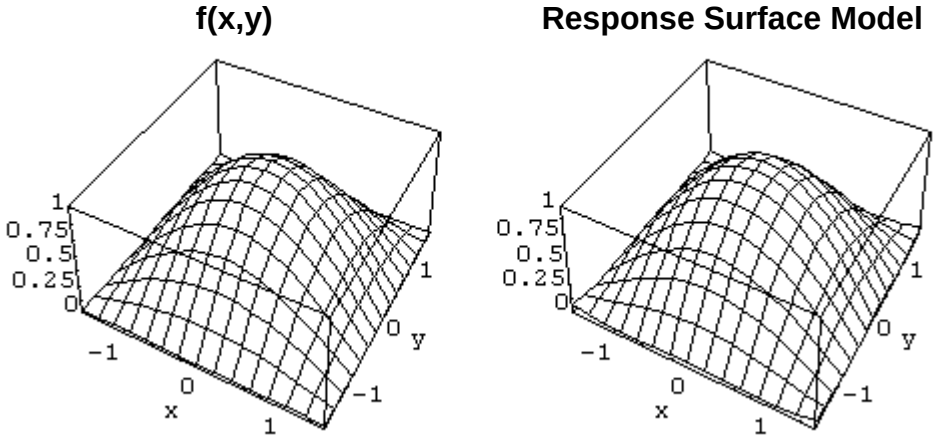

Figure 9 Function and response surface comparison in valid region

$$f(x,y) = Cos(x)Cos(y) \qquad \{71\}$$

This system can be approximated by the following fourth order polynomial in x and y, also plotted in Figure 9.

$$RSM = c_0 + c_1x + c_2y + c_{11}x^2 + c_{12}xy + c_{22}y^2 + c_{111}x^3 + c_{122}xy^2 + c_{112}x^2y + c_{222}y^3 + c_{1111}x^4 + c_{1112}x^3y + c_{1122}x^2y^2 + c_{1222}xy^3 + c_{2222}y^4 \qquad \{72\}$$

This polynomial very accurately models the system in the range of $-\frac{\pi}{2} \le x \le \frac{\pi}{2}$ and $-\frac{\pi}{2} \le y \le \frac{\pi}{2}$. However, outside of this range, the functions are very different (Figure 10).

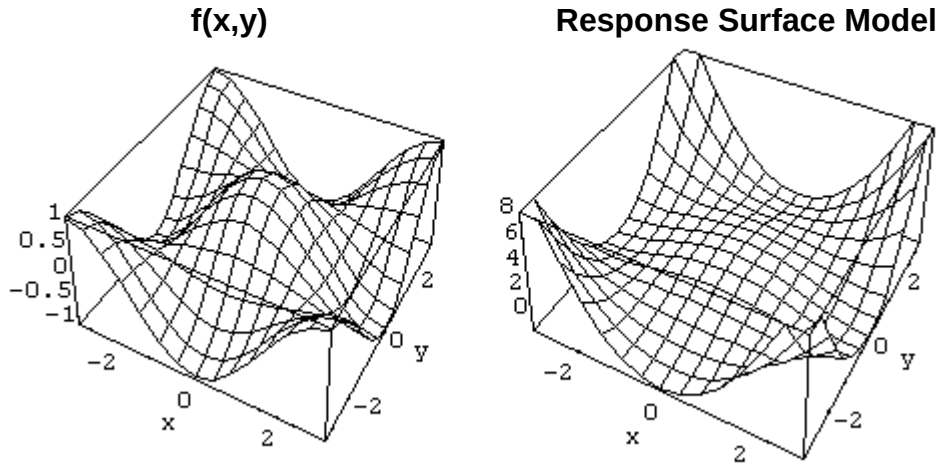

Figure 10 Function and response surface comparison over larger than valid region

Care must be taken when using a response surface model to ensure that the portion of the model being used is within the valid region of the model. It is possible, even likely, for an optimization strategy to direct the design point outside of the valid region of the response surface. In that case, the significant errors of the response surface may give an infeasible design that appears very good.

3.2.1—Response surface model development

The response surface models the buckling load of the composite cylinder in terms of the cylinder wall thickness, *h*, the two in-plane stiffness parameters V_1^* and V_3^*, and the two bending stiffness parameters W_1^* and W_3^*. The response surface is then incorporated into the genetic algorithm analysis to evaluate the imposed buckling load constraint.

The first step in the development of the response surface model is the construction of the design variable data set. Three possible methods existed for selecting the designs which would be used to calculate the response surface model. The first, and theoretically more desirable option, was to calculate the set of designs according to the |X'X| criterion [19]. The second option would be to use a factorial or lattice design, which filled the design space, according to a regular

grid. The third method would be to develop a distribution of designs to randomly fill the design space. Ultimately, this was the method that was chosen.

The |X'X| criterion attempts to maximize the value of |X'X|, where X is the least squares matrix. For a five variable, sixth order polynomial, the least squares matrix is 462x924. Each term in the matrix is a variable in the maximization problem. While it is possible to maximize this criterion without too much difficulty for smaller problems, the size of this problem made utilization of this method impossible due to computational limitations.

The factorial design was not utilized due to the difficulty in determining a set of designs which was independent of the polynomial being fit to the data. A rectangular grid was not used because of the bounding parabola on the V_1^*-V_3^* and W_1^*-W_3^* data and projecting a grid onto the parabolic space resulted in data which was not independent of the polynomial. Therefore, a random selection of the design points was used.

A set of 2000 design points was developed randomly and subsequent STAGS analyses were performed. A distribution of the $\left(V_1^*, V_3^*\right)$ and $\left(W_1^*, W_3^*\right)$ data is shown in Figures 11 and 12. Buckling load information was collected from the analyses, and third, fourth, fifth and sixth order polynomials in h, V_1^*, V_3^*, W_1^*, and W_3^* were then fit to the data using a linear regression analysis. Each regression used a number of data points equal to double the number of terms in each polynomial. The resulting response surface models are given by:

$$\lambda_{RSM} = c_0 + c_1 h + c_2 V_1^* + c_3 V_3^* + etc. \qquad \{73\}$$

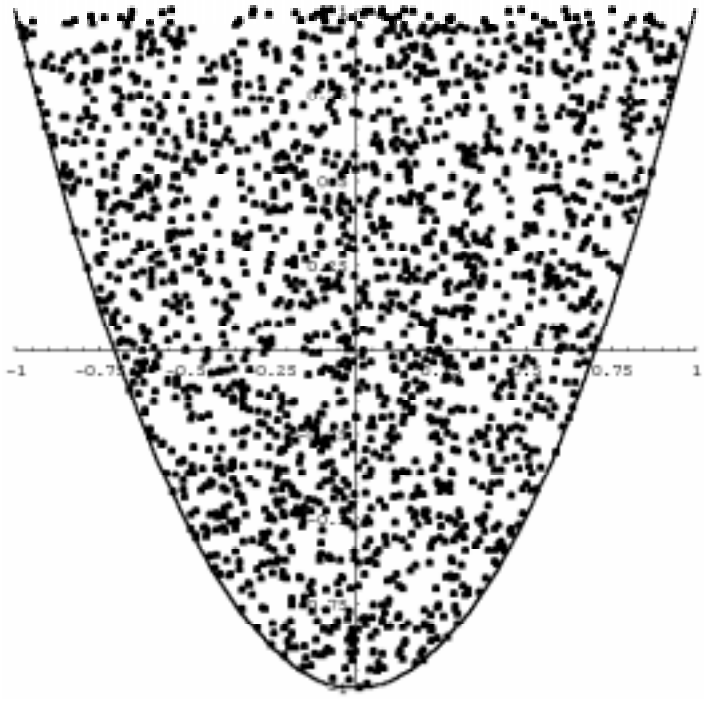

Figure 11 (V_1^*, V_3^*) Distribution

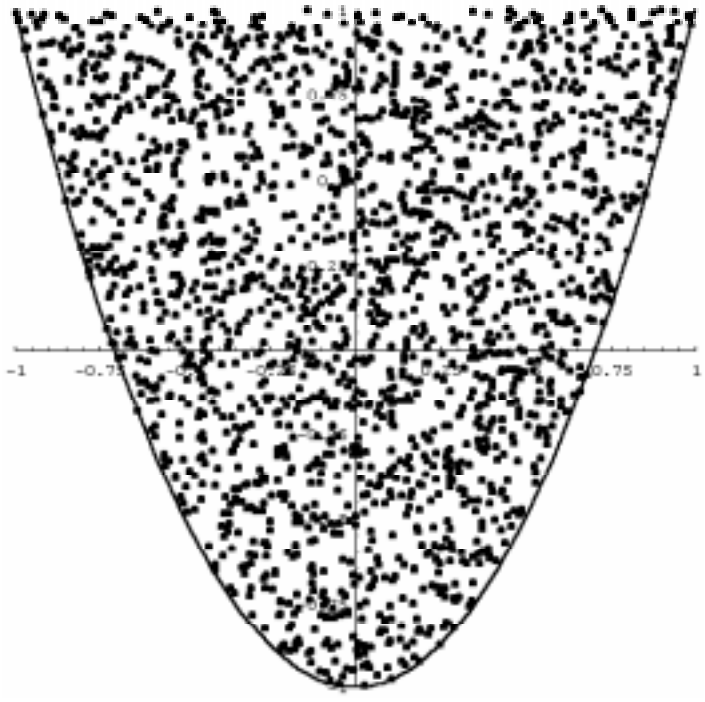

Figure 12 (W_1^*, W_3^*) Distribution

Table 3 details the statistical information of the least squares fit to each polynomial. The sixth order polynomial was chosen due to its greater degree of accuracy (particularly its better estimated variance) when compared to the other three response surface models. Computational limitations prevented higher order polynomials from being explored.

Table 3 RSM Linear Regression Data

Order	Number of Terms	Number of Data Points	R Squared Value	Adjusted R Squared Value	Estimated Variance ($x10^6$)
3	56	112	0.994151	0.988407	5.77815
4	126	252	0.996947	0.993919	3.21904
5	252	504	0.998026	0.996060	1.99156
6	462	924	0.99873	0.997463	1.32713

Response surface model use eliminated the two most significant problems with the implementation of the SLP algorithm. Execution of the response surface was extremely inexpensive, requiring only a simple set of calculations. It also provided the opportunity for the user to examine the data before fitting the polynomial. Any problems that are found in the data can be resolved before fitting the surface and beginning an expensive optimization run.

3.3 Genetic Algorithms

Now that an inexpensive response surface had been developed to replace the direct STAGS analyses, optimization studies could begin. However, the extremely reduced computational cost of the response surface no longer made the SLP algorithm the best choice. With computational expense no longer an issue, the drawbacks of gradient based search algorithms were more important than their benefits. The sixth order response surface presents a design space which likely has a number of local minima. In addition, the need to optimize with respect to discrete design variables make gradient based algorithms less desirable. Thus, an investigation into the use of genetic algorithms was begun.

Genetic algorithms (GAs) are optimization algorithms which search the design space using the principles of evolution. A design's success or failure is determined by its fitness. Survival of the fittest ultimately allows the algorithm to converge to an optimum design.

GAs are have significant advantages and disadvantages. Their ability to search an entire design space gives them the ability to handle optimization problems with highly non-linear objective functions with many local minima. In addition, since they are not gradient based algorithms, they are ideally suited to optimization problems which utilize discrete design variables, such as the optimization of composite laminate stacking sequence. Soremekun utilized GAs in his study of composite laminate design [20]. The GA code used in this study was written by Soremekun for that study. On the other hand, genetic algorithms can be extremely expensive. Each member of a population of designs requires an evaluation of the fitness function. Tens of thousands of fitness function evaluations may be required over the course of a single GA run. Only computationally inexpensive problems are well suited to GA use.

GAs utilize a string of numeric values, which are analogous to the biological chromosome, to describe a potential design in terms of its design variables. These numeric values may be the values of the design variables themselves or the chromosome may require decoding to arrive at the design variables. Table 4 shows examples of GA chromosomes and their decoding.

Table 4 Chromosome Encoding

Chromosome	Alphabet Encoding Type	Decoded Chromosome
{1,0,1,1,0,1,0}	Binary encoding	180
{1,1,2,1,3}	$1 = [0^o]_2$, $2 = [+45^o/-45^o]$, $3 = [90^o]_2$	$[0^o/0^o/0^o/0^o/+45^o/-45^o/0^o/0^o/90^o/90^o]_s$
{10,24,17}	Direct	{10,24,17}

Figure 13 shows a schematic of a typical GA. To begin a GA run, an initial population of designs is randomly determined. This initial population is then decoded, and the fitness of the design can be determined by evaluating the value of the fitness function for the design. Often, this fitness function incorporates the constraints required by the optimization problem in the form of penalty terms. These penalty terms penalize the value of the fitness function for violation of

constraints. For a structural weight minimization problem, the fitness function might include a penalty term which added "weight" to the structure for violating an imposed stiffness or load requirement.

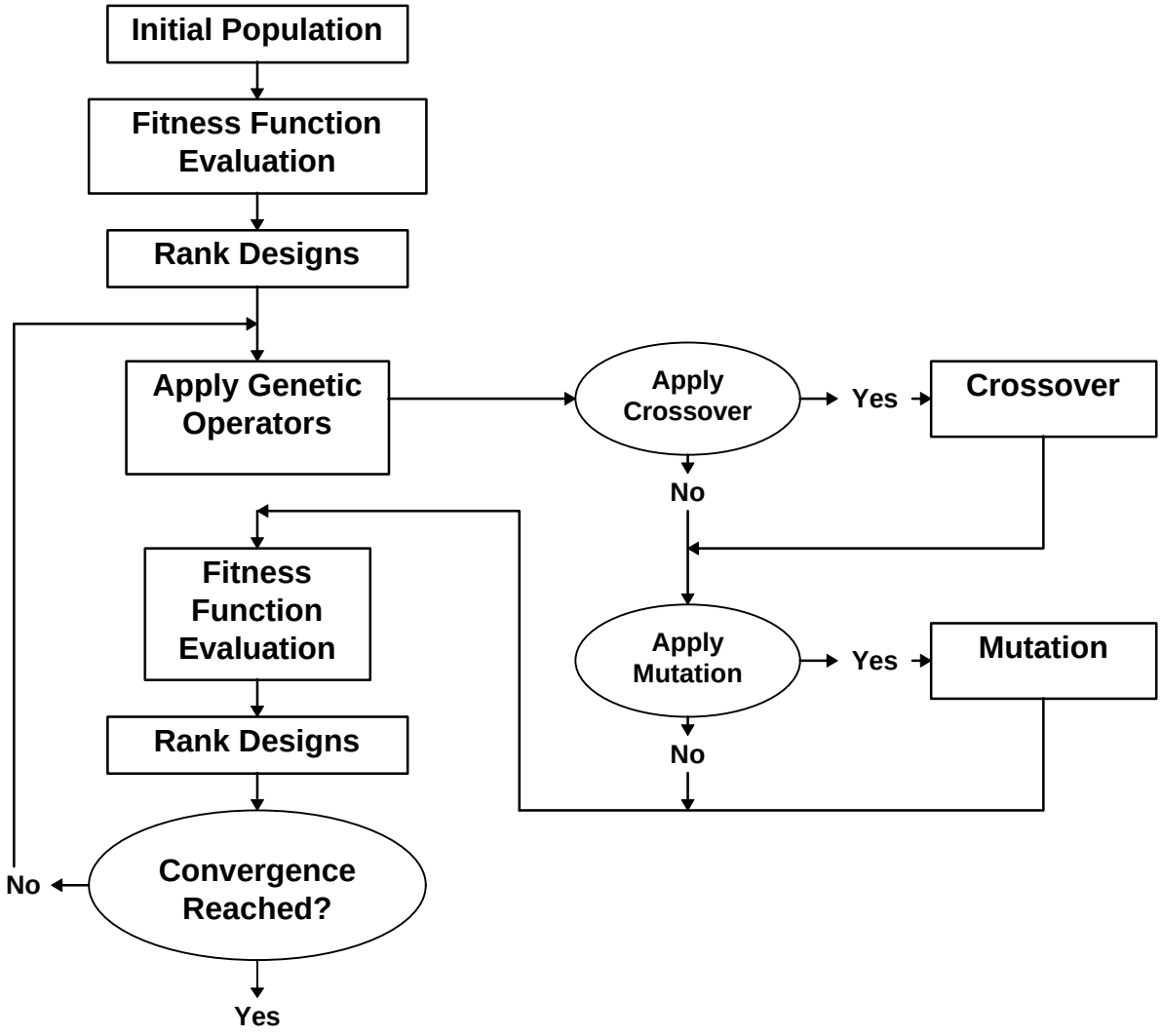

Figure 13 Genetic Algorithm Schematic

After the fitness of each design is determined, the designs are ranked and selected for mating according to this fitness value. A "roulette wheel" is used to select parent designs for

mating. Designs which have the best values of the fitness function are more likely to be selected than designs with poor fitnesses.

A series of genetic operators is performed on two selected designs to arrive at two new (child) designs. The two most common genetic operators are crossover and mutation. Crossover works by splitting the two design chromosomes at a randomly determined point and switching portions of the chromosome. Mutation randomly selects a gene in the chromosome and randomly changes it to another value. Tables 5 and 6 show examples of these genetic operators.

Table 5 Example of Crossover

Genetic Operator	Parent Chromosome	Child Chromosome
Crossover	*{1,0,0,**1,1,0,1,0**}* {1,0,1,**0,1,1,0,1**}	*{1,0,0,**0,1,1,0,1**}* {1,0,1,***1,1,0,1,0***}

Table 6 Example of Mutation

Genetic Operator	Initial Chromosome	Final Chromosome
Mutation	{1,0,1,0,1,**1**,0,1}	{1,0,1,0,1,**0**,0,1}

Whether or not a given genetic operator is performed on a chromosome is determined by user defined probabilities. Typically, crossover is performed all of the time (>90% probability). Mutation is often set to occur very rarely (<10% probability). Selection and genetic operations are performed until a new generation has been filled.

After an entire child generation has been determined, the process of fitness function evaluation, ranking, selection, and mating repeats until convergence is reached. Often, an elitist scheme is used, which incorporates the top design, or a number of the top designs, from the parent generation into the child generation. This ensures that the information contained in the best design of one generation is not lost to the next. Convergence is reached when the fitness function of the best design no longer improves. A variety of convergence criteria can be used, but a typical criteria is to set the number of generations which must pass without improvement in the fitness function.

Chapter 4—Model Description

4.1—Physical Model

The physical structure modeled in this work is a monocoque, fiber reinforced composite cylinder, shown in Figure 14. It's dimensions are approximately those of a narrow body fuselage aircraft. The radius of the cylinder is 74.5 inches, with a length of 60 inches. The thickness of the cylinder wall is treated as a design variable.

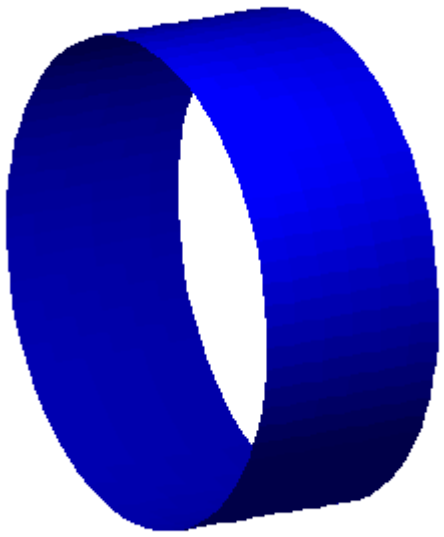

Figure 14 Cylinder model

The dimensions of this model correspond to the portion of a narrow body fuselage aircraft which surrounds a window cutout. In a current, conventional aluminum aircraft, there would be four ring stiffeners, spaced 20 inches apart, and 50 longitudinal stringers spaced evenly around the circumference. While the dimensions are similar, for this design study, a monocoque composite cylinder is modeled. Future investigations in this topic could be expanded to include stiffening structures and cutouts.

4.2—Finite Element Model

Analyses performed in this design study utilized a finite element model of the cylinder. The model was developed in STAGS, using the 410 element. A typical finite element mesh is shown in Figure 15. The global x coordinate is directed along the axis of the shell, while the global y coordinate is directed circumferencialy and the global z direction is taken to be the outward normal of the shell surface. There are 5 elements in the axial direction and 39 around the circumference. Reasons for choosing the particular mesh used in this study will be described later in the discussion on convergence study.

A linear buckling analysis was performed on the model to calculate the minimum buckling load of the structure. Studies by Palazotto indicate that the linear calculations will provide results that are significantly greater than observed collapse loads, but are still useful for design work and relative comparison [21].

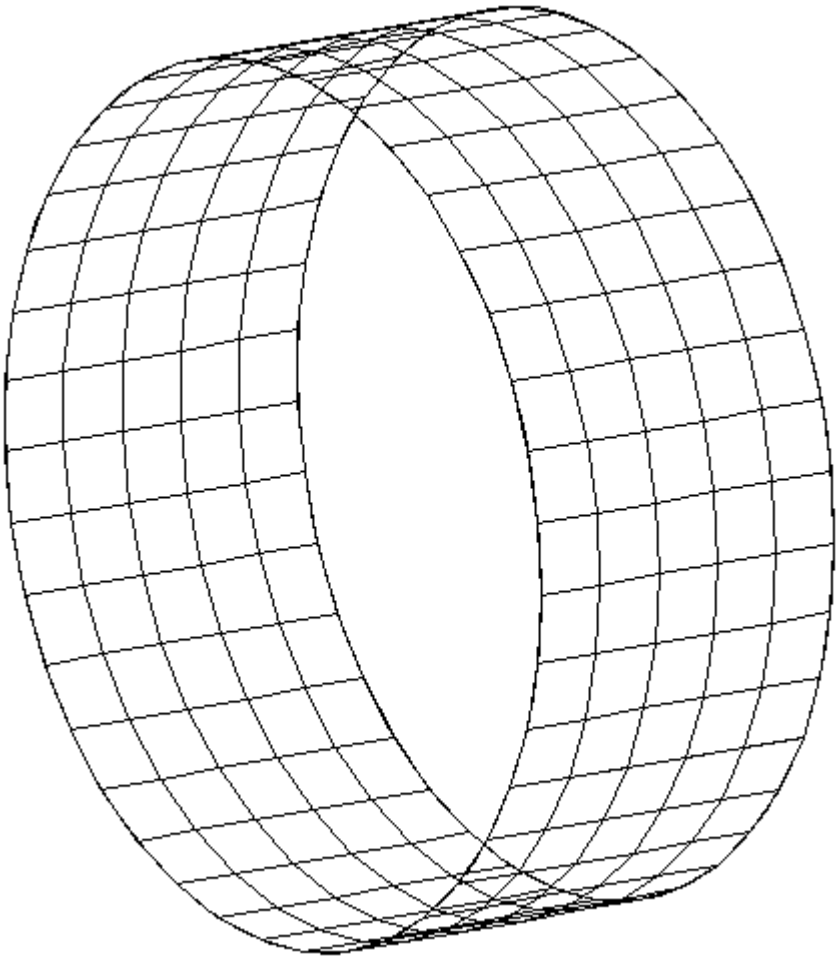

Figure 15 Undeformed mesh

4.3—Design Variables

The finite element model is described via an input deck of various parameters. Utilizing the Mathematica® programming environment, a function was written which could construct the input deck from the design variables used in the study. This allowed the automated construction of the required finite element models, and subsequently, the automated execution of the STAGS analysis.

A group of five design variables was used in this study. They are outlined in Table 7.

Table 7 Design Variable Descriptions

Design Variables	Description
h	Shell wall thickness
V_1^*	In-plane stiffness parameter
V_3^*	In-plane stiffness parameter
W_1^*	Bending stiffness parameter
W_3^*	Bending stiffness parameter

4.4—Material Properties

The material properties used throughout this study are shown in Table 8. These properties are for a T300/5208 graphite-epoxy material system.

Table 8 Material Properties (Graphite-Epoxy)

Property	Value
E_1	$26.25 \cdot 10^6$ lbs/in^2
E_2	$1.49 \cdot 10^6$ lbs/in^2
G_{12}	$1.04 \cdot 10^6$ lbs/in^2
ν_{12}	0.28
ρ	0.074 lbs/in^3

The invariant U terms for this material are given by:

Table 9 Invariant Properties (Graphite-Epoxy)

Invariant Term	Value
U_1	$1.11 \cdot 10^7$
U_2	$1.24 \cdot 10^7$
U_3	$2.86 \cdot 10^6$
U_4	$3.28 \cdot 10^6$
U_5	$3.90 \cdot 10^6$

4.5—Mesh Convergence

A convergence study was performed to determine the appropriate finite element mesh to be used in the linear buckling analysis of the cylinder model. Three meshes were developed, with increasing numbers of elements in the axial and circumfrential directions. These are shown in Figure 16.

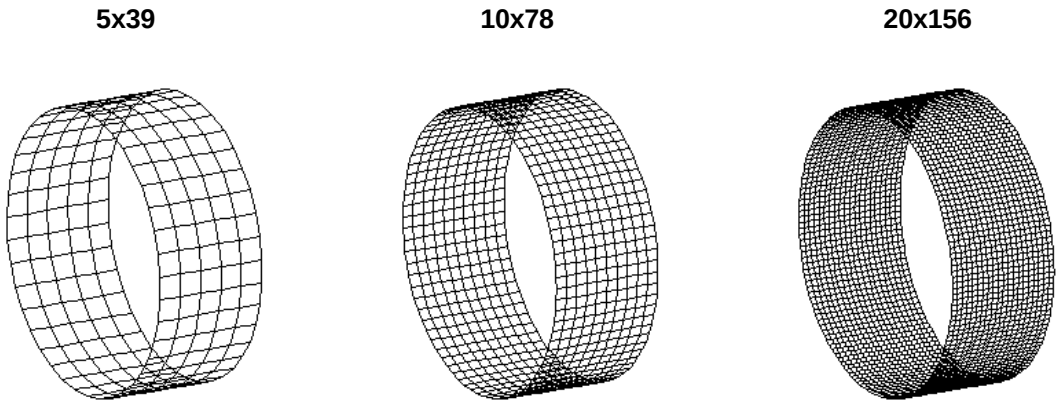

Figure 16 Convergence study meshes

The buckling loads for each of these models is shown in Table 10. There is only a 0.6% difference between the load calculated for mesh 1 (5x39) and mesh 2 (10x78). A smaller difference (0.1%) is observed between mesh 2 and mesh 3(20x156). This indicates that the coarsest mesh is capable of performing the analysis within a reasonable degree of accuracy. The deformed shape of mesh 3 is shown in Figure 17.

Table 10 Convergence study mesh data

Mesh	Number of Elements		Element Dimensions	Buckling Load
	Axial	Circumfrential	(in. x in.)	(lb.)
1	5	39	12 x 12	84900
2	10	78	6 x 6	84400
3	20	156	3 x 3	84300

There is a significant difference in the time required to perform a STAGS analysis of mesh 1 and mesh 3. Mesh 1 requires approximately 18 seconds to complete the analysis, while the refined mesh 3 requires up to 12 minutes, or more. Since a large number of runs were required to collect enough data for the response surface, the time savings observed by using mesh 1 were significant.

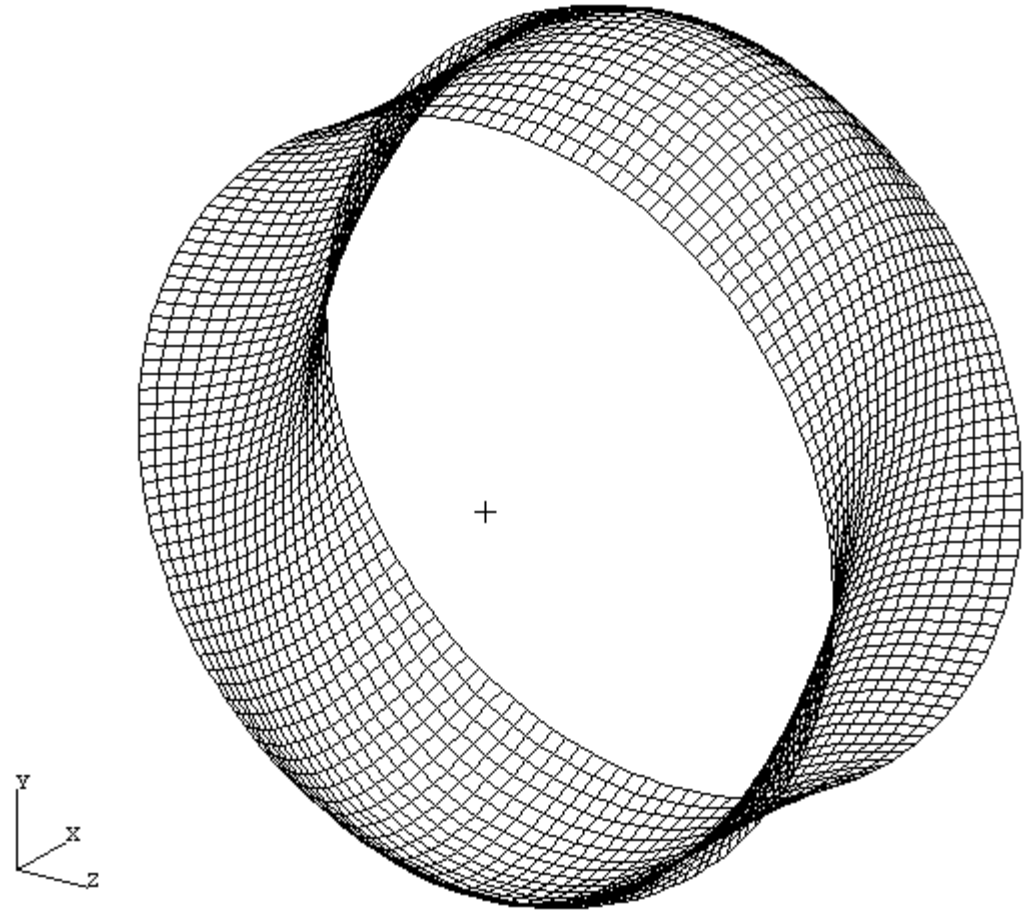

Figure 17 Deformed mesh

Chapter 5—GA Results

Optimization results are presented for 3 different target buckling loads and 4 different optimization variable formulations. The four variable formulations reflect different approaches to the relationship between (V_1^*, V_3^*) and (W_1^*, W_3^*). These approaches are outlined in Table 11. The first approach (Elliptical) limits the values of (W_1^*, W_3^*) to those found on the ellipsoid described in Chapter 2. The second approach (Interior) expands the design space to include the area inside the ellipsoid. Both of these approaches utilize continuous variation in the shell wall thickness (h) and the four stiffness parameters. The final two approaches manipulate the stacking sequence of the composite laminate in an effort to find the best laminate design. In both approaches, the shell wall thickness is a function of the number of layers in the laminate. Only balanced symmetric laminate designs are permitted. The third approach (Stacking) allows continuous variation in the fiber orientation angles, while the fourth approach (Discrete Stacking) limits fiber orientation angles to 0^o, $\pm 30^o$, $\pm 45^o$, $\pm 60^o$, or 90^o. Single layer thickness was assumed to be 0.005". Each approach utilizes a unique GA chromosome formulation.

Table 11 Design Study Approach

Approach	Design Variables	Continuous or Discrete Variation	Imposed Constraints
Elliptical	h, V_1^*, V_3^*, W_1^*, W_3^*	Continuous	(W_1^*, W_3^*) are limited to values on the ellipsoid
Interior	h, V_1^*, V_3^*, W_1^*, W_3^*	Continuous	(W_1^*, W_3^*) are limited to values on or within the ellipsoid
Stacking	Stacking Sequence	Fiber orientation angles are continuous, h is discrete	
Discrete Stacking	Stacking Sequence	Discrete	Fiber orientation angles are limited to 0^o, $\pm 30^o$, $\pm 45^o$, $\pm 60^o$, or 90^o

Three different load cases are optimized. Buckling load targets of 75,000, 100,000, and 125,000 pounds are each utilized. Since the response surface is not expected to give buckling load values which are of acceptable accuracy for the final analysis, and it is likely that the design determined by the optimizer will have a buckling load under the required value, a number of additional cases are run with inflated buckling load constraints. These load cases are outlined in Table 12. To verify that the optimized design has an acceptable buckling load, a final STAGS analysis of the optimized design is performed.

Table 12 Buckling load targets and constraints

Minimum Buckling Load Target	Case Number	Imposed Buckling Load Constraint
75,000 pounds	1	75,000 pounds
	2	77,500 pounds
	3	80,000 pounds
	4	82,500 pounds
	5	85,000 pounds
100,000 pounds	6	100,000 pounds
	7	102,500 pounds
	8	105,000 pounds
	9	107,500 pounds
	10	110,000 pounds
125,000 pounds	11	125,000 pounds
	12	127,500 pounds
	13	130,000 pounds
	14	132,500 pounds
	15	135,000 pounds

Upon completion of the response surface model, the optimization process is begun. Because there are a number of constraints which must be satisfied while the weight optimization problem is being solved, a number of penalty terms are added to the expression for the weight of the cylinder (equation 74).

$$weight = \rho\left(l\pi\left(r_o^2 - r_i^2\right)\right) \quad \{74\}$$

where:

l = cylinder length = 60.0 inches

$r_o = r + \frac{h}{2}$ = cylinder outer radius

$r_o = r - \frac{h}{2}$ = cylinder inner radius

r = nominal radius = 74.5 inches

The balanced-symmetric requirement is automatically satisfied by the decoding of the GA chromosomes, so it does not require any additional terms. All other constraint penalties are handled by artificially reducing the buckling load calculated by the RSM to a value below the minimum buckling load value. The objective function is then expressed as:

Fitness Function = If $\lambda_{RSM} < \lambda_{\min}$ $\quad -\frac{weight}{weightnorm} + penalty \cdot \frac{\lambda_{\min} - \lambda_{RSM}}{\lambda_{norm}}$

Else $\quad -\frac{weight}{weightnorm} - \frac{\lambda_{RSM} - \lambda_{\min}}{\lambda_{norm}}$

where

weightnorm = the weight of a cylinder for h = 0.050”

penalty = 1000

λ_{norm} = 75,000 pounds

The objective function is negative because the GA used only maximizes its fitness function. The use of this fitness function is intended to give designs which give the maximum buckling load for a given shell wall thickness.

5.1—Elliptical Approach

The elliptical approach uses the stiffness parameters, V_1^*, V_3^*, W_1^*, and W_3^*, and the shell wall thickness, *h*, as design variables. These parameters are coded into a genetic chromosome for GA optimization. While the design variables are considered to be continuous, the nature of the chromosomal formulation limits them to be finitely variable. Table 13 shows an example of the elliptical approach chromosomal formulation. Details of the decoding relationships are given in Appendix B.

Table 13 Elliptical Approach Genetic Formulation

Genetic Alphabet	1-10			
Design Variables	h	t	v1star	w3star
Example Chromosome	6 3	8 1	10 4	6 9
Decoded Chromosome	0.13	0.4	0.86	0.16

Equations 36 and 37 govern the relationship between the W_1^* and W_3^* parameters and the parameter *t*. Given values for V_1^*, V_3^*, and *t*, the values of W_1^* and W_3^* can be determined. The *t* parameter is allowed to vary in the range $-1 \le t \le 1$. For values of *t* in the range $0 < t < 1$, the first parts of equations 36 and 37 are used, while for *t* in the range $-1 < t < 0$, *t* is set equal to *-t* and the second parts of equations 36 and 37 are used. The points represented by *t*=0 and *t*=1 are singular points which satisfy both parts of the equations. This is shown in Figure 18.

The results of the elliptical approach are shown in Tables 14 through 19, and Figures 19 through 21. For each required buckling load, the optimizer, as expected, found a design for which the response surface model predicted a buckling load greater than that required. However, the STAGS analysis of the resulting design was lower for all optimized designs. Such error is expected in the use of a response surface model because the response surface only approximates the physical system being modeled. To account for this error, additional cases were run for each buckling load target.

Table 14 Elliptical Approach Optimization Results
75,000 pound target

Case	Buckling Constraint	λ-RSM (pounds)	λ-STAGS (pounds)	Error (%)	Fitness
1	75000	79131.2	69282.8	-14.2	-0.694
2	77500	79131.2	69282.8	-14.2	-0.694
3	80000	80064.0	78886.0	-1.5	-0.943
4	82500	82600.3	81842.3	-0.9	-1.090
5	85000	85260.2	84705.4	-0.7	-1.236

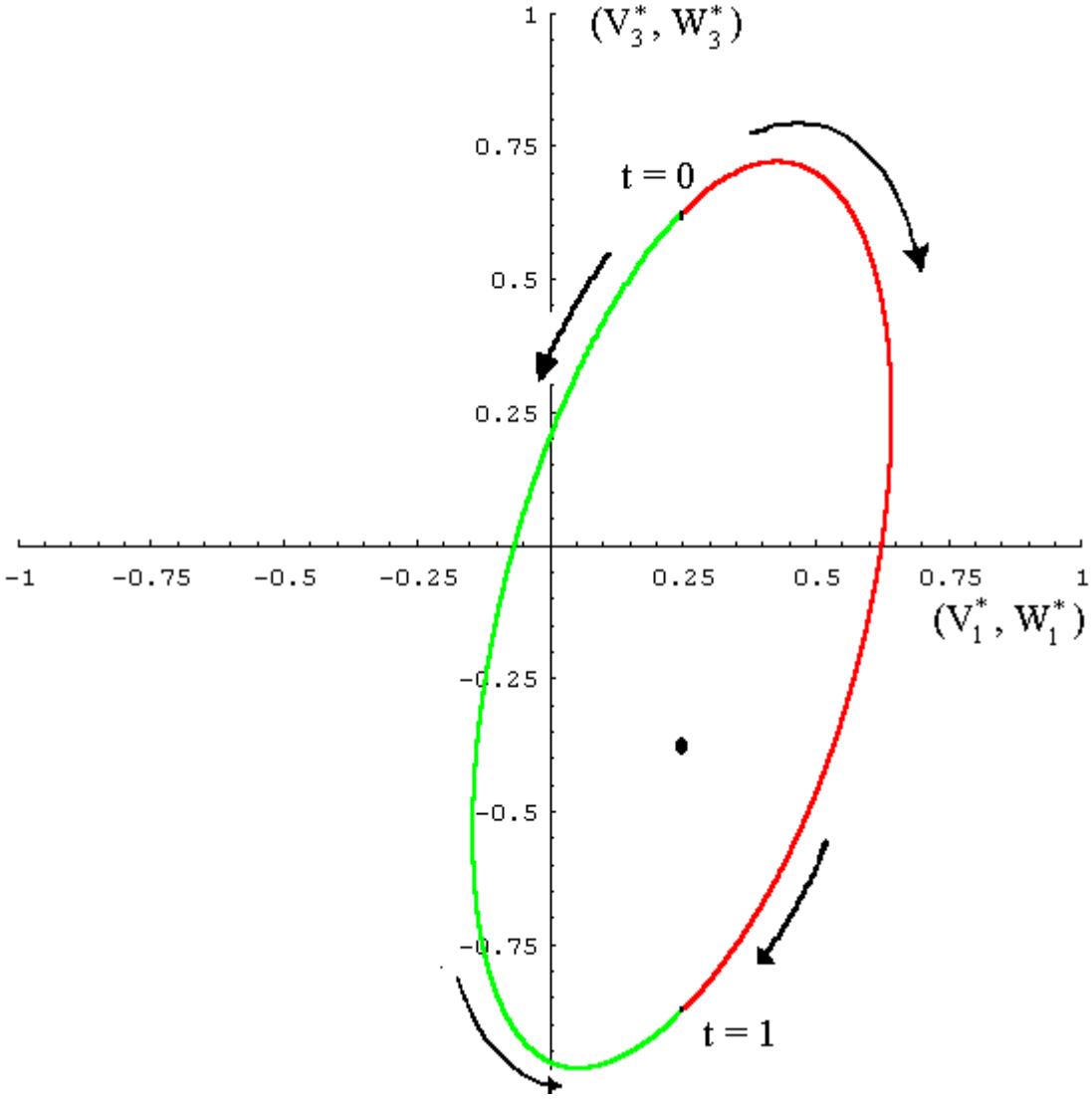

Figure 18 Elliptical Optimization Formulation

Table 15 Elliptical Approach Parameter Results
75,000 pound target

Case	h (in)	t	v1star	v3star	w1star	w3star
1	0.040	0.980	0.900	0.620	0.900	0.620
2	0.040	0.980	0.900	0.620	0.900	0.620
3	0.052	0.540	0.240	0.220	0.781	0.610
4	0.060	0.480	0.200	0.120	0.748	0.621
5	0.068	0.520	0.220	0.160	0.759	0.571

A significant error between the response surface and the STAGS analysis was observed for the cases 1 and 2 of this approach. This is likely due to the fact that the design is close to the edge of the design space, in terms of both its thickness (0.040 inches) and the stiffness parameters (as shown in Figure 19). The edges of the design space are likely areas of inaccuracy for the response surface. The error drops off significantly as the design moves towards those with greater thickness and at the center of the design space.

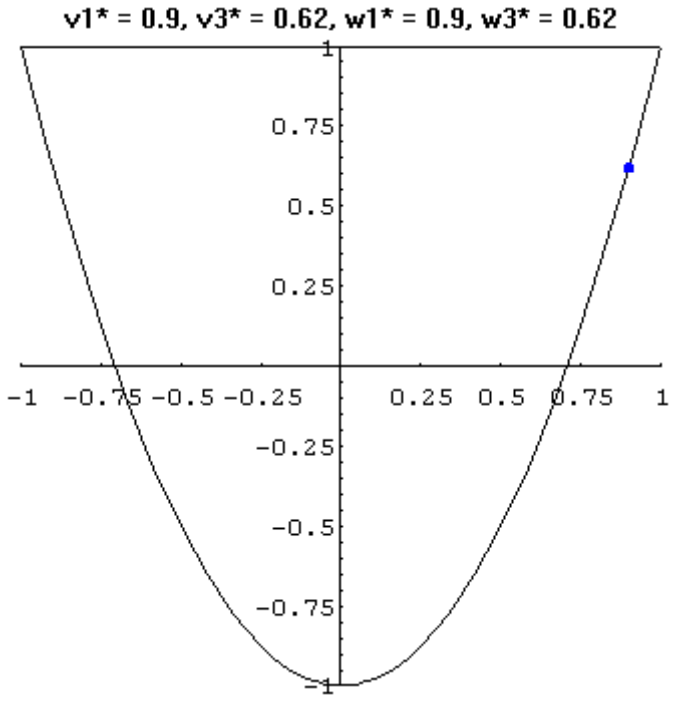

Figure 19 Elliptical approach, Cases 1 and 2

In all results figures, the point in blue indicates the inplane stiffness parameters, while the red point indicates the bending stiffness parameters. The green curve marks the ellipsoidal region for the given inplane stiffness parameters. For the ellipsoidal case, the bending stiffness parameters are constrained to this curve.

The optimizer found identical designs for case 1 and case 2. Having minimized the thickness as much as possible, the optimizer sets out to maximize the buckling load. Since the buckling load for case 1 exceeded the constraint value for case 2, this design satisfied both cases.

The STAGS analysis indicates that the optimized designs found using the 75,000 and 77,500 pound constraint produces a design which does not satisfy the 75,000 pound target. Thus,

further optimization runs with increasingly rigid buckling load constraints were necessary to find an optimum design which met the target load constraint.

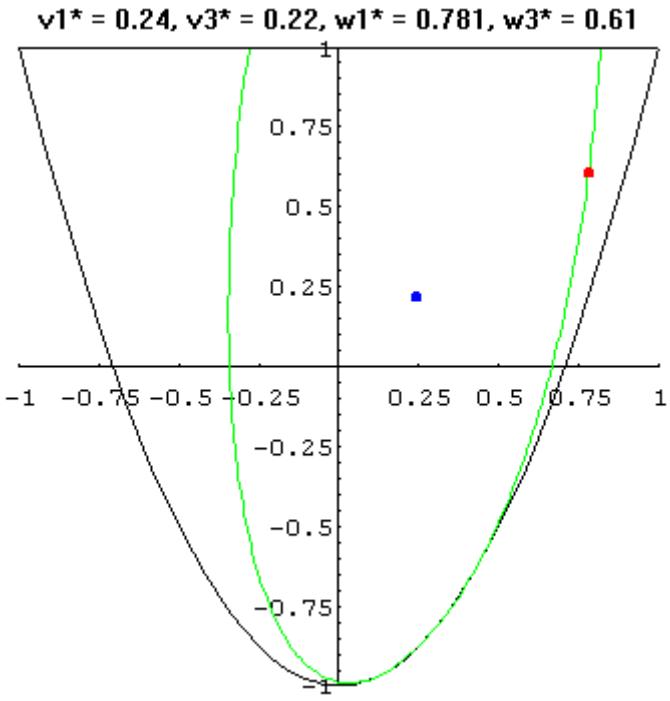

Figure 20 Elliptical approach, Case 3

The optimization produced a satisfactory designs for the 80,000 pound load and greater constraints. Each of these designs have similar parameter values, and vary primarily in the thickness of the shell wall. If further accuracy were desired, further refinement of the buckling load constraint could be done until an optimum design was found in which the STAGS analysis matched the target load or an additional response surface could be constructed which focused in on the region of the design space. By modeling a smaller region of the design space, accuracy of the response surface is likely to increase.

Results for the second target load (100,000 pounds) are shown in Tables 16 and 17 and Figure 21. Unlike the first target load, the designs found by the optimizer are in the more robust area of the response surface. While the first case does not find a satisfactory design, the designs for the second and higher load cases are satisfactory. Only small variations in shell wall thickness and parameter values separate these five designs. Similar observations can be made for the third target load, as seen in Tables 18 and 19 and Figures $$$ through $$$.

Table 16 Elliptical Case Optimization Results
100,000 pound target

Case	Buckling Constraint	λ-RSM (pounds)	λ-STAGS (pounds)	Error (%)	Fitness
6	100000	100937.2	98846.3	-2.1	-2.015
7	102500	103226.3	101608.8	-1.6	-2.112
8	105000	105517.5	103204.5	-2.2	-2.209
9	107500	107821.5	105469.2	-2.2	-2.306
10	110000	110137.7	108248.5	-1.7	-2.403

Table 17 Elliptical Approach Parameter Results
100,000 pound target

Case	h (in)	t	v1star	v3star	w1star	w3star
6	0.107	0.520	-0.080	-0.160	0.396	-0.361
7	0.113	0.520	-0.080	-0.180	0.390	-0.378
8	0.117	0.540	-0.100	-0.180	0.360	-0.458
9	0.122	0.540	-0.120	-0.200	0.332	-0.507
10	0.128	0.540	-0.140	-0.220	0.303	-0.555

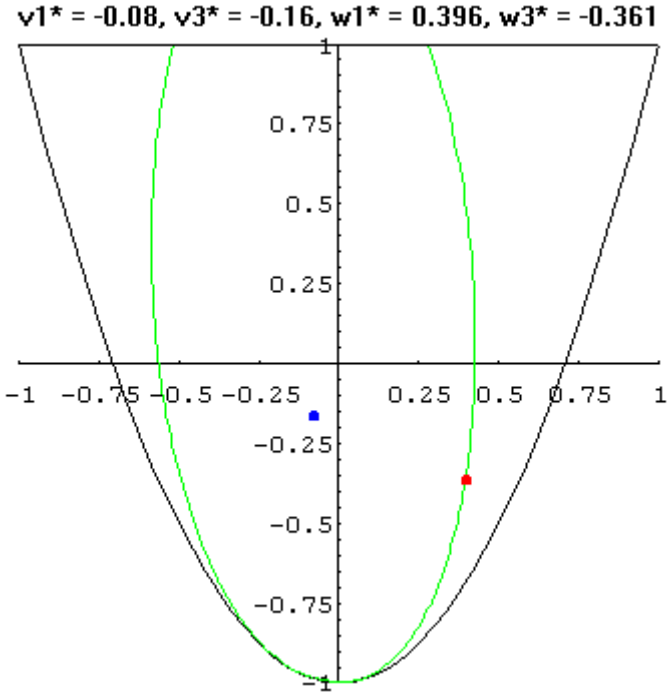

Figure 21 Elliptical approach, Case 6

Table 18 Elliptical Approach Optimization Results
125,000 pound target

Case	Buckling Constraint	λ-RSM (pounds)	λ-STAGS (pounds)	Error (%)	Fitness
11	125000	125237.5	123482.5	-1.4	-3.033
12	127500	127521.4	125947.4	-1.2	-3.130
13	130000	130915.5	128895.6	-1.6	-3.275
14	132500	133148.9	130913.6	-1.7	-3.372
15	135000	135352.8	132849.4	-1.9	-3.470

Table 19 Elliptical Approach Parameter Results
125,000 pound target

Case	h (in)	t	v1star	v3star	w1star	w3star
11	0.160	0.580	-0.220	-0.280	0.171	-0.766
12	0.165	0.580	-0.220	-0.280	0.171	-0.766
13	0.172	0.580	-0.220	-0.300	0.165	-0.776
14	0.177	0.580	-0.220	-0.320	0.158	-0.786
15	0.182	0.600	-0.220	-0.320	0.150	-0.809

Full graphical results for the elliptical approach are shown in Appendix C.

5.2—Interior Approach

For the second approach, the bending stiffness parameters were allowed to vary within the ellipsoid determined by the inplane parameters. This required an additional parameter within the genetic chromosome. Table 20 shows the genetic formulation used. Decoding relationships are given in Appendix B.

Table 20 Interior Approach Genetic Formulation

Genetic Alphabet	1-10				
Design Variables	h	t	tp	v1star	w3star
Example Chromosome	6 3	8 1	1 8	10 4	6 9
Decoded Chromosome	0.13	0.4	0.07	0.86	0.16

The calculation of the W_1^* and W_3^* parameters is similar for this approach as that used in the elliptical approach. However, in order to make the interior of the ellipsoid a feasible region, the use of the t_p parameter was required. Temporary values of W_1^* and W_3^* are calculated as in

the previous formulation. The t_p parameter defines a percentage of the vector equal to $\left(W_1^*, W_3^*\right)$-$\left(V_1^*, V_3^*\right)$. This vector is then added to $\left(V_1^*, V_3^*\right)$ to calculate the new $\left(W_1^*, W_3^*\right)$ values. This is shown in Figure 22.

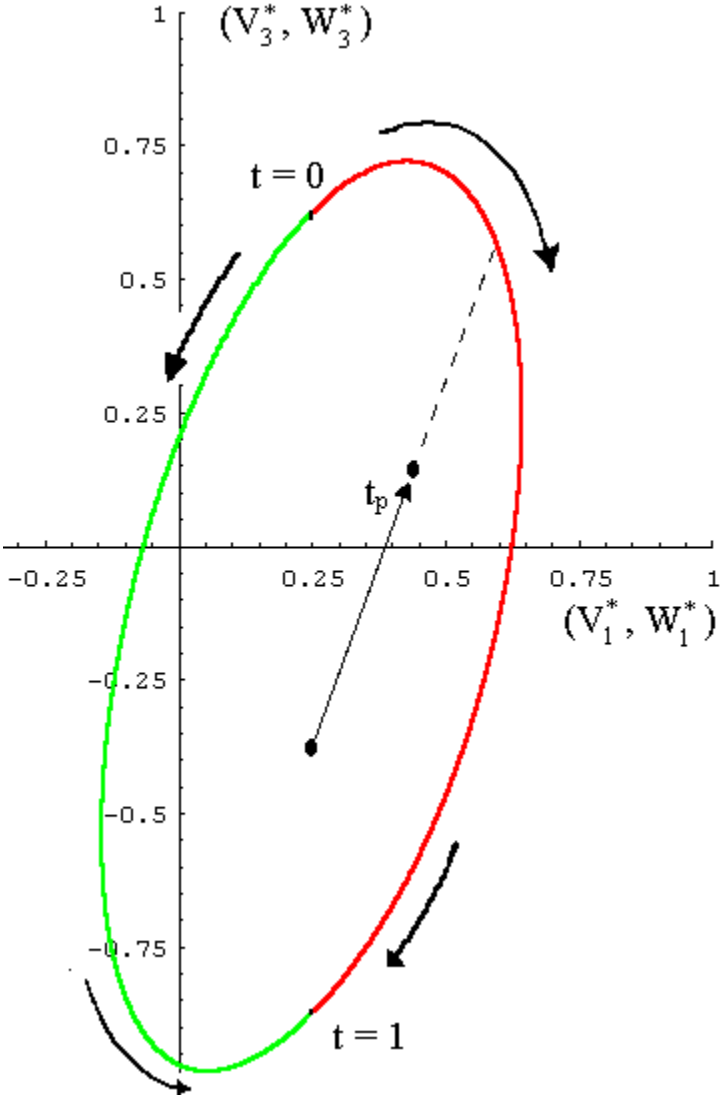

Figure 22 Interior Optimization Formulation

Tables 21 through 26 show the results for this formulation. As can be seen in Figures 23 through 24, for each target load and each load constraint, the optimizer found designs with bending stiffness parameters located on the ellipsoid. Errors similar to those observed for the ellipsoidal approach are observed for the lowest target load, again likely due to inaccuracies in the response surface model at the edges of the design space.

Table 21 Interior Approach Optimization Results
75,000 pound target

Case	Buckling Constraint	λ-RSM (pounds)	λ-STAGS (pounds)	Error (%)	Fitness
1	75000	79794.4	68415.4	-16.6	-0.736
2	77500	79802.6	68390.1	-16.7	-0.769
3	80000	80103.1	68708.8	-16.6	-0.849
4	82500	83227.8	82437.5	-1.0	-1.240
5	85000	85832.9	85434.0	-0.5	-1.389

Table 22 Interior Approach Parameter Results
75,000 pound target

Case	h (in)	t	tp	v1star	v3star	w1star	w3star
1	0.040	0.760	0.080	0.880	0.560	0.883	0.571
2	0.040	0.980	0.290	0.880	0.560	0.883	0.568
3	0.043	0.980	0.290	0.880	0.560	0.883	0.568
4	0.062	0.460	1.000	0.180	0.100	0.732	0.625
5	0.070	0.460	1.000	0.180	0.080	0.727	0.599

From a parameter view point, cases 1, 2, and 3 are virtually indistinguishable. Cases 1 and 2 vary slightly in their W_3^* value, and cases 2 and 3 differ only in *h*. Only results for case 1 are shown, in Figure 23. These three cases are also the only cases in the interior approach for which t_p was not found to be equal to 1. This can be explained primarily by the observation that the (V_1^*, V_3^*) values are nearly on the bordering parabola, on which the ellipsoid collapses to a point.

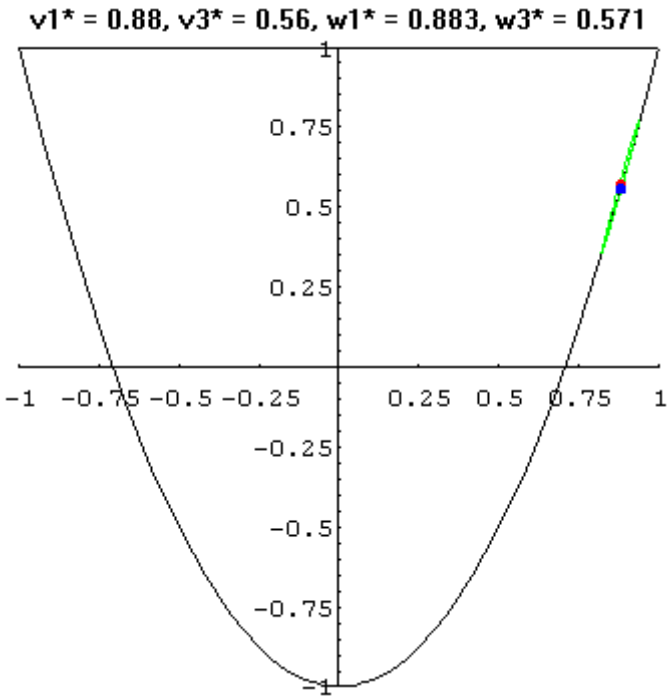

Figure 23 Interior approach, Case 1

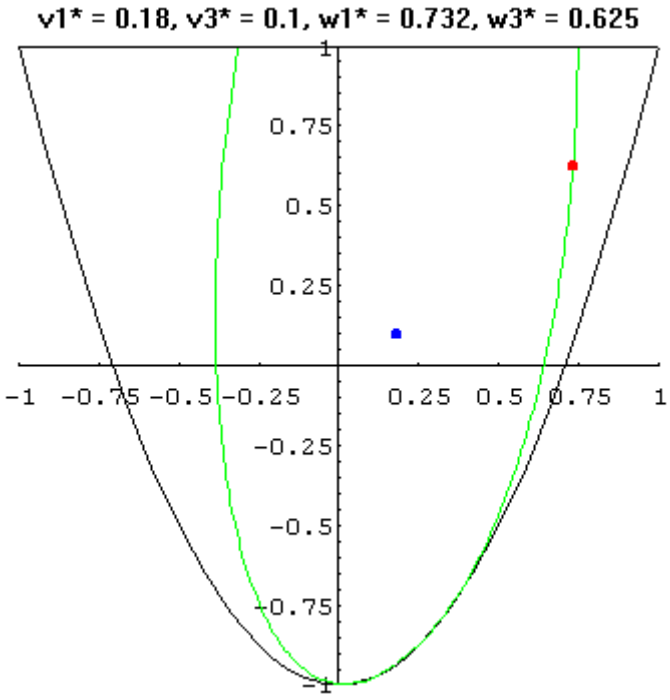

Figure 24 Interior approach, Case 4

Tables 23 and 24 show the results for the 100,000 pound target load. For each of these cases, the value of the optimal t_p parameter was found to be 1. This indicates that the bending stiffness parameters are on the ellipsoid. Comparing the results for these cases and the corresponding cases for the elliptical approach shows that the GA found the same design despite being able to explore designs within the ellipsoid.

Table 23 Interior Approach Optimization Results
100,000 pound target

Case	Buckling Constraint	λ-RSM (pounds)	λ-STAGS (pounds)	Error (%)	Fitness
6	100000	100937.2	98846.3	-2.1	-2.138
7	102500	103226.3	101608.8	-1.6	-2.240
8	105000	105517.5	103204.7	-2.2	-2.343
9	107500	107821.5	105469.2	-2.2	-2.446
10	110000	110137.7	108248.5	-1.7	-2.548

Table 24 Interior Approach Parameter Results
100,000 pound target

Case	h (in)	t	tp	v1star	v3star	w1star	w3star
6	0.107	0.520	1.000	-0.080	-0.160	0.396	-0.361
7	0.113	0.520	1.000	-0.080	-0.180	0.390	-0.378
8	0.117	0.540	1.000	-0.100	-0.180	0.360	-0.458
9	0.122	0.540	1.000	-0.120	-0.200	0.332	-0.507
10	0.128	0.540	1.000	-0.140	-0.220	0.303	-0.555

Table 25 Interior Approach Optimization Results
125,000 pound target

Case	Buckling Constraint	λ-RSM (pounds)	λ-STAGS (pounds)	Error (%)	Fitness
11	125000	125237.5	123482.5	-1.4	-3.197
12	127500	127521.4	125947.4	-1.2	-3.300
13	130000	130915.5	128895.6	-1.6	-3.438
14	132500	133134.1	131143.9	-1.5	-3.542
15	135000	135352.8	132849.4	-1.9	-3.645

Table 26 Interior Approach Parameter Results
125,000 pound target

Case	h (in)	t	tp	v1star	v3star	w1star	w3star
11	0.160	0.580	1.000	-0.220	-0.280	0.171	-0.766
12	0.165	0.580	1.000	-0.220	-0.280	0.171	-0.766
13	0.172	0.580	1.000	-0.220	-0.300	0.165	-0.776
14	0.177	0.600	1.000	-0.220	-0.320	0.150	-0.809
15	0.182	0.600	1.000	-0.220	-0.320	0.150	-0.809

Full graphical results for the interior approach are shown in Appendix C.

5.3—Stacking Approach

In this approach, the inplane and bending stiffness parameters were not optimized directly, but were derived from continuous fiber orientation angles and stacking sequences that were the design variables for the optimization. This approach also uses a discretely varying shell wall thickness, which results from the use of discrete numbers of layers of material.

A significantly different genetic formulation was required for this approach. Since fiber orientation angles are being allowed to vary continuously, decoding similar to that found in the elliptical and interior approaches was used. Shell wall thickness was calculated from the number of layers of fiber used. Table 27 shows the genetic formulation. The decoding process is explained in Appendix B.

Table 27 Stacking Approach Genetic Formulation

Genetic Alphabet	0-20									
Design Variables	t1	t2	t3	t4	t5	t6	t7	t8	t9	t10
Example Chromosome	0 0	0 0	0 8	4 6	3 6	4 8	9 3	10 4	2 8	6 9
Decoded Chromosome	NA	NA	7	35	25	37	82	-87	17	58
Design Variables	o1	o2	o3	o4	o5	o6	o7	o8	o9	o10
Example Chromosome	9	5	20	20	9	13	13	20	2	12
Decoded Chromosome	7	3	14	13	5	6	5	8	1	3
Design Variables	o11	o12	o13	o14	o15	o16	o17	o18	o19	o20
Example Chromosome	4	17	12	17	8	2	4	1	8	5
Decoded Chromosome	1	3	1	1	1	1	2	0	4	3
Decoded Fiber Stacking Sequence	[17/25/-7/-35/-87/-58/58/-37/7/82/35/87/37/-17/82/-82/-25]s									

While this approach limits thickness variation to discrete increments, it allows the GA to explore areas of the design space outside of the ellipsoid previously examined.

Table 28 Stacking Approach Optimization Results
75,000 pound target

Case	Buckling Constraint	λ-RSM (pounds)	λ-STAGS (pounds)	Error (%)	Fitness
1	75000	79843.0	67906.9	-17.6	-0.735
2	77500	79843.0	67906.9	-17.6	-0.770
3	80000	82964.0	82150.7	-1.0	-1.163
4	82500	90099.0	89968.8	-0.1	-1.508
5	85000	90099.0	89968.8	-0.1	-1.540

Table 29 Stacking Approach Parameter Results
75,000 pound target

Case	h (in)	v1star	v3star	w1star	w3star
1	0.040	0.879	0.545	0.878	0.542
2	0.040	0.879	0.545	0.878	0.542
3	0.060	0.199	0.211	0.778	0.538
4	0.080	0.161	0.107	0.744	0.440
5	0.080	0.161	0.107	0.744	0.440

Again, at the lower thickness range, the response surface demonstrates some inaccuracies. An interesting observation can be made by comparing the results of the first and second cases and the third and fourth cases. Since the designs found by the optimizer should be those that maximize buckling load for a given thickness, it should be expected that if the design found for one load constraint exceeds not only that load constraint, but also the next higher constraint, that the same design should be found for both cases. This is can be seen in Table 29.

The stacking sequences for this case are given in Table 30.

Table 30 Stacking Approach Stacking Sequence Results
75,000 pound target

Case	h	Stacking Sequence
1	0.04	[-14.5/14/-14/14.5/]s
2	0.04	[-14.5/-14/14/14.5/]s
3	0.06	[72/-72/-33/33/1.5/-1.5]s
4	0.08	[75.5/-75.5/49/-49/24.5/-24.5/0/0]s
5	0.08	[-75.5/75.5/-49/49/24.5/-24.5/0/0]s

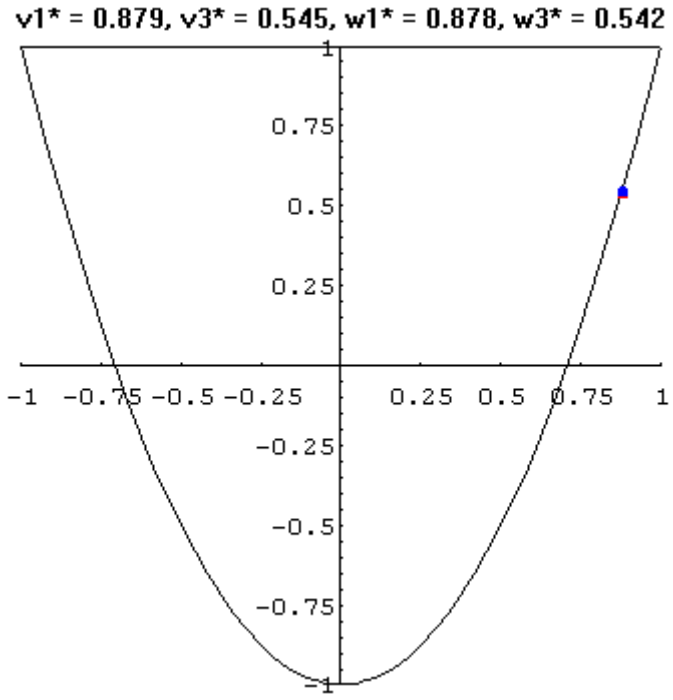

Figure 25 Stacking approach, Cases 1 and 2

The stacking sequence results for case 3 through 15 of the stacking approach produce designs which have greater than 3 fiber orientation angles. Since this is greater than the two fiber orientation angles that were used to develop the (V_1^*, V_3^*)-(W_1^*, W_3^*) relationship, it is possible for the (W_1^*, W_3^*) point to fall outside of the ellipsoid. For the optimized designs found in this study, most of the designs have (W_1^*, W_3^*) points outside of the ellipsoid. This is shown in Figure 26.

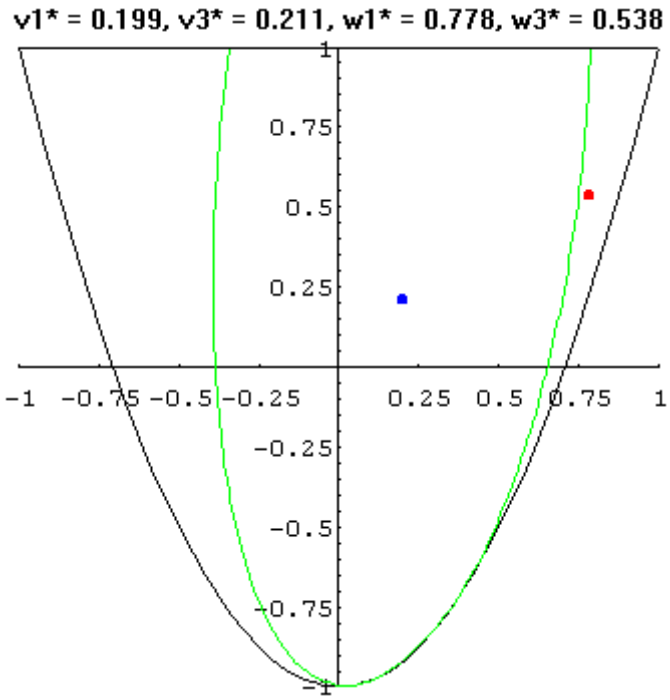

Figure 26 Stacking approach, Case 3

Results for the 100,000 pound target load are similar to those for the 75,000 pound target load. Again, the accuracy of the response surface appears to improve as the optimizer drives the design towards the center of the design space. Duplication of the designs is now seen between the first, second and third load constraints and the fourth and fifth. Comparing the values of the stiffness parameters and the stacking sequences for these designs show some minor variations in the stacking sequence. This slight variation indicates that in this case the optimizer had difficulty negotiating extremely close regions of the design space. However, the major features of the designs are the same. Similar observations can be made for the 125,000 pound target load.

Table 31 Stacking Approach Optimization Results
100,000 pound target

Case	Buckling Constraint	λ-RSM (pounds)	λ-STAGS (pounds)	Error (%)	Fitness
6	100000	107953.3	106080.8	-1.8	-2.320
7	102500	107954.1	106051.1	-1.8	-2.347
8	105000	107954.2	106093.8	-1.8	-2.372
9	107500	116977.8	115276.7	-1.5	-2.712
10	110000	116975.2	115218.7	-1.5	-2.737

Table 32 Stacking Approach Parameter Results
100,000 pound target

Case	h (in)	v1star	v3star	w1star	w3star
6	0.120	-0.124	-0.213	0.384	-0.447
7	0.120	-0.126	-0.213	0.381	-0.456
8	0.120	-0.124	-0.218	0.383	-0.451
9	0.140	-0.193	-0.262	0.278	-0.641
10	0.140	-0.192	-0.261	0.276	-0.649

Table 33 Stacking Approach Stacking Sequence Results
100,000 pound target

Case	h	Stacking Sequence
6	0.12	[-89.5/89.5/71/-71/52.5/-52.5/-39.5/39.5/-31.5/31.5/24.5/-24.5]s
7	0.12	[90/-90/71.5/-71.5/52/-52/-40/40/31/-31/-25/25]s
8	0.12	[90/-90/-71/71/-52/52/40/-40/31.5/-31.5/24.5/-24.5]s
9	0.14	[-90/90/81.5/-81.5/-58.5/58.5/46.5/-46.5/-39/39/33.5/-33.5/-29.5/29.5]s
10	0.14	[-89.5/89.5/-85/85/57/-57/-46.5/46.5/39/-39/-34/34/29.5/-29.5]s

Table 34 Stacking Approach Optimization Results
125,000 pound target

Case	Buckling Constraint	λ-RSM (pounds)	λ-STAGS (pounds)	Error (%)	Fitness
11	125000	126130.2	125021.4	-0.9	-3.191
12	127500	135163.0	132427.0	-2.1	-3.540
13	130000	135255.7	132616.4	-2.0	-3.560
14	132500	135256.5	132556.1	-2.0	-3.579
15	135000	144237.6	140186.0	-2.9	-3.932

Table 35 Stacking Approach Parameter Results
125,000 pound target

Case	h (in)	v1star	v3star	w1star	w3star
11	0.160	-0.226	-0.301	0.213	-0.745
12	0.180	-0.239	-0.339	0.176	-0.789
13	0.180	-0.237	-0.342	0.180	-0.794
14	0.180	-0.237	-0.340	0.182	-0.791
15	0.200	-0.236	-0.391	0.166	-0.806

Table 36 Stacking Approach Stacking Sequence Results
125,000 pound target

Case	h	Stacking Sequence
11	0.18	[-90/90/90/-90/-65/65/51/-51/-43/43/-38.5/38.5/35/-35/-33/33]s
12	0.18	[-89.5/75/89.5/78.5/-78.5/-75/-53.5/53.5/47.5/-47.5/-41/41/39/-39/-36/36/-34.5/34.5]s
13	0.18	[89.5/-88.5/-89.5/88.5/-70/70/53.5/-53.5/47/-47/-42/42/-38.5/38.5/36.5/-36.5/34/-34]s
14	0.18	[90/89.5/-89.5/-90/70/-70/53.5/-53.5/47/-47/42.5/-42.5/-38.5/38.5/36/-36/-34/34]s
15	0.20	[87.5/89.5/-87.5/-89.5/-68/58.5/68/-58.5/50.5/-50.5/45.5/-45.5/-41.5/41.5/-39/39/36/-36/34/-34]s

Full graphical results for the stacking approach are shown in Appendix C.

5.4—Discrete Stacking Approach

The discrete stacking approach represents the most restricted of the four approaches. In addition to the discretely varying shell wall thickness due to the discrete number of layers of material, fiber orientation angles are now limited to a finite number of possibilities (0^o, $\pm 30^o$, $\pm 45^o$, $\pm 60^o$, $\pm 90^o$). Although the design is not bounded by the ellipsoid, the possible combinations of stiffness parameters are severely limited by the discrete fiber orientation angles, and therefore the overall number of design possibilities is also limited.

The genetic formulation for this approach is very similar to that of the previously discussed stacking approach. The major difference is that the fiber orientation angles are decoded to members of a discrete set, and not permitted to vary continuously. Appendix B contains details of the chromosome decoding process.

Table 37 Discrete Stacking Approach Genetic Formulation

Genetic Alphabet	0-20									
Design Variables	t1	t2	t3	t4	t5	t6	t7	t8	t9	t10
Example Chromosome	0	0	0	2	20	15	2	10	9	9
Decoded Chromosome	NA	NA	NA	0	90	45	0	90	90	90
Design Variables	o1	o2	o3	o4	o5	o6	o7	o8	o9	o10
Example Chromosome	19	15	16	10	17	9	12	14	1	9
Decoded Chromosome	13	9	9	5	8	4	4	4	1	2
Design Variables	o11	o12	o13	o14	o15	o16	o17	o18	o19	o20
Example Chromosome	7	18	14	20	10	15	8	4	3	11
Decoded Chromosome	1	2	1	1	1	1	1	1	1	1
Decoded Fiber Stacking Sequence	[-90/-90/-90/90/0/0/90/90/90/0/90/45/-45/-90/0]s									

Results for the 75,000 pound target are shown in Table 38 and 39, and corresponding stacking sequences are presented in Table 40. Note that the thickness for case 1 is 50% greater than the corresponding design which utilized continuous fiber orientation angles.

Table 38 Discrete Stacking Approach Optimization Results
75,000 pound target

Case	Buckling Constraint	λ-RSM (pounds)	λ-STAGS (pounds)	Error (%)	Fitness
1	75000	80186.2	71080.1	-12.8	-1.131
2	77500	80186.2	71080.1	-12.8	-1.165
3	80000	80186.2	71080.1	-12.8	-1.198
4	82500	89505.9	89470.3	0.0	-1.515
5	85000	89505.9	89470.3	0.0	-1.547

Table 39 Discrete Stacking Approach Parameter Results
75,000 pound target

Case	h (in)	v1star	v3star	w1star	w3star
1	0.060	0.833	0.500	0.856	0.569
2	0.060	0.833	0.500	0.856	0.569
3	0.060	0.833	0.500	0.856	0.569
4	0.080	0.125	0.125	0.711	0.336
5	0.080	0.125	0.125	0.711	0.336

Similar errors are noted for cases 1, 2 and 3 as were present in the previous approaches. While the thickness of this design is not at the edge of the design space, the values of the stiffness parameters are close to the edge. This can be seen in Figure 27. However, the error for the satisfactory design found in cases 4 and 5 is noted to be quite small.

Table 40 Discrete Stacking Sequence Results
75,000 pound target

Case	h	Stacking Sequence
1	0.06	[-30/0/0/0/30/0]s
2	0.06	[30/0/0/0/-30/0]s
3	0.06	[30/0/0/0/-30/0]s
4	0.08	[-90/90/-45/45/30/-30/0/0]s
5	0.08	[90/-90/45/-45/-30/30/0/0]s

Since the optimum design found by the GA for case 1 has a λ_{rsm} greater than the buckling constraint for cases 2 and 3, it is expected that the optimum design for all three of these cases would be the same. This is confirmed by both the values of the stiffness parameters and the stacking sequences found by the GA. Similar observations can be made for cases 4 and 5. There are slight differences in these laminate designs, but these differences have no effect on either the laminate stiffness parameters or its buckling response.

Figures 27 and 28 show the parameter values for both of these designs.

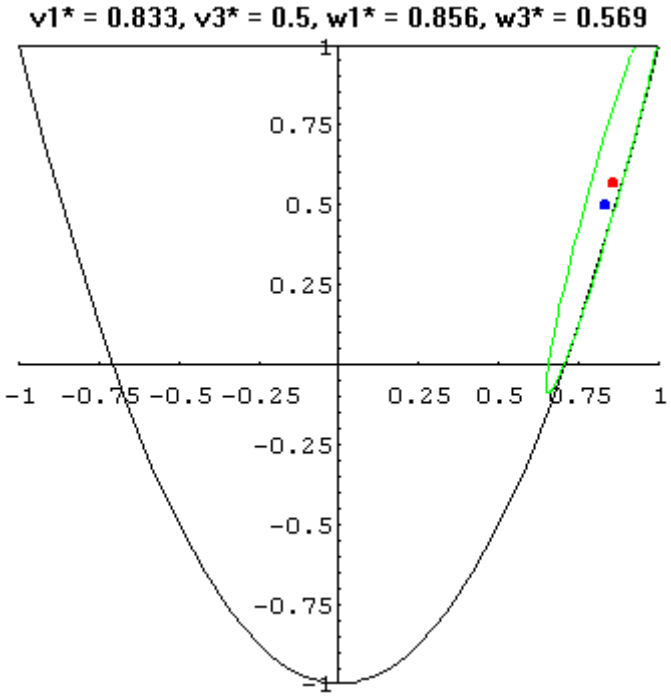

Figure 27 Discrete Stacking approach, Cases 1, 2, and 3

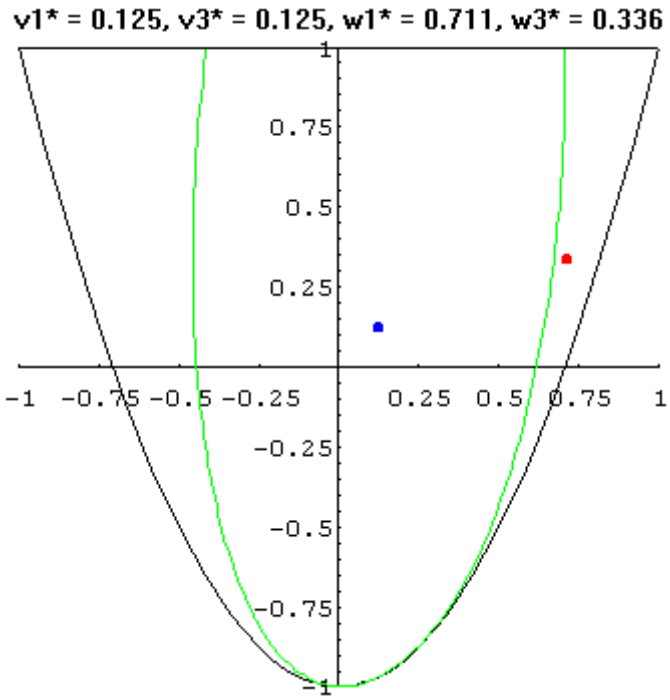

Figure 28 Discrete Stacking approach, Cases 4 and 5

Tables 41 and 42 present the results for the 100,000 pound target load. As with previous approaches, the error in the response surface for this load range is acceptably small. Note that identical designs are again found by the GA for cases 6, 7 and 8 and cases 9 and 10.

Table 41 Discrete Stacking Approach Optimization Results 100,000 pound target

Case	Buckling Constraint	λ-RSM (pounds)	λ-STAGS (pounds)	Error (%)	Fitness
6	100000	107230.2	104798.3	-2.3	-2.328
7	102500	107230.2	104798.3	-2.3	-2.354
8	105000	107230.2	104798.3	-2.3	-2.379
9	107500	116511.9	114820.7	-1.5	-2.716
10	110000	116511.9	114820.7	-1.5	-2.741

Table 42 Discrete Stacking Parameter Results
100,000 pound target

Case	h (in)	v1star	v3star	w1star	w3star
6	0.120	-0.167	-0.167	0.315	-0.574
7	0.120	-0.167	-0.167	0.315	-0.574
8	0.120	-0.167	-0.167	0.315	-0.574
9	0.140	-0.214	-0.214	0.267	-0.608
10	0.140	-0.214	-0.214	0.267	-0.608

Small variations in the stacking sequences, as shown in Table 43 are present, but as with the 75,000 pound load target, these do not affect the stiffness parameters or the buckling response.

Table 43 Discrete Stacking Sequence Results
100,000 pound target

Case	h	Stacking Sequence
6	0.12	[-90/90/90/-90/45/-45/45/-45/-30/30/30/-30]s
7	0.12	[90/-90/-90/90/45/-45/-45/45/-30/-30/30/30]s
8	0.12	[-90/-90/90/90/45/-45/-45/45/30/-30/30/-30]s
9	0.14	[-90/90/90/-90/60/-60/45/-45/-45/45/30/30/-30/-30]s
10	0.14	[-90/90/-90/90/60/-60/-45/45/-45/45/-30/-30/30/30]s

Results for the 125,000 pound load target are similar to those found for the previous two target loads. Independent designs are found for case 11, cases 12, 13, and 14, and case 15. Results are shown in Tables 44 and 45, with corresponding stacking sequences given in Table 46.

Table 44 Discrete Stacking Approach Optimization Results
125,000 pound target

Case	Buckling Constraint	λ-RSM (pounds)	λ-STAGS (pounds)	Error (%)	Fitness
11	125000	125474.6	124740.0	-0.6	-3.196
12	127500	134212.4	131320.8	-2.2	-3.547
13	130000	134212.4	131320.8	-2.2	-3.568
14	132500	134212.4	131320.8	-2.2	-3.587
15	135000	142953.7	139545.4	-2.4	-3.941

Table 45 Discrete Stacking Approach Parameter Results
125,000 pound target

Case	h (in)	v1star	v3star	w1star	w3star
11	0.160	-0.188	-0.313	0.255	-0.661
12	0.180	-0.222	-0.333	0.215	-0.675
13	0.180	-0.222	-0.333	0.215	-0.675
14	0.180	-0.222	-0.333	0.215	-0.675
15	0.200	-0.200	-0.400	0.208	-0.712

Table 46 Discrete Stacking Sequence Results
125,000 pound target

Case	h	Stacking Sequence
11	0.16	[-90/90/90/-90/60/-60/-45/45/45/45/-45/-45/30/-30]s
12	0.18	[-90/90/-90/90/-60/60/60/-60/-45/45/-45/-45/45/45/30/30/-30/-30]s
13	0.18	[-90/90/90/-90/60/-60/60/-60/-45/-45/45/-45/45/45/30/-30/30/-30]s
14	0.18	[90/-90/90/-90/-60/60/-60/60/45/-45/45/-45/45/-45/30/30/-30/-30]s
15	0.20	[90/-90/-90/90/-60/60/60/-60/-45/45/45/45/45/-45/-45/-45/-30/30/30/-30]s

Full graphical results for the discrete stacking approach are shown in Appendix C.

Chapter 6—Conclusions and Recommendations for Future Work

6.1—Conclusions

This study has shown that it is possible to develop an efficient optimization strategy for composite cylinders, making use of finite element analysis, simplified laminate parameters, response surface techniques, and genetic algorithms. The resulting optimization strategy is an efficient, cost effective method of optimizing a complex structure.

Structural Analysis of General Shells is widely accepted as one of the best packages for analyzing complex shell structures. Given the large number of analyses that were required in the course of this study, the speed and efficiency of the STAGS package allowed exploration of high order response surface models without straining computational resources.

The use of the Miki stiffness parameters offers significant potential for composite optimization. While utilizing the bounding ellipsoid did not offer significant insights into what could be expected from full stacking sequence optimization, the parameters allowed a simplified description of a complex stacking sequence. Consider the results from the stacking sequence and discrete stacking sequence approach. For the higher load targets, a comparatively large number of layers of material were required. For both approaches, case 15 required a forty layer laminate. For a balanced symmetric stacking sequence, ten different fiber orientations angles are possible, with 20! possible stacking sequence combinations. Use of the Miki parameters allowed this design space to be fully explored by the genetic algorithm using only a five variable response surface model. A response surface model which utilized 10 individual fiber orientation angles as variables would have required a significantly greater number of STAGS analyses to construct than the approximately 1000 analyses used for this response surface model.

The use of the genetic algorithm is also especially well suited to this study. The advantages of the genetic algorithm were exploited, while the major drawback was avoided. Genetic algorithms excel at optimizing difficult design spaces and discrete design variable problems. This problem combined both in terms of a high order polynomial analysis and stacking sequence optimization. Genetic algorithms are also notorious for the high numbers of function evaluations required. Use of a response surface model alleviated that penalty. Usually, optimization is simpler if a closed form expression for an objective function is known. In this case, even though a closed form expression was known for the response surface model, navigating the design space with a gradient-based optimization method would be extremely difficult. Since the response surface model is 6^{th} order, it likely contains a number of local minima and maxima that a gradient based method is likely to get caught in. The genetic algorithm is capable of avoiding these regions by searching large areas of the design space, not just a single path through it.

Discrete design variables present another problem area for optimization. While methods do exist for solving such problems (branch and bound techniques), these methods often leave large portions of the design space untouched. They are also difficult to implement for problems in which only discrete values can be analyzed. A genetic algorithm's ability to optimize using only the value of a fitness function allows it to fully explore a complex discrete design space without gradient calculation.

Because of the use of the response surface model, the extremely large number of function evaluations that were required for each GA run did not pose a computational burden. With a population size of 500 and as many as 1000 generations, 500,000 fitness function evaluations would be required. Using a STAGS analysis that requires 15 seconds of computer processor time would require over 12 weeks to run. The use of a response surface model make function evaluations virtually instantaneous.

This study proved the efficiency of using a response surface model in place of direct analysis for optimization work. The response surface allowed the use of an advanced analysis without imposing excessive demands on computational resources. The reduced computational time required to evaluate the response surface allowed the use of a genetic algorithm, which allowed stacking sequence optimization to be completed. Detailed optimization such as this will

allow optimization to become a more useful tool throughout the development of composite structures.

6.2—Future Work

Considering the significant differences between the results for both the elliptical and interior approaches and the stacking sequence and discrete stacking sequence approaches, further work in this area should concentrate on the use of discrete stacking sequence optimization. While use of the Miki parameters and bounding ellipsoid offers some idea of the relationship between the inplane and bending stiffnesses of a laminate, it does not capture the complex interactions between inplane and bending properties that are possible with laminates with more than two fiber orientation angles.

Use of the Miki parameters to reduce the number of design variables encountered in a problem appears to offer a good deal of promise. The ability to reduce a full description of a laminate to four parameters would be a powerful tool in optimization work. Shrinking the design space makes the search process significantly easier to handle, regardless of optimization technique being used.

The response surface technique seems to offer significant improvements to the computational cost of optimization. While the construction of an accurate response surface model can be extremely expensive, the resulting optimizations that can be made with that model make up for this expense. Unlimited numbers of optimizations can subsequently be carried out using the response surface without undue computer cost. Expanding the use of response surfaces to more complex problems with greater numbers of variables offers interesting possibilities.

While it has been known that genetic algorithms have been well suited to composite laminate optimization problems, the combination of GAs with a response surface model seems to be very successful. The speed with which the response surface can be evaluated allows a GA to explore a design space with large population sizes and high numbers of generations without incurring high computer costs. Optimizations can be run repeatedly if necessary. Further work utilizing this combination holds significant potential.

References

[1] Brogan, Frank A., Charles C. Rankin, and Harold D. Cabiness. STAGS User Manual, Version 2.0. Palo Alto, CA: Lockheed Palo Alto Research Laboratory, 1994.

[2] Almroth, B. O. and F. A. Brogan. "The STAGS Computer Code." NASA CR-2950, 1978.

[3] Chao, C. C., C. T. Sun, and S. L. Koh. "Strength Optimization for Cylindrical Shells of Laminated Composites." Journal of Composite Materials, vol. 9 (1975): 53-66.

[4] Prucz, Jacky, J. Sivan, and P. C. Upadhyay. "On the Optimum Design of Composite Ducts and Cylinders under Combined Loading." Composites: Proceedings of the 8th International Conference on Composite Materials (ICCM/8), Honolulu, HI: July 15-19, 1991, Section 1-11.

[5] ZitzEvancih, L. D. "Designing Graphite Cylinders to Resist Buckling." AIAA Paper No. 85-1101, 1985. AIAA/SAE.ASME/ASEE 21st Joint Propoulsion Conference, Monterey, CA: July 8-10, 1985.

[6] Zimmerman, Rolf. "Optimization of Axially Compressed Fiber Composite Cylindrical Shells." Optimization: Methods and applications, possibilities and limitations; Proceedings of the International Seminar, Bonn, Federal Republic of Germany: June 7-8, 1989. p. 63-82.

[7] Chattopadhyay, Aditi and Jay Ferreira. "Design Sensitivity and Optimization of Composite Cylinders." Composites Engineering, vol 3 (1993): p. 169-179

[8] Narducci, R., B. Grossman, M. Valorani, A. Dadone, and R. T. Haftka. "Optimization Methods for Non-Smooth or Noisy Objective Functions in Fluid Design Problems." AIAA Paper 95-1648-CP, June 1995.

[9] Ragon, S. A., Z. Gurdal, R. T. Haftka, and T. J. Tzong. "Global/Local Structural Wing Design Using Reponse Surface Techniques." AIAA Paper 97-1051, 1997.

[10] Whitney, James M. Structural Analysis of Laminated Anisotropic Plates. Lancaster: Technomic Publishing Co., Inc., 1987.

[11] Jones, Robert M. Mechanics of Composite Materials. New York: Hemishpere Publishing Corporation, 1975.

[12] Haftka, Raphael T. and Zafer Gürdal. Elements of Structural Optimization. 3rd ed. Boston: Kluwer Academic Publishers, 1992.

[13] Almroth, B. O., F. A. Brogan, and G. M. Stanley. "User's Manual for STAGS, Volume 1: Theory." NASA CR-165670, March 1978.

[14] Rankin, Charles and Frank Brogan. "The Computational Structural Mechanics Testbed Structural Element Processor ES5: STAGS Shell Element." NASA CR-4358, 1991.

[15] Rankin, C. C., P. Stehlin, and F. A. Brogan. "Enhancements to the STAGS Computer Code." NASA CR-4000, 1986.

[16] Arora, Jasbir S. Introduction to Optimum Design. New York: McGraw-Hill Inc., 1989.

[17] Wolfram, Stephen. Mathematica: A System for Doing Mathematics by Computer. 2nd ed. New York: Addison-Wesley Publishing Company, Inc., 1991.

[18] Davis, Randall C. and Fred Carder. "Buckling Tests of a 10-Foot Diameter Stiffened Cylinder with Rectangular Cutouts." NASA TM-88996, February, 1987.

[19] Box, M. J. and N. R. Draper. "Factorial Designs, the |X'X| Criterion, and Some Related Matters." Technometrics, vol. 13 (1971): p. 731-742.

[20] Soremekun, Grant A. E. "Genetic Algorithms for Composite Laminate Design and Optimization." Master's Thesis, Virginia Polytechnic Institute and State University: February, 1997.

[21] Palazotto, A. N. "Bifurcation and collapse analysis of stringer and ring-stringer stiffened cylindrical shells with cutouts." NASA CR-146777, 1975.

Appendices

Appendix A

Modified zbuck.f STAGS subroutine

```
      c
      c $Id: zbuck.F,v 1.2 1993/11/23 03:23:04 stags Stab $
      c $Locker:  $
      c $Log: zbuck.F,v $
      c Revision 1.2  1993/11/23  03:23:04  stags
      c added RCS keyword substitution flags to file
      c
      c
      c
      #include "keydefs.h"
      c
      C=DECK    ZBUCK
      c
            SUBROUTINE ZBUCK
(NEIG,SHIFT,EPSD,PLD,PA,PB,K,B,NVC,JVEC,EIGB)
      C
      C=PURPOSE   Find NEIG eigenvalues and eigenvectors closest
to SHIFT
      C
      C
            COMMON /NITNOT/ NIT,NOT
      #include "zsys.h"
      #if _double_
      CUPD  DEC31,89
            DOUBLE PRECISION D0,D1,DD,EIGB,PLD,PA,PB,SHIFT,EPSD
            DOUBLE PRECISION SHF,APA,BTA
      CEND  DEC31,89
      #endif _double_
            COMMON /PREC/ IPREC
            DIMENSION JVEC(1),EIGB(1)
            INTEGER K,B,J
            COMMON /EIGCM1/ MXK,MXB,ASSM,VSKY,VBNDA,VMASS,VSCRA
            COMMON /EIGCM2/ VINIT(10),VX(40),VY(40),VZ(40)
            COMMON /EIGCM3/ NVEC,IVEC(20)
            INTEGER MXK,MXB,ASSM,VSKY,VBNDA,VMASS,VSCRA
            INTEGER VINIT,VX,VY
            COMMON /CON5/ DM1,DM2,DEL,rdummy(18)
            COMMON /CON6/ IS1,IS2,IVA,IVB,IVC,IVD,IVE
            COMMON /PARAM/
N,NCLST,LCPS,NEVAL,NPRNT,NCOF,NSEC,NBOUND,NEV,
           $ SHFT,ALPHA,BETA,INU,IOU,INDIC,NXEV
            COMMON /EVCM1/ SHF,APA,BTA
            COMMON /FQG   / AP1,AP2,PSLD,PSLDB,PSLA,PST
            COMMON /VIB1/ NLDS,ILDS,PLDS(20)
      C
      C
            D0=0.
            DEL=EPSD
            SHFT=SHIFT
```

```
      EIG1=APA
      EIG2=BTA
      MXK=K
      MXB=B
      PSLD=PA
      PSLDB=PB
      ILDS=max(ILDS,1)
      PLDS(ILDS)=PLD
      NVEC=NVC
      DO 5 I=1,NEIG
    5 IVEC(I)=JVEC(I)
C
C.............CALL EIGBUC FOR EIGEN SOLUTION
C
      CALL EIGBUC (NEIG,SHFT,EIG1,EIG2,EIGB)
C
C.............SET EIGB TO "CRITICAL" LOAD
C
      NVC=NVEC
      DO 10 I=1,NVEC
   10 EIGB(I)=PLD+PA*EIGB(I)
C-------------------------------------------------
C    MODIFICATIONS MADE BY JON RICH
C    FRIDAY, FEB 16, 1995
C-------------------------------------------------
      OPEN( UNIT = 100, FILE = 'buckling.DAT',
     +  ACCESS = 'SEQUENTIAL', STATUS = 'UNKNOWN')
      DO 110 J = 1,NVEC
  110 WRITE(100,*) EIGB(J)
      CLOSE(100)
C-------------------------------------------------
C    END MODIFICATIONS
C-------------------------------------------------
      IVAS=IVA
      IVA=60
      NEV=NVEC
CXXX  CALL ZDATA (-----)
      IVA=IVAS
      RETURN
      END
```

Appendix B

Genetic Formulation Descriptions

Elliptical Formulation:

Genetic Alphabet	1-10			
Design Variables	h	t	v1star	w3star
Example Chromosome	6 3	8 1	10 4	6 9
Decoded Chromosome	0.13	0.4	0.86	0.16

Each of the eight genes can hold values from 1-10.

Variables are allowed to vary in the ranges:

$0 < h \le 0.25$

$-1 \le t, V_1^*, V_3^* \le 1$

Variables are decoded as follows:

$$h = 0.25\left(\frac{10(h_1 - 1) + (h_2)}{100}\right)$$

$$t = \left(\frac{10(t_1 - 1) + (t_2 - 1)}{50}\right) - 1$$

$$V_1^* = \left(\frac{10(v1_1 - 1) + (v1_2 - 1)}{50}\right) - 1$$

$$V_3^* = \left(\frac{10(v3_1 - 1) + (v3_2 - 1)}{50}\right) - 1$$

Interior Formulation

Genetic Alphabet	1-10				
Design Variables	h	t	tp	v1star	w3star
Example Chromosome	6 3	8 1	1 8	10 4	6 9
Decoded Chromosome	0.13	0.4	0.07	0.86	0.16

The variable ranges and decoding equations are identical to those for the Elliptical Formulation, except for the additional t_p parameter.

$$0 < t_p \le 1$$

$$t_p = \left(\frac{10\left(tp_1 - 1\right) + \left(tp_2\right)}{100} \right)$$

Stacking Sequence Formulation

Genetic Alphabet	0-20									
Design Variables	t1	t2	t3	t4	t5	t6	t7	t8	t9	t10
Example Chromosome	0 0	0 0	0 8	4 6	3 6	4 8	9 3	10 4	2 8	6 9
Decoded Chromosome	NA	NA	7	35	25	37	82	-87	17	58
Design Variables	o1	o2	o3	o4	o5	o6	o7	o8	o9	o10
Example Chromosome	9	5	20	20	9	13	13	20	2	12
Decoded Chromosome	7	3	14	13	5	6	5	8	1	3
Design Variables	o11	o12	o13	o14	o15	o16	o17	o18	o19	o20
Example Chromosome	4	17	12	17	8	2	4	1	8	5
Decoded Chromosome	1	3	1	1	1	1	2	0	4	3
Decoded Fiber Stacking Sequence	[17/25/-7/-35/-87/-58/58/-37/7/82/35/87/37/-17/82/-82/-25]s									

The first 20 genes in the chromosome represent the fiber orientation angles the laminate will be constructed from. The second 20 genes in the chromosome represent a selection order to determine the stacking sequence. This formulation makes use of the GA utility to stack 0 terms at the beginning of the chromosome.

For t_1 through t_{10},

If $10(t_{i1} - 1) + (t_{i2} - 1) \le 90$ $\qquad t_i = 10(t_{i1} - 1) + (t_{i2} - 1)$

Else $\qquad t_i = 10(t_{i1} - 1) + (t_{i2} - 1) - 180$

The fiber orientation angles are then concatenated into an array with their negatives:

$$\left\{ t_1 \quad t_2 \quad t_3 \quad t_4 \quad t_5 \quad t_6 \quad t_7 \quad t_8 \quad t_9 \quad t_{10} \quad -t_{10} \quad -t_9 \quad -t_8 \quad -t_7 \quad -t_6 \quad -t_5 \quad -t_4 \quad -t_3 \quad -t_2 \quad -t_1 \right.$$

The order genes determine what order the fiber orientations will be strung into:

$$o_i = INT\left(\frac{o_{i1}}{\left(\frac{20}{nangles - i + 1} \right)} \right)$$ for i = 1, number of angles (up to 20)

The stacking sequence is then built from the array of fiber orientation angles sequentially by using the o_i^{th} member of the array, and then removing that member.

Discrete Stacking Sequence Formulation

Genetic Alphabet	0-20									
Design Variables	t1	t2	t3	t4	t5	t6	t7	t8	t9	t10
Example Chromosome	0	0	0	19	3	4	8	8	8	6
Decoded Chromosome	NA	NA	NA	90	30	30	60	60	60	45
Design Variables	o1	o2	o3	o4	o5	o6	o7	o8	o9	o10
Example Chromosome	19	15	16	10	17	9	12	14	1	9
Decoded Chromosome	13	9	9	5	8	4	4	4	1	2
Design Variables	o11	o12	o13	o14	o15	o16	o17	o18	o19	o20
Example Chromosome	7	18	14	20	10	15	8	4	3	11
Decoded Chromosome	1	2	1	1	1	1	1	1	1	1
Decoded Fiber Stacking Sequence	[-30/-60/-60/60/-60/60/60/60/45/90/30/30/-30/-45/-90]s									

The formulation for the Discrete Stacking Sequence formulation is the same as that for the Stacking Sequence formulation, except for the decoding of the fiber orientation angles.

For $_{t1}$ through t_{10}:

If $t_i > 10$ $\quad t_i = t_i - 10$

If $t_i \geq 9$ $\quad \theta_i = 90^o$

Else If $t_i \geq 7$ $\quad \theta_i = 60^o$

Else If $t_i \geq 5$ $\quad \theta_i = 45^o$

Else If $t_i \geq 3$ $\quad \theta_i = 30^o$

Else $\quad \theta_i = 0^o$

Appendix C

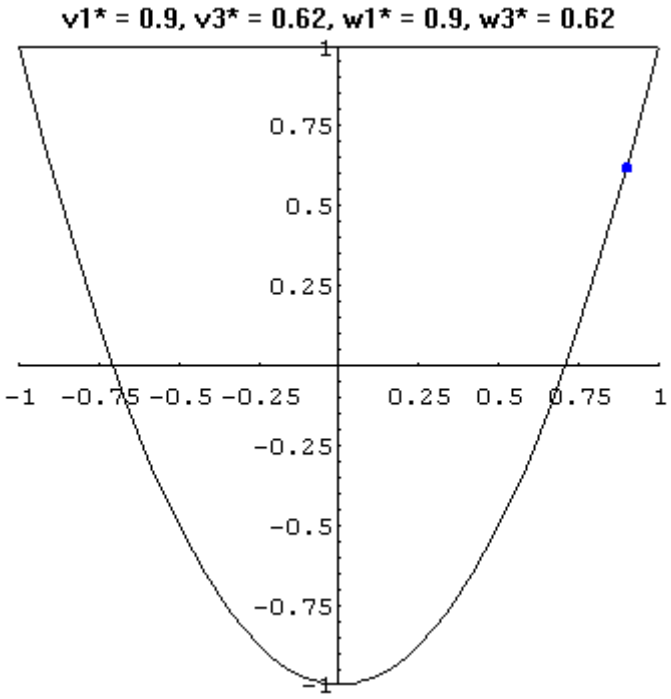

Figure 29 Elliptical approach, Cases 1 and 2

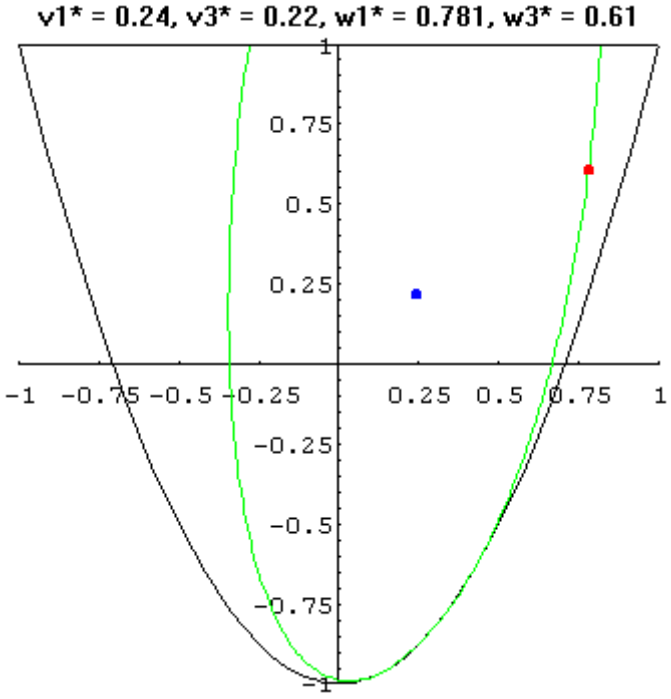

Figure 30 Elliptical Approach, Case 3

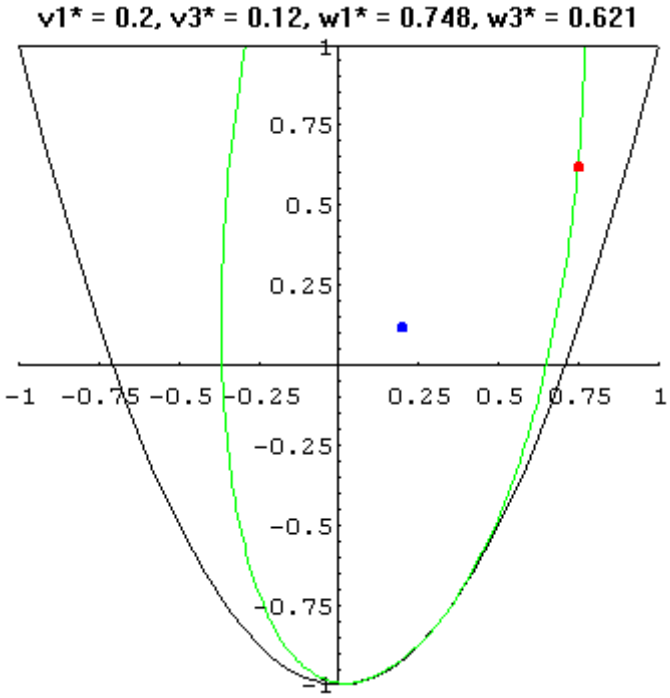

Figure 31 Elliptical Approach, Case 4

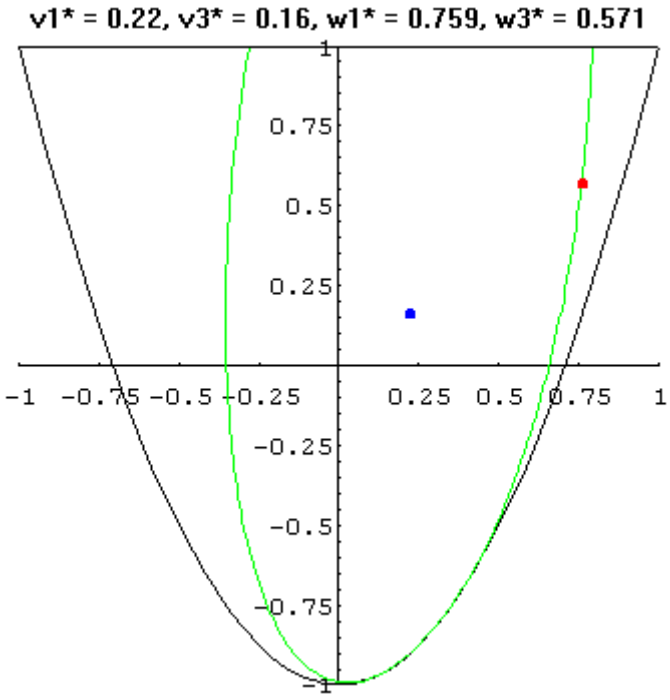

Figure 32 Elliptical Approach, Case 5

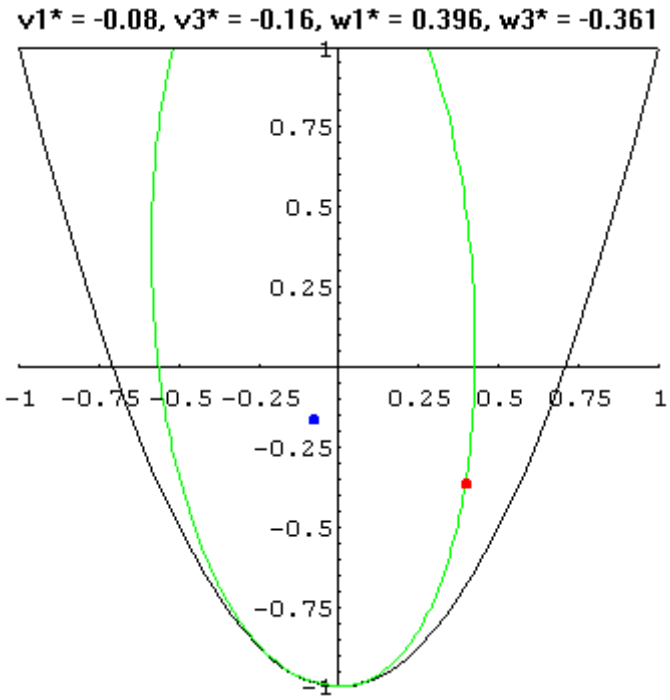

Figure 33 Elliptical Approach, Case 6

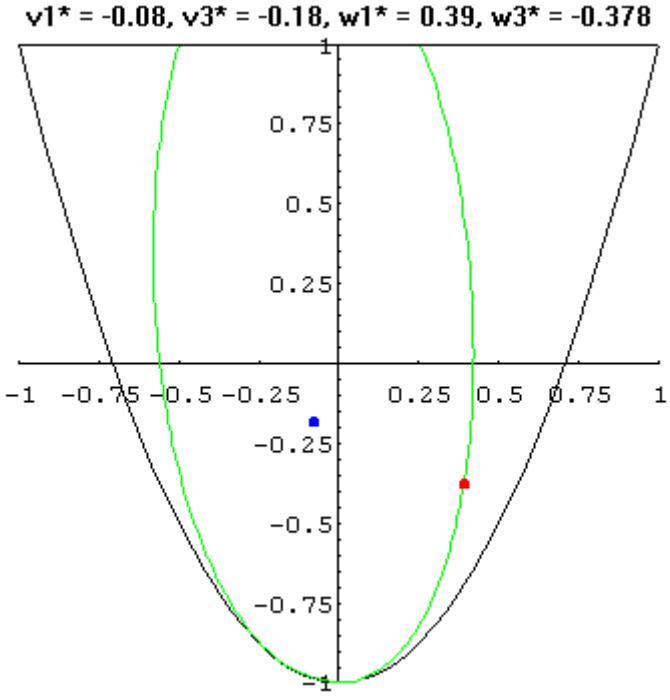

Figure 34 Elliptical Approach, Case 7

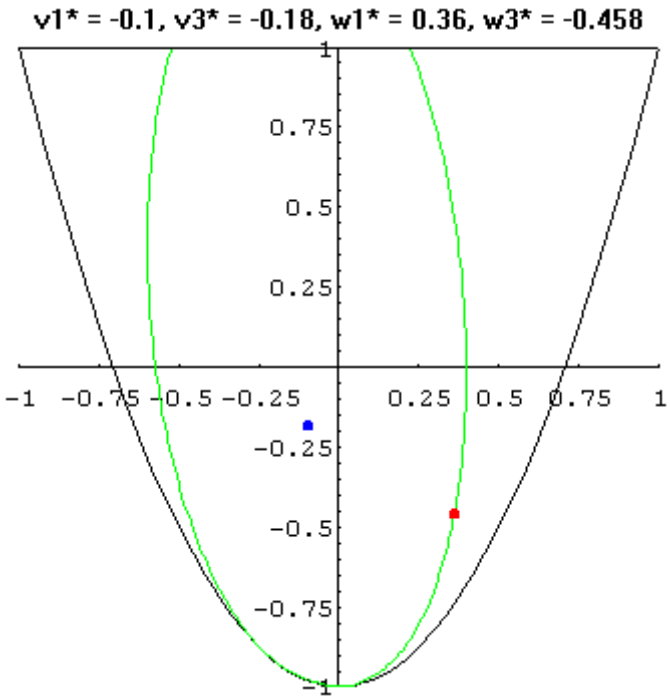

Figure 35 Elliptical Approach, Case 8

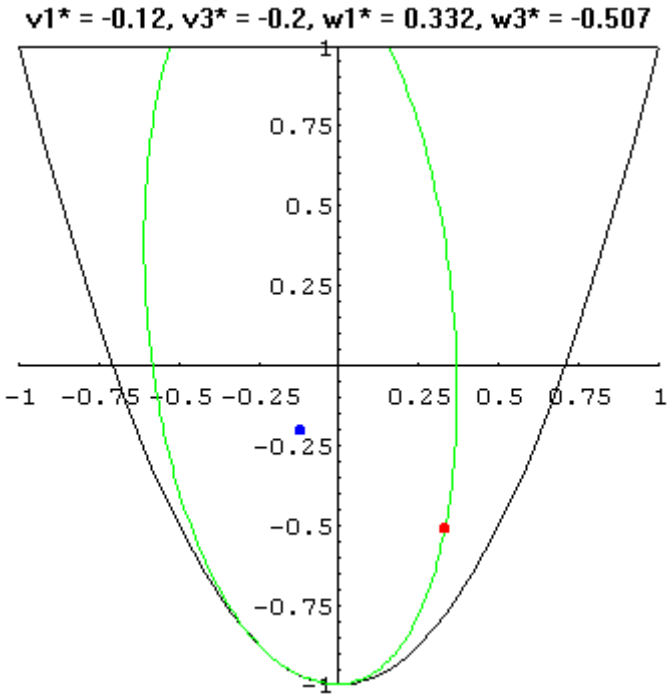

Figure 36 Elliptical Approach, Case 9

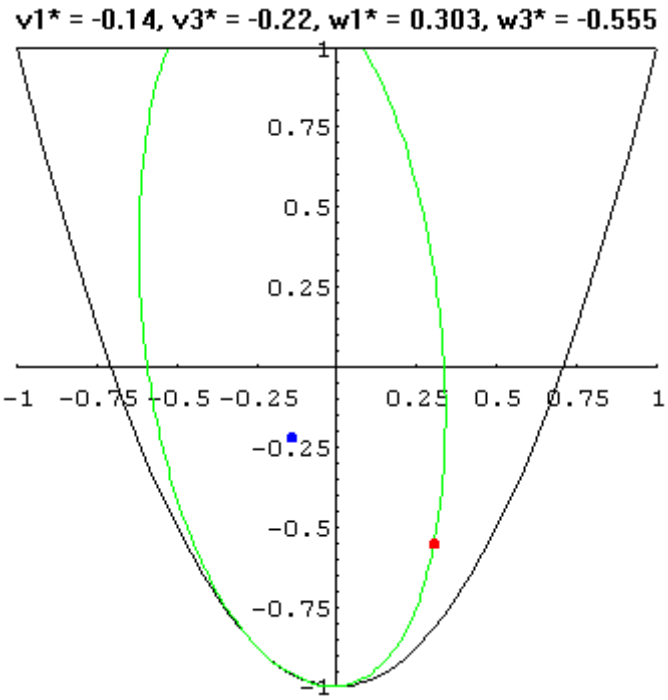

Figure 37 Elliptical Approach, Case 10

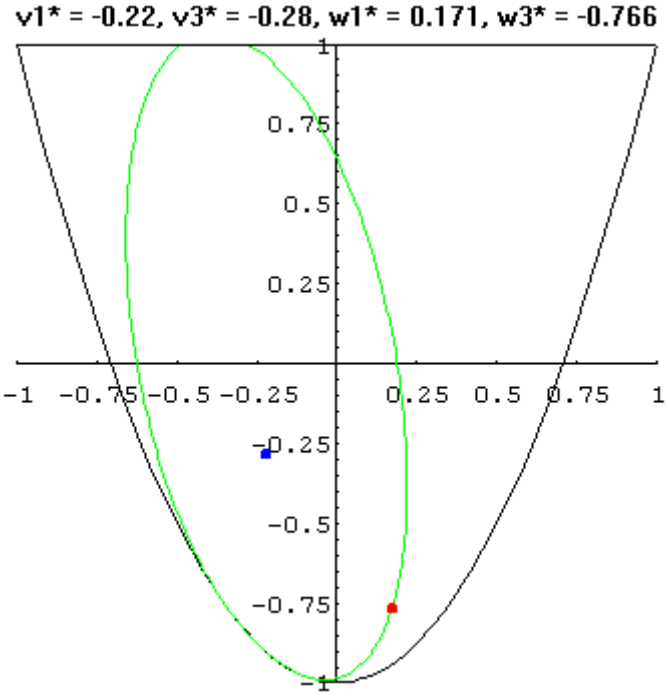

Figure 38 Elliptical Approach, Case 11

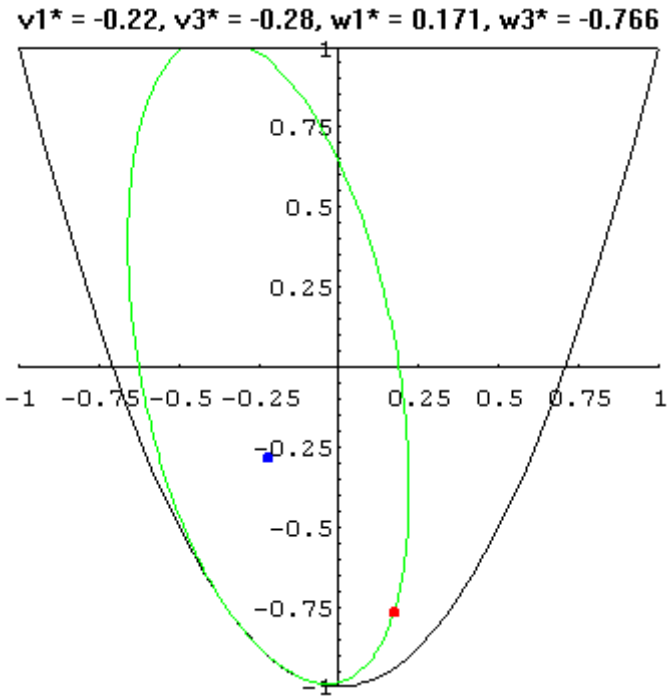

Figure 39 Elliptical Approach, Case 12

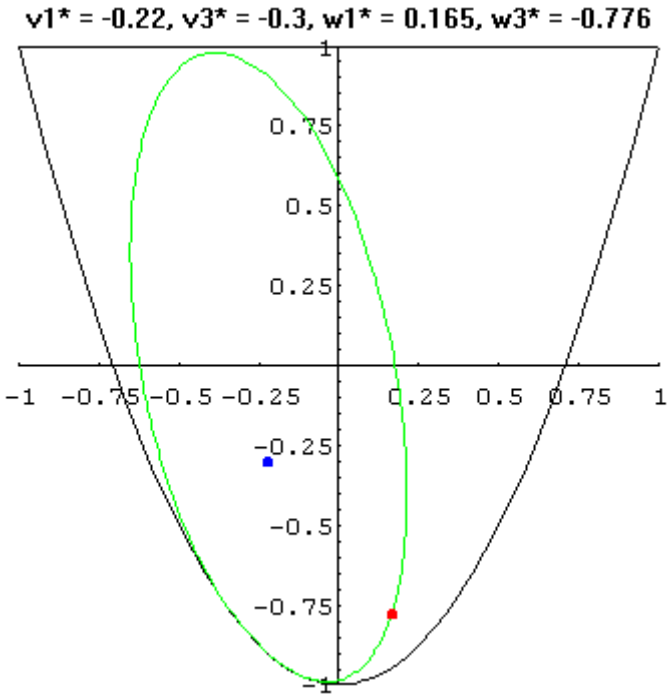

Figure 40 Elliptical Approach, Case 13

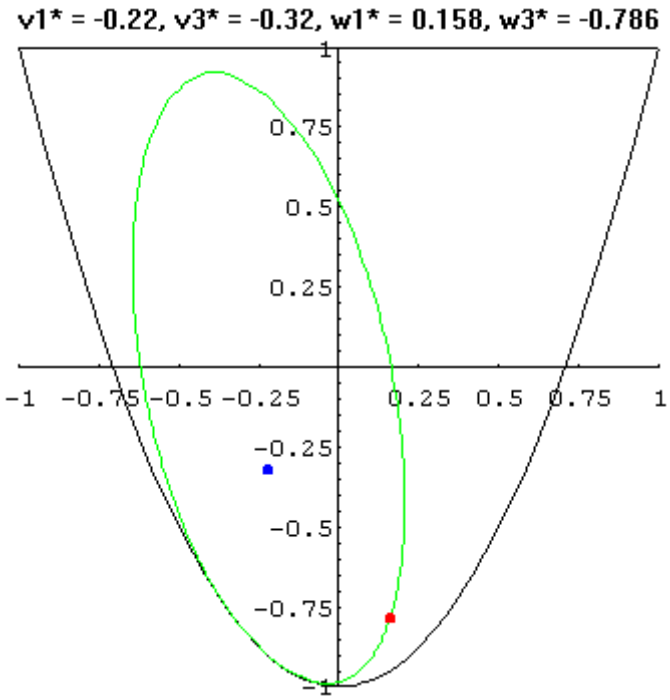

Figure 41 Elliptical Approach, Case 14

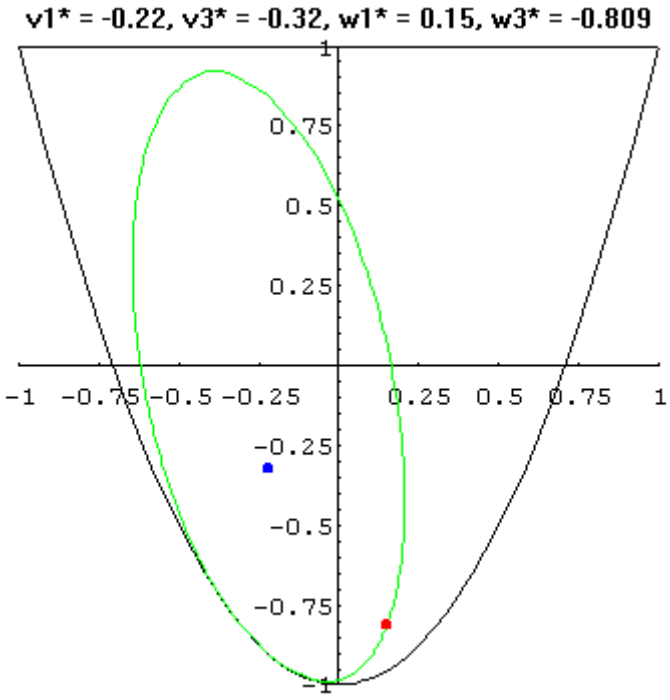

Figure 42 Elliptical Approach, Case 15

Interior Approach

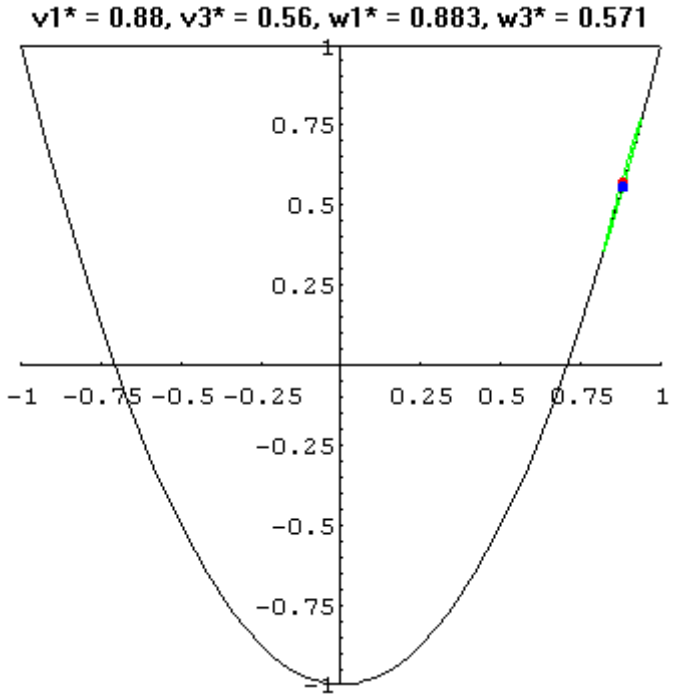

Figure 43 Interior Approach, Case 1

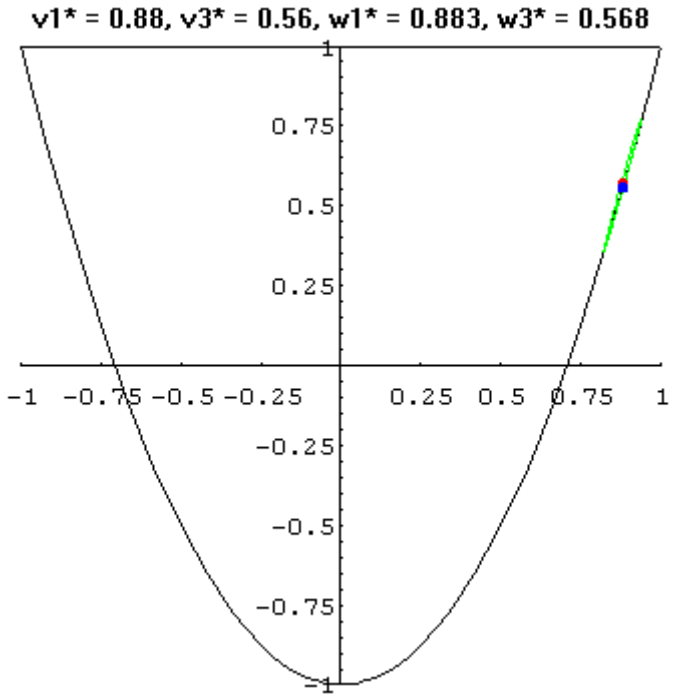

Figure 44 Interior Approach, Case 2

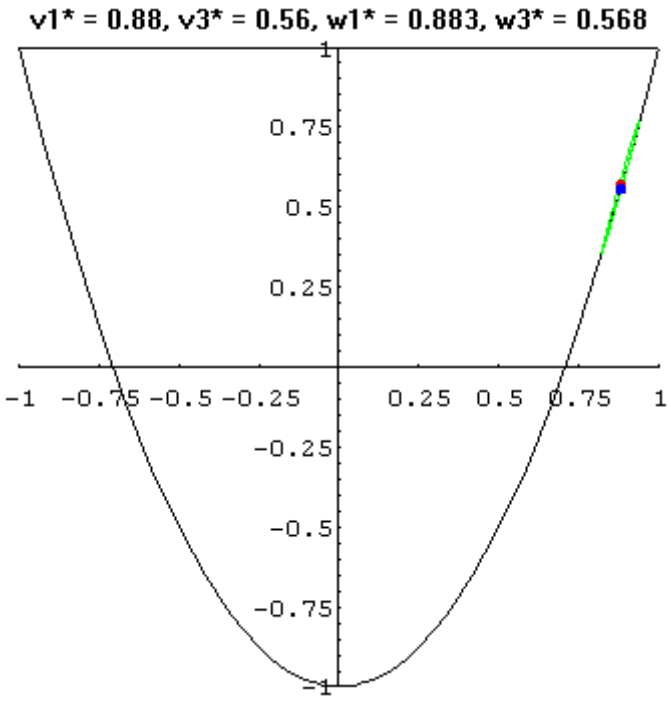

Figure 45 Interior Approach, Case 3

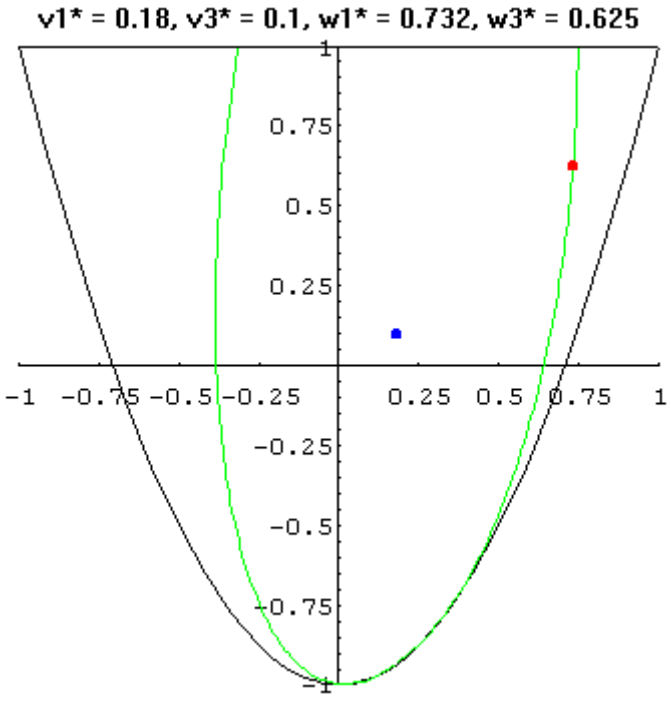

Figure 46 Interior Approach, Case 4

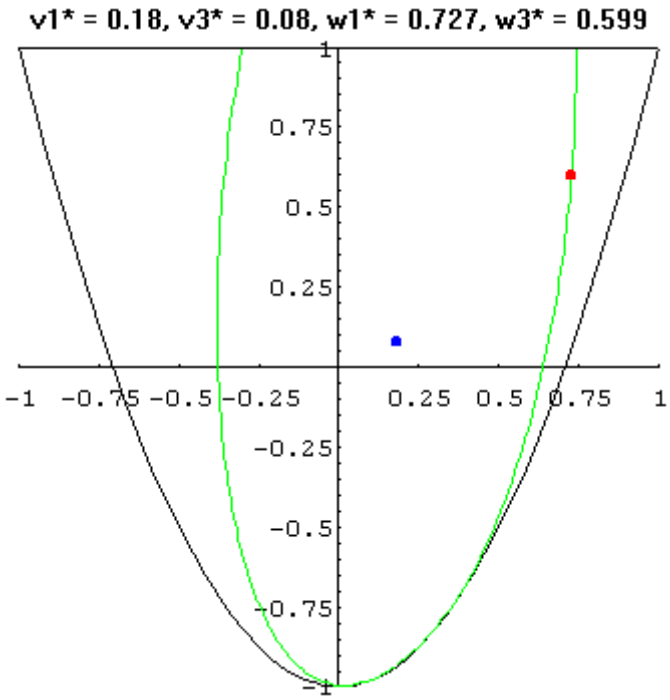

Figure 47 Interior Approach, Case 5

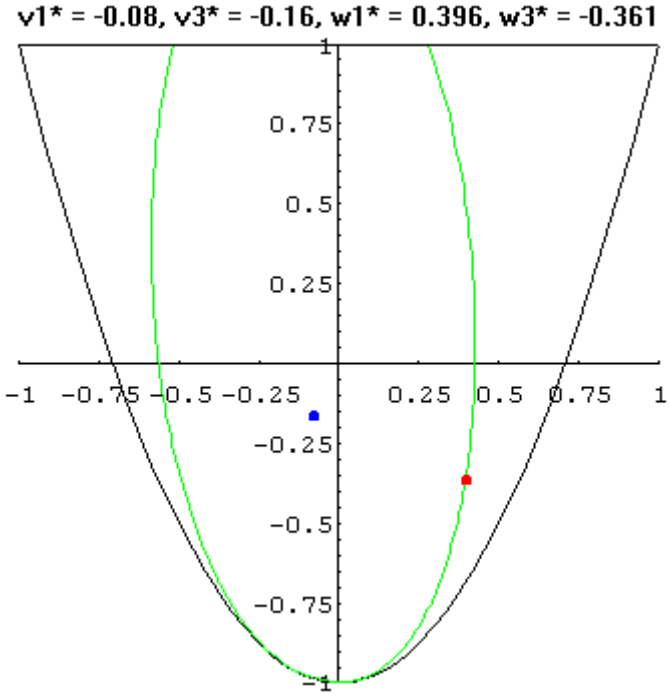

Figure 48 Interior Approach, Case 6

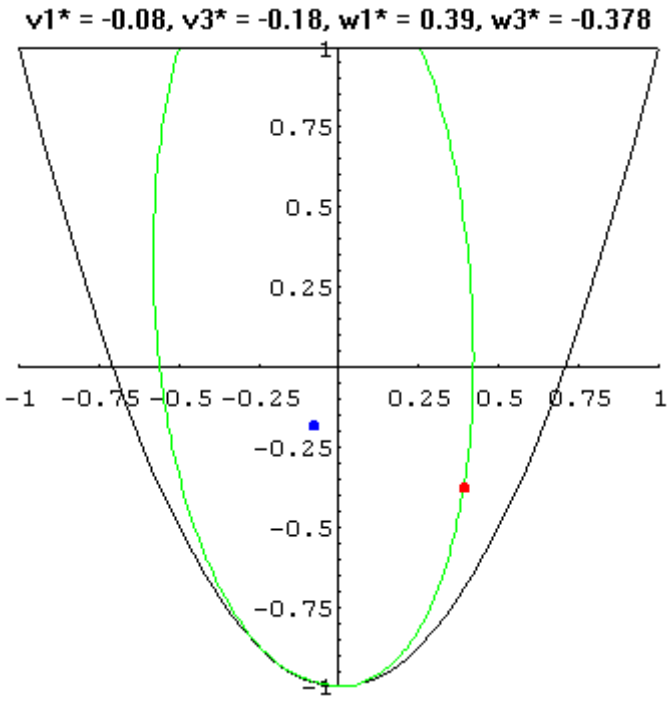

Figure 49 Interior Approach, Case 7

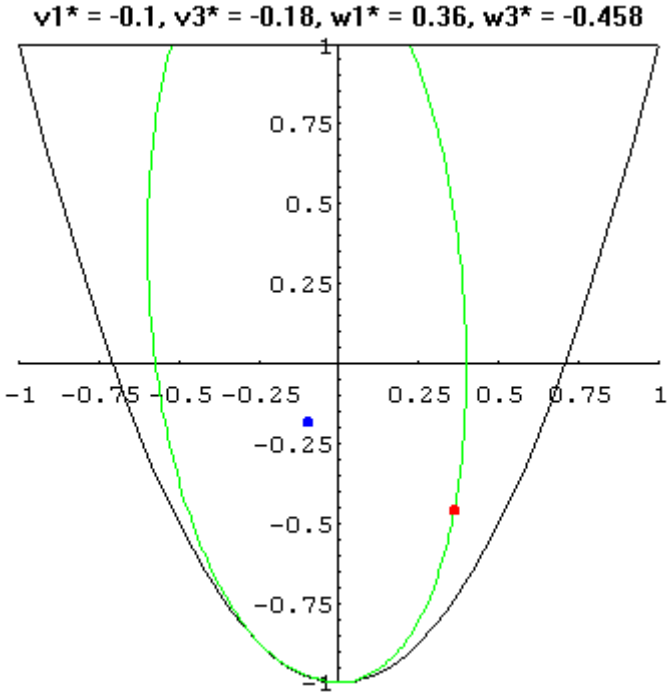

Figure 50 Interior Approach, Case 8

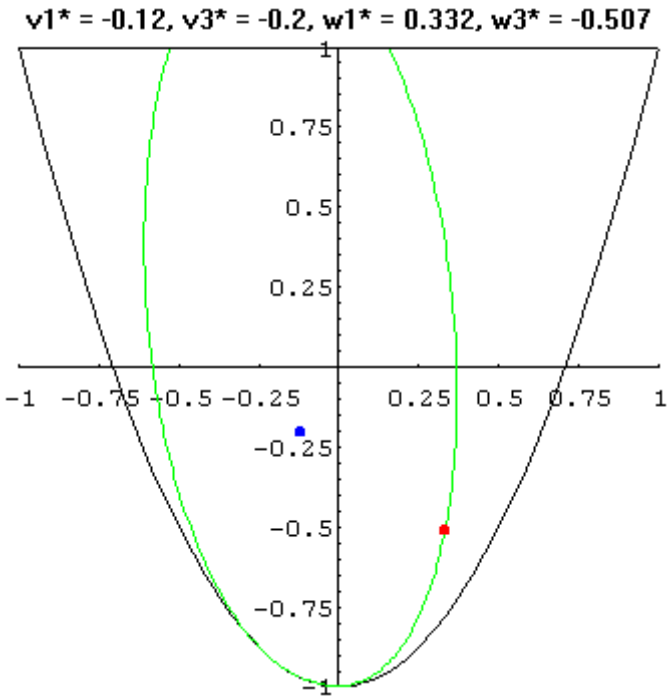

Figure 51 Interior Approach, Case 9

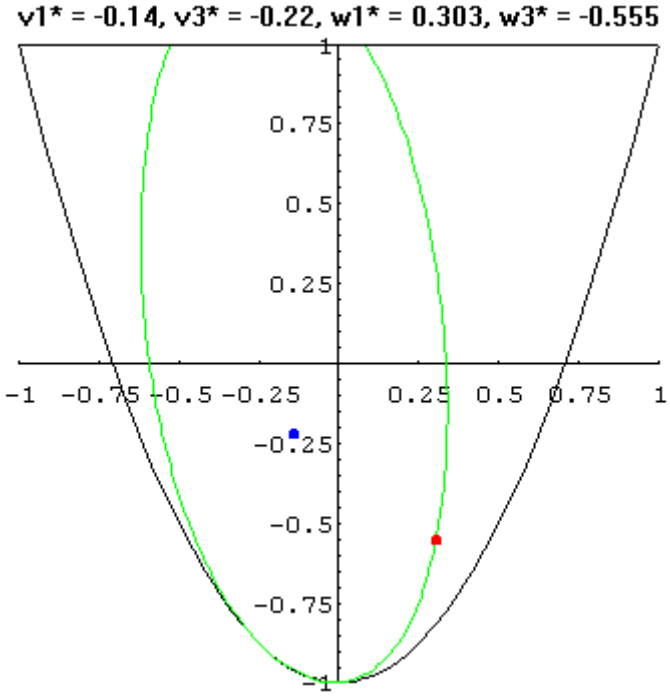

Figure 52 Interior Approach, Case 10

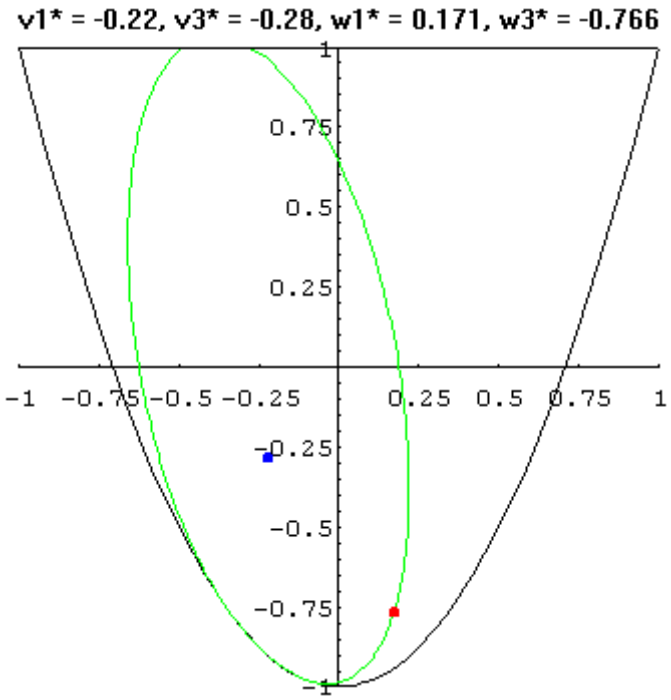

Figure 53 Interior Approach, Case 11

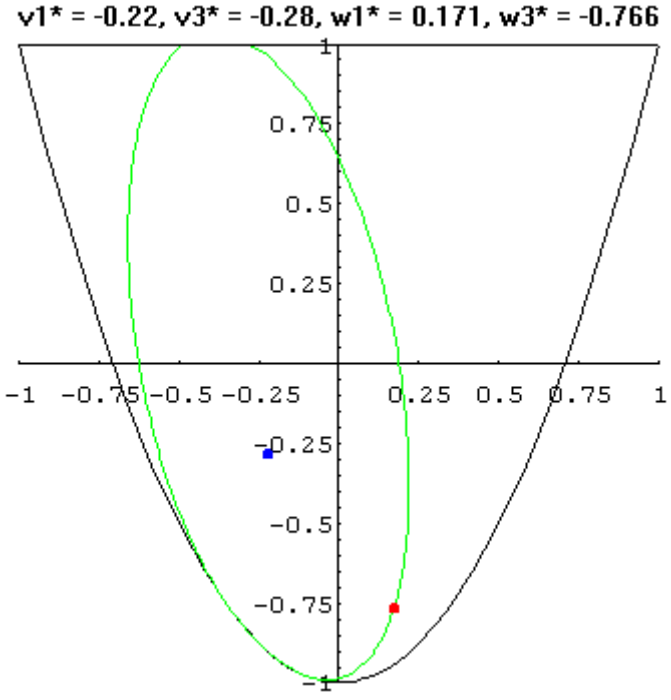

Figure 54 Interior Approach, Case 12

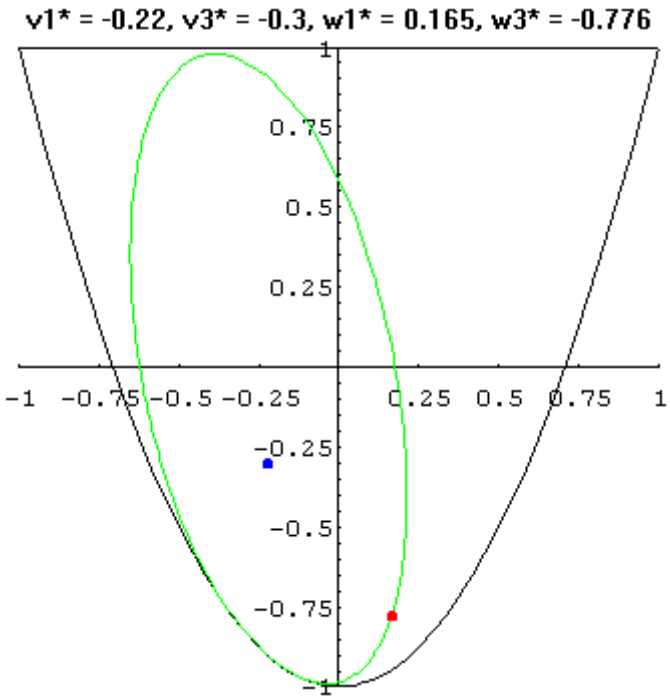

Figure 55 Interior Approach, Case 13

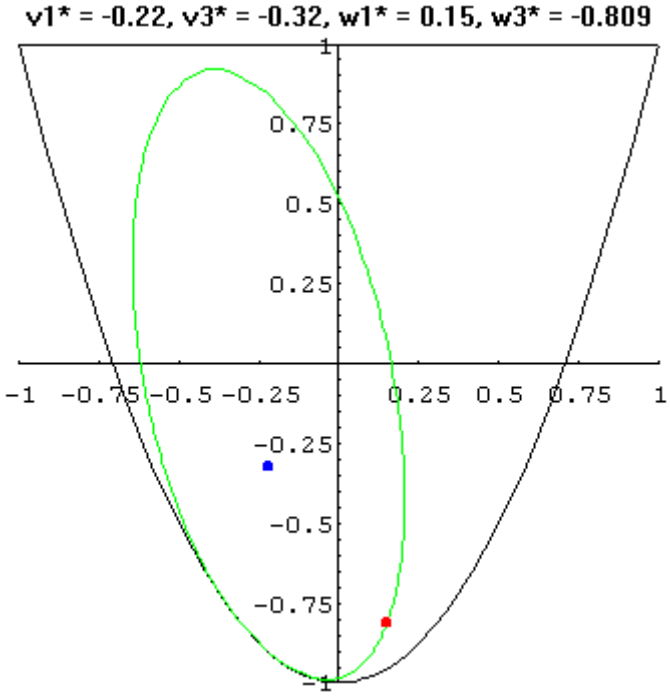

Figure 56 Interior Approach, Case 14

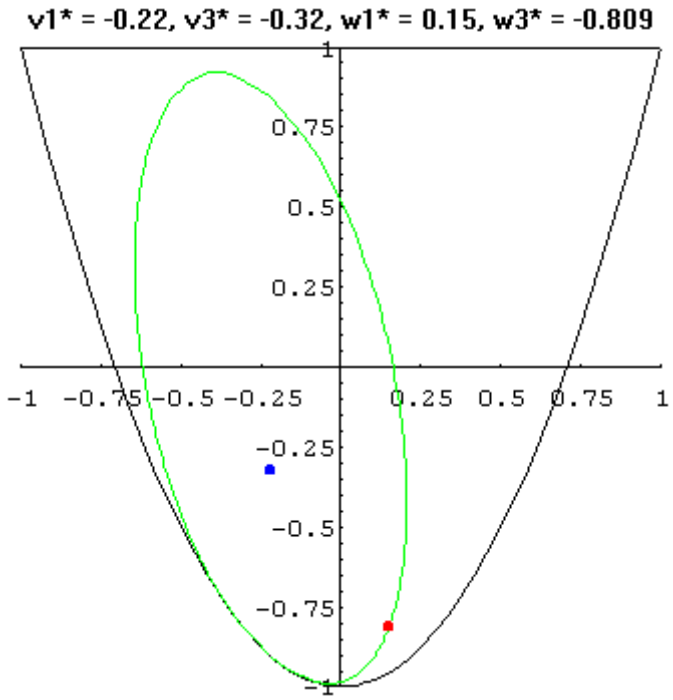

Figure 57 Interior Approach, Case 15

Stacking Approach

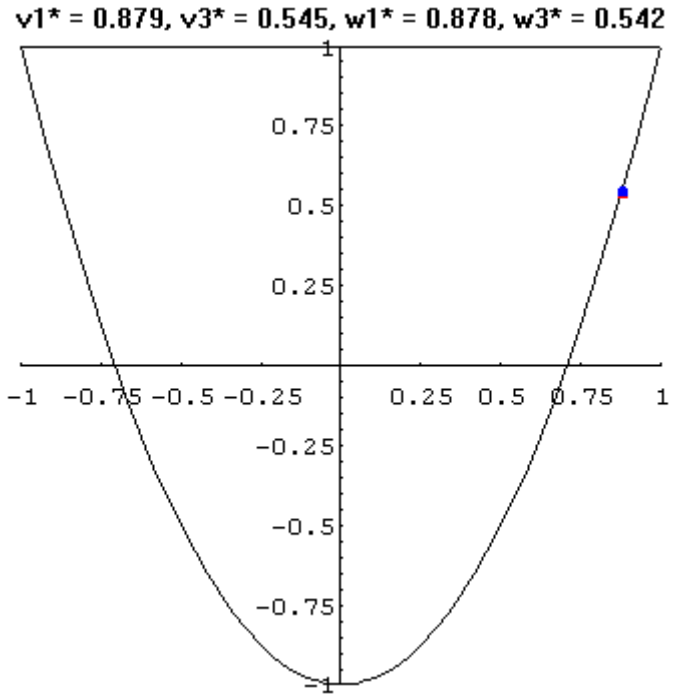

Figure 58 Stacking Approach, Cases 1 and 2

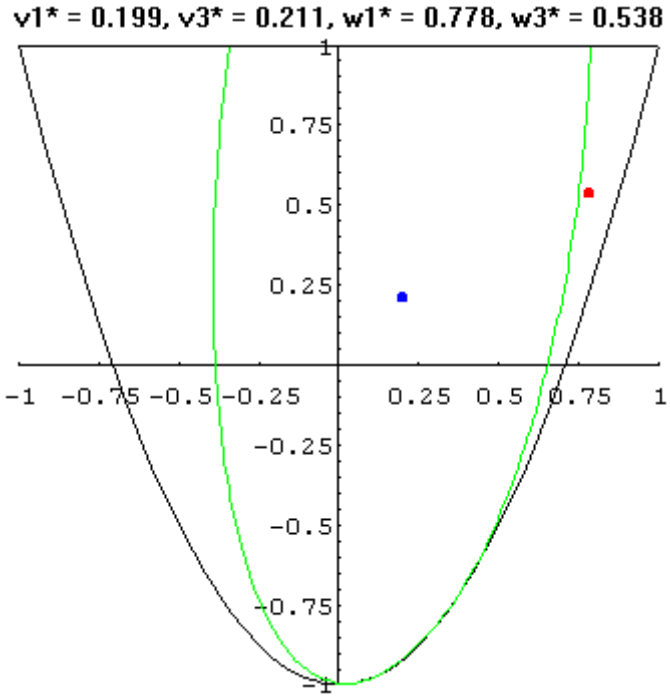

Figure 59 Stacking Approach, Case 3

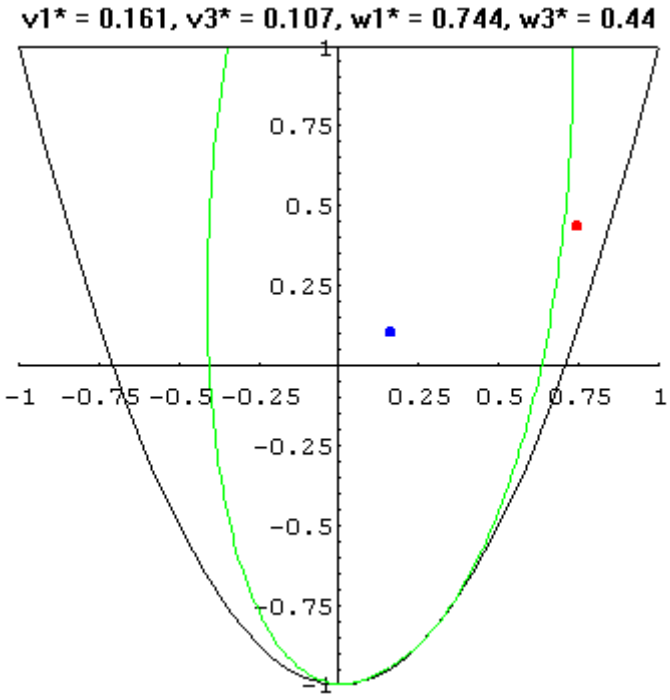

Figure 60 Stacking Approach, Cases 4 and 5

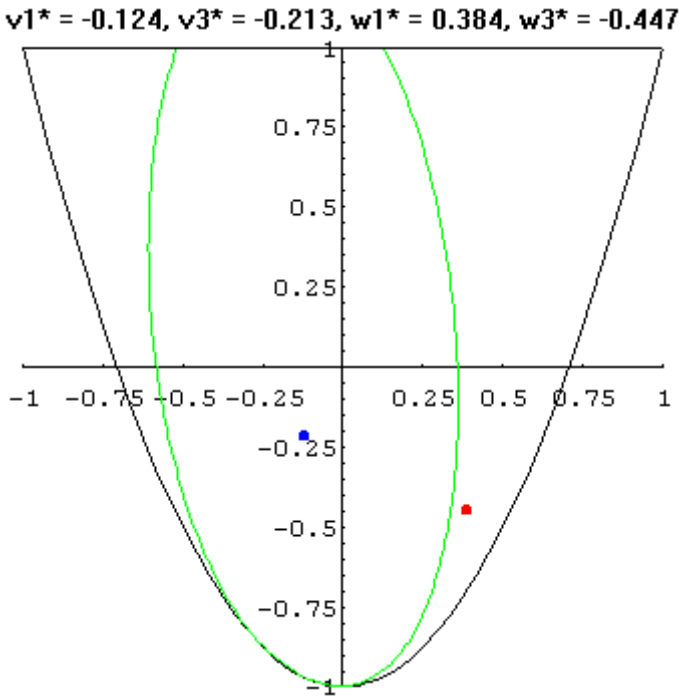

Figure 61 Stacking Approach, Cases 6, 7, and 8

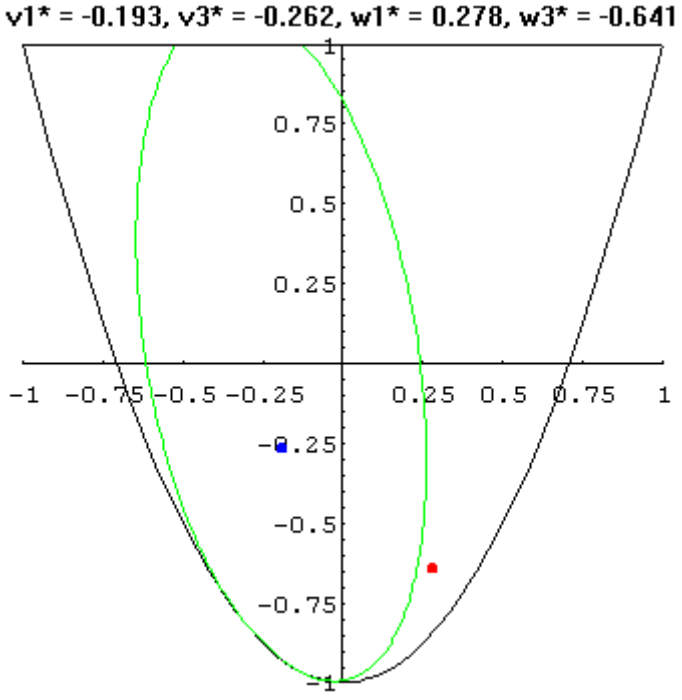

Figure 62 Stacking Approach, Cases 9 and 10

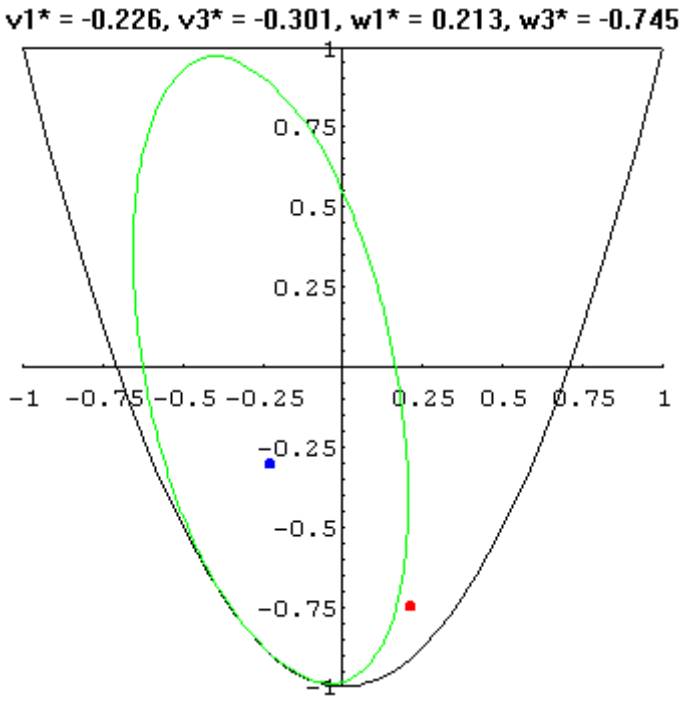

Figure 63 Stacking Approach, Case 11

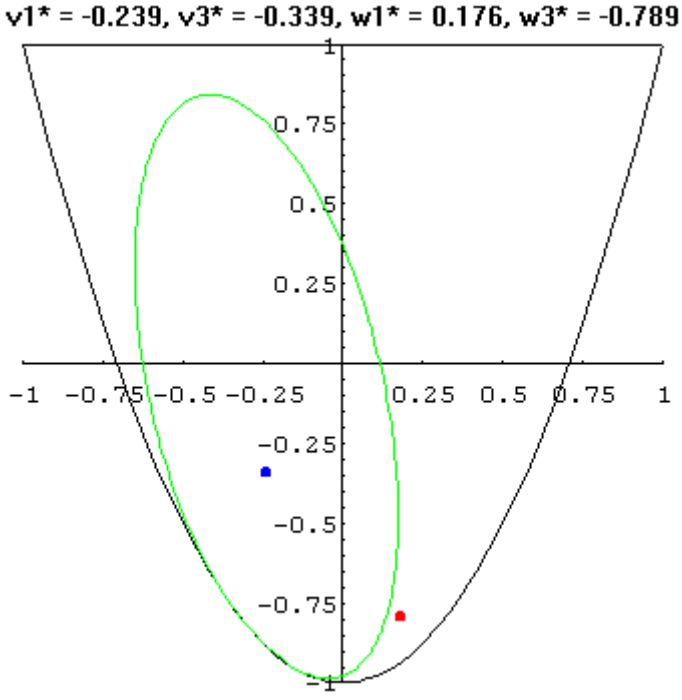

Figure 64 Stacking Approach, Cases 12, 13, and 14

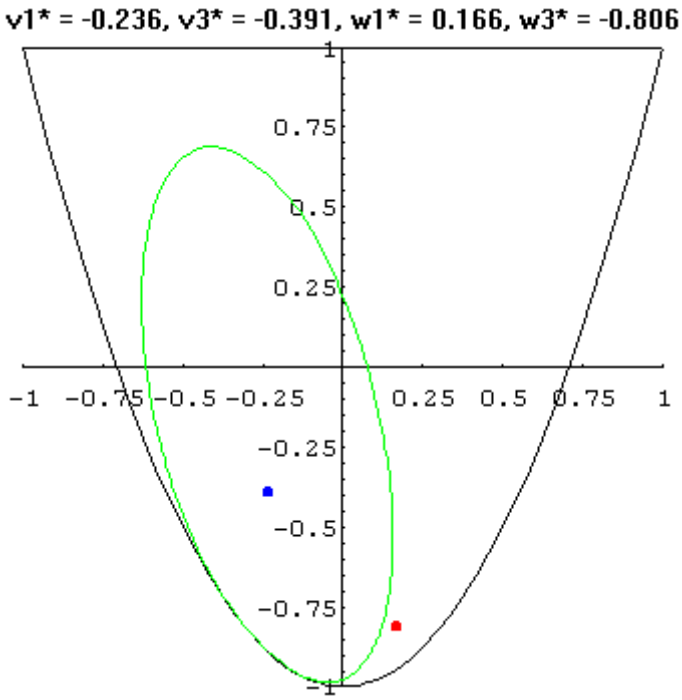

Figure 65 Stacking Approach, Case 15

Discrete Stacking Approach

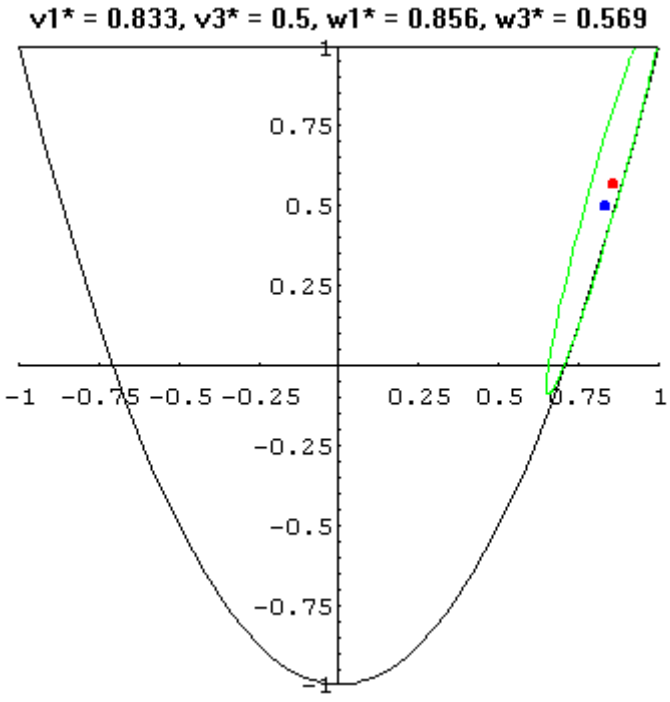

Figure 66 Discrete Stacking Approach, Cases 1, 2, and 3

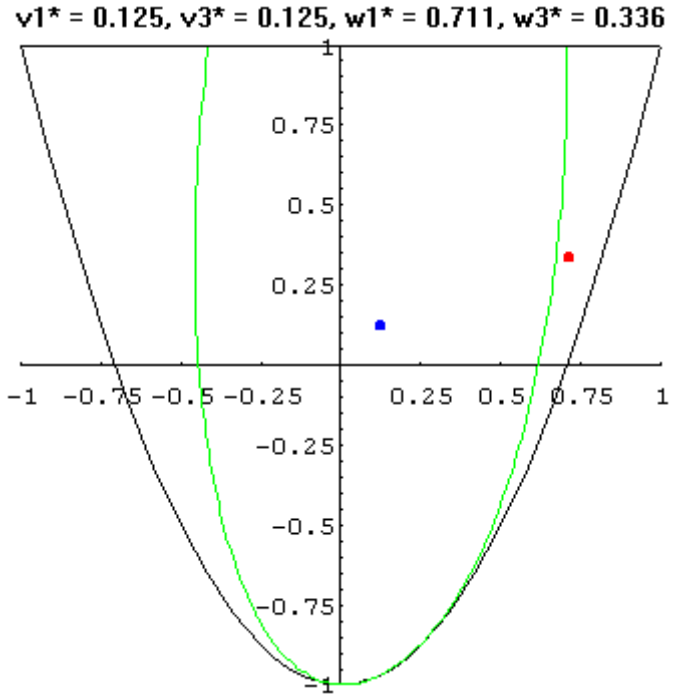

Figure 67 Discrete Stacking Approach, Cases 4 and 5

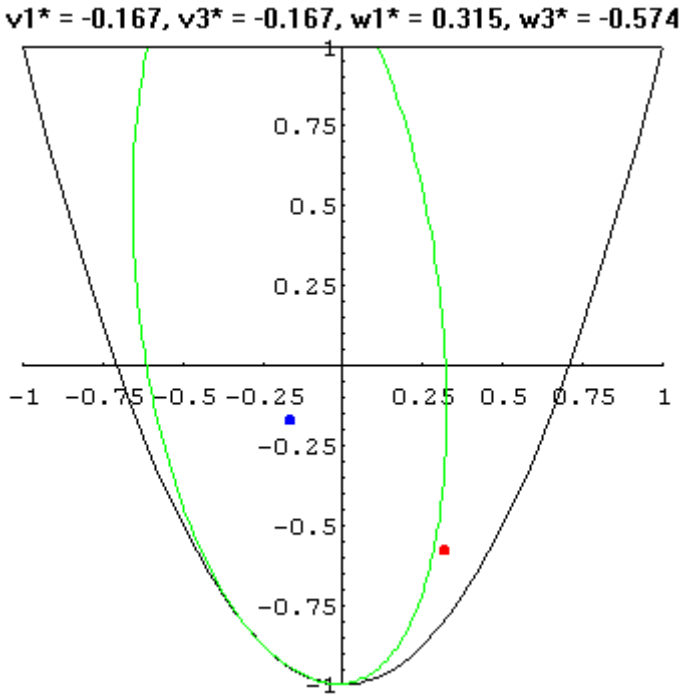

Figure 68 Discrete Stacking Approach, Cases 6, 7, and 8

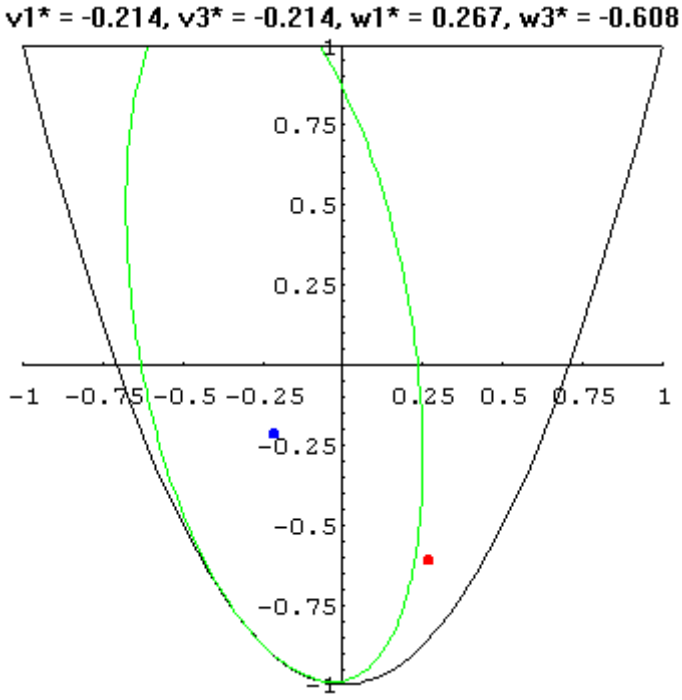

Figure 69 Discrete Stacking Approach, Cases 9 and 10

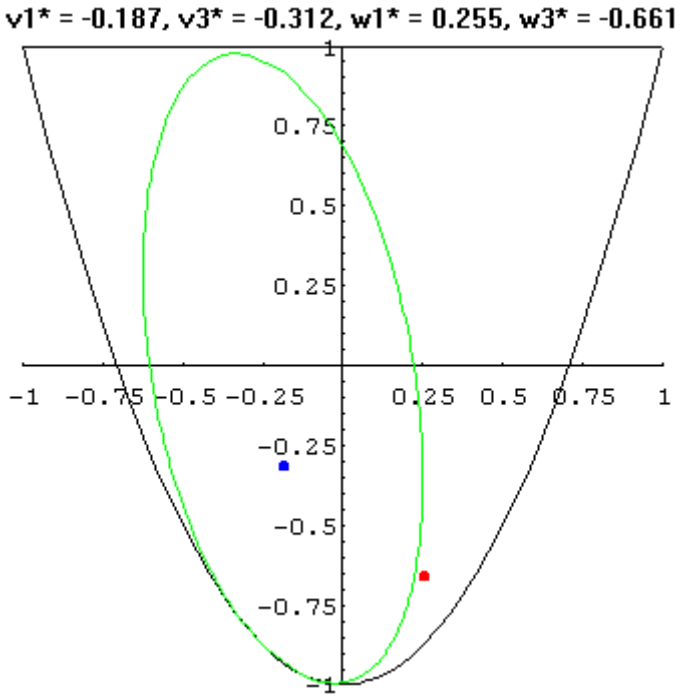

Figure 70 Discrete Stacking Approach, Case 11

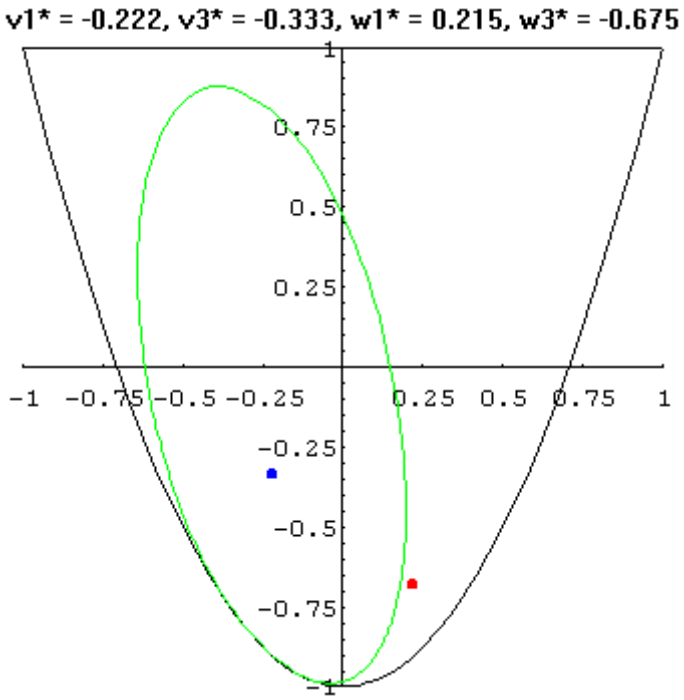

Figure 71 Discrete Stacking Approach, Case 12, 13 and 14

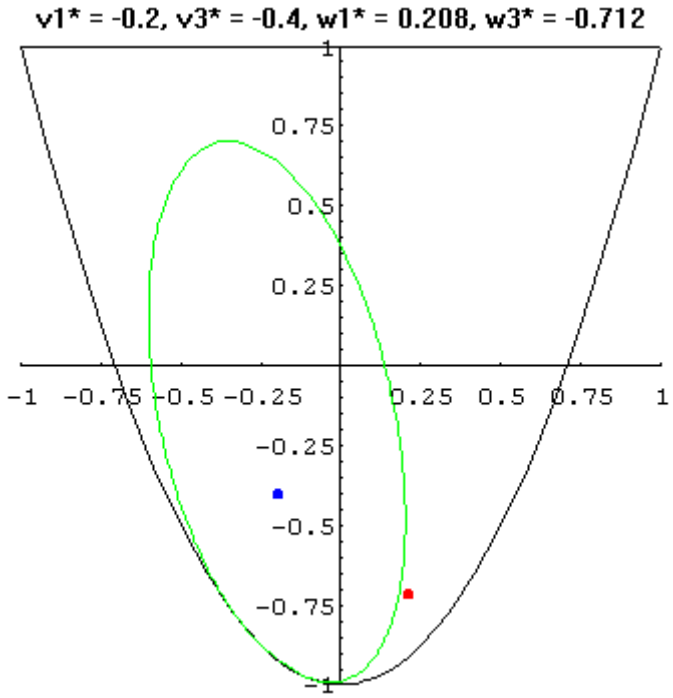

Figure 72 Discrete Stacking Approach, Case 15

Vita

Jonathan E. Rich

The author was born on July 12, 1973 in Parma, Ohio. After living in Ohio, Maryland, and New York, he graduated from Yorktown High School in Yorktown, NY in June 1991. He attended Rose-Hulman Institute of Technology, where he graduated magna cum laude with a B.S. in Mechanical Engineering. After graduation, he began his graduate studies in the Engineering Science and Mechanics Department at Virginia Tech in 1995. Prior to completing his graduate work, he was married to Alice Elizabeth Kaufman on August 30, 1997.